Doctoral Dissertation (Shinshu University)

Molecular mechanism underlying phosphorus transfer in arbuscular mycorrhizal symbiosis

September 2022

Nguyen Thi Cuc

Submitted in fulfilment of the requirement

For the degree of

Doctor of Philosophy

Laboratory of Soil Biology

Department of Bioscience and Food Production Science

Interdisciplinary Graduate School of Science and Technology

Shinshu University

Nagano, Japan

SHINSHU UNIVERSITY | Graduate School of Science and Technology

TO WHOM IT MAY CONCERN

We hereby certify this copy is a typical copy of the original PhD thesis of:

Nguyen Thi Cuc

Thesis title

Molecular mechanism underlying phosphorus transfer in arbuscular mycorrhizal symbiosis

Contents

Abstract

Phosphorus (P) is an essential element for plant growth and development. However, the concentration of available P in soil is low. Thus, plants have evolved several strategies for P acquisition in P-limiting environments. One of these strategies is the formation of symbiotic associations with arbuscular mycorrhizal (AM) fungi belonging to the subphylum Glomeromycotina. AM fungi provide soil P to host plants via hyphae that interconnect the roots and surrounding soil, thereby improving plant P nutrition and growth. Investigating the P delivery process of AM fungi at the molecular level is important to comprehensively understand this symbiotic association. This study investigates the metabolism and distribution of polyphosphate (polyP), a linear polymer of phosphate (Pi), in AM fungi and symbiotic interfaces to elucidate the P transfer mechanism between AM fungi and the host.

AM fungi accumulate a large amount of polyP in their mycelia, which plays a role in P storage and translocation. The vacuolar transporter chaperone 4 (VTC4) localized in the tonoplast is responsible for polyP synthesis in budding yeast and protozoan parasites. In Chapter II, the biochemical properties of the VTC4 protein of the AM fungus *Rhizophagus irregularis* were investigated. The *R. irregularis* VTC4 protein could catalyze polyP synthesis using ATP as a substrate. Notably, the VTC4 protein also catalyzed the reverse reaction (polyP-depolymerizing reaction), in which ATP was generated from polyP in the presence of high ADP concentration. The direction of the reaction was switched at ATP:ADP ratios of 2:1–5:1. These results indicate that AM fungal VTC4 not only synthesizes polyP but also regenerates ATP from polyP, which may be involved in the regulation of polyP and ATP levels in AM fungal cells.

Arbuscules, highly branched fungal structures, are the main site for P exchange. Arbuscules are surrounded by a host-derived periarbuscular membrane with localized symbiotic Pi transporters and H^+-ATPase HA1. The mutation of *HA1* impairs P acquisition through the mycorrhizal pathway. In Chapter III, the subcellular localization of polyP in mature arbuscules colonizing the roots of a *Lotus japonicus ha1-1* mutant was investigated to understand P transfer at the arbuscular interface. PolyP accumulated in the cell walls of trunk hyphae of the wild-type and *ha1-1* mutant, but most fine branches of arbuscules lacked polyP. Double staining of polyP and acid phosphatase (ACP) activity revealed their contrasting distribution patterns in arbuscules, i.e., ACPs were active around fine branches. Notably, polyP was observed in the cell wall of some fine branches formed in the *ha1-1* mutant, indicating that P was released from fungal cells to apoplastic regions. These observations indicate that polyP in fungal cell walls and apoplastic ACPs may play an important role in P transfer at the symbiotic interface of arbuscules.

Based on the findings, the model of P transfer from AM fungi to the host plant was proposed. The polyP accumulated in vacuoles was translocated to arbuscules, depolymerized by VTC4 to short-chain polyP, and released into the cell wall of fine branches. The secreted polyP was hydrolyzed to Pi by ACP located on the apoplastic region between the AM fungus and the host. The liberated Pi was delivered to host cells by symbiotic Pi transporters driven by the H^+ gradient generated across the periarbuscular membrane of the HA1 H^+-ATPase. The data presented herein indicate that VTC4 and ACP participate in the synthesis and hydrolysis of polyP metabolism during AM symbiosis, which may affect the growth and P nutrition of AM plants. The present work will promote the production of P-efficient crops and reduce the application of P fertilizer in sustainable agriculture by developing molecular diagnostic tools such as polyP, VTC4, and ACP for the evaluation of AM functions.

Chapter I

Introduction

Phosphorus (P) is the main nutrient necessary for plant growth and development. However, acquiring this element in plants is difficult. In soil, P is present in relatively large amounts, but it is mostly unavailable due to the low solubility of phosphate (Pi) iron, aluminum, and calcium (Schachtman *et al.*, 1998). Therefore, the P utilization efficiency of plants is typically low and P supplied by fertilizers is almost adsorbed by soil particles. Excessive P fertilizer application increases P concentration in agriculture ecosystems, leading to environmental problems. In addition, most P fertilizers are sourced from phosphate rock (P rock), a nonrenewable resource with no feasible substitute (Cooper & Carliell-marquet, 2013; Li *et al.*, 2016). Thus, developing the efficient use of P fertilizers would address environmental and resource scarcity issues. In natural and agricultural ecosystems, the association of plants with a number of microbes can contribute to the efficient use of P fertilizers (Richardson *et al.*, 2011). Among the microbes, the symbiotic relationship with arbuscular mycorrhizal (AM) fungi is the most ubiquitous, ancient, and ecologically important (Remy *et al.*, 1994; Redecker *et al.*, 2000; Strullu-Derrien *et al.*, 2018).

AM fungi belonging to the subphylum Glomeromycotina are symbiotic microorganisms that form a mutualistic relationship with most land plants (Brundrett & Tedersoo, 2018). In exchange for carbon, AM fungi provide mineral nutrients, particularly P, to the host plants via hyphae that interconnect the roots and surrounding soil (Smith & Read, 2008). Improving plant nutrition through AM symbiosis under P-deficient conditions is important. Other attributes of AM symbiosis include important determinants of plant community structure and ecosystem productivity (Heijden *et al.*, 2015; Martin *et al*., 2017), which represent a crucial asset for sustainable agriculture (Rooney *et al.*, 2009). In addition, AM symbiosis can stimulate the synthesis of plant secondary metabolites, which may improve plant fitness, including increased tolerance of or resistance to some diseases and improved water relation, soil structure, and structural stability (Newsham *et al.*, 1995; Miller & Jastrow, 2000). Moreover, AM fungi could increase the uptake of macronutrients other than P, including nitrogen (N), potassium (K), and magnesium (Mg) (Hodge *et al.*, 2001; Clark & Zeto, 2008; Smith & Read, 2008), and increase the uptake of some micronutrients (Li *et al*., 1991; Azaizeh *et al.*, 1995; Dfaz & Honrubia, 1996; Gildon & Tinder, 2016).

Among the benefits that AM fungi provide to host plants, improved P nutrient has received considerable attention from researchers. During symbiosis, host plants can acquire soil Pi via two

pathways, namely, the mycorrhizal pathway and direct pathway. The mycorrhizal pathway is a route via AM fungal hyphae (Smith *et al*., 2003; Smith *et al*., 2011). In the direct pathway, Pi is directly absorbed by plant roots. The mycorrhizal pathway is usually activated even in nonresponsive AM plants, for which AM fungal colonization does not positively affect growth or P nutrition (Smith *et al*., 2003; Smith *et al.*, 2004). The overall flow of P through the mycorrhizal pathway includes (1) P uptake from soil by AM fungal extraradical hyphae that extend far beyond the P depletion zone surrounding the root system, (2) long-distance P translocation through extraradical and intraradical hyphae, (3) P release from arbuscules that have a highly branched fungal structure formed in root cortical cells, and (4) P transfer into host plant cells (Saito & Ezawa, 2016; Ezawa & Saito, 2018). However, the mechanism of P metabolism and transport in AM symbiosis are unknown.

AM fungi absorb Pi from the soil through the Pi transporters localized on the plasma membrane of extraradical hyphae (Harrison & van Buuren, 1995; Maldonado-Mendoza *et al.*, 2001; Benedetto *et al.*, 2005; Fiorilli *et al.*, 2013; Xie *et al.*, 2016). The absorbed Pi is rapidly converted into polyphosphate (polyP) that is sequestered into tubular vacuoles (Rasmussen *et al.*, 2000; Uetake *et al.*, 2002; Ezawa *et al.*, 2004; Viereck *et al.*, 2004; Kuga *et al.*, 2008; Hijikata *et al.*, 2010; Nayuki *et al.*, 2014; Kikuchi *et al.*, 2014, 2016). PolyP is a linear polymer of Pi linked by high-energy phosphoanhydride bonds, which could be synthesized by the vacuolar transporter chaperone (VTC) complex consisting of subunits VTC1, VTC2, and VTC4 using ATP as substrate (Tani *et al.*, 2009; Tisserant *et al.*, 2012; Kikuchi *et al.*, 2014; Ezawa & Saito, 2018). P translocation in extraradical hyphae is bidirectional. However, the net flow of P is toward intraradical hyphae that are the main sink for P (Nielsen *et al.*, 2002; Viereck *et al.*, 2004; Hijikata *et al.*, 2010). Thus, a water potential gradient in AM fungal hyphae has been proposed as a driving force for the long-distance translocation of P (Kikuchi *et al.*, 2016). Once polyP is delivered to the intraradical hyphae, its chain length is shortened (Solaiman *et al.*, 1999; Viereck *et al.*, 2004; Ohtomo & Saito, 2005; Takanishi *et al.*, 2009) in a reaction that is possibly catalyzed by fungal endopolyphosphatases. This depolymerized polyP in arbuscules may be an important source of P for host plants (Solaiman & Saito, 2001; Takanishi *et al.*, 2009). Therefore, arbuscule plays a vital role in P supply through P release from fungal cells. Several hypotheses of mechanism underlining Pi export from AM fungi have been proposed. First, Pi is released by the hydrolysis of polyP and exported by Pi exporters on the fungal plasma membrane or by Golgi/trans-Golgi network-mediated vesicle trafficking (Saito & Ezawa, 2016; Ezawa & Saito, 2018). Second, Pi is directly exported from arbuscules (Saito & Ezawa, 2016). The Pi in the periarbuscular (PA) space is absorbed by mycorrhizal/inducible Pi transporters that are localized in the PA membrane (Harrison *et al.*, 2002; Javot *et al.*, 2007; Kobae & Hata, 2010; Pumplin *et al.*, 2012). These transporters are driven by the proton motive force generated by P-type

H^+-ATPase across the plasma membrane (Pao *et al.*, 1998). The mycorrhizal Pi transporter likely plays an essential role in Pi uptake through the mycorrhizal pathway (Javot *et al.*, 2007; Yang *et al.*, 2012a; Willmann *et al.*, 2013). The mycorrhiza-inducible transporter *LjPT3* and mycorrhiza-specific Pi transporter *LjPT4* have been identified in *Lotus japonicus* (Maeda *et al.*, 2006). The presence of acid phosphatase (ACP) activity in the PA space and PA membrane (Gianinazzi-Pearson *et al.*, 1991; Dreyer *et al.*, 2008) plays a role in the liberation of Pi from polyP (Saito & Ezawa, 2016).

It is important to investigate the P delivery of AM fungi at the molecular level to comprehensively understand this symbiotic association. Here, the metabolism and distribution of polyP in AM fungi and symbiotic interfaces were investigated to elucidate the P transfer mechanism between AM fungi and the host. In Chapter II, biochemical analysis of the AM fungi VTC4 protein was performed to determine whether AM fungal VTC4 is involved in the polymerization and depolymerization of polyP. In Chapter III, the subcellular localization of polyP in mature arbuscules of *Rhizophagus irregularis* colonizing the roots of a *L. japonicus* wild-type and H^+-ATPase *ha1-1* mutant was analyzed, which is defective in P acquisition through the mycorrhizal pathway, to elucidate P transfer at the arbuscular interface. The findings of this study indicate the importance of comprehensively understanding the mechanism of the symbiotic P acquisition at molecular and genetic levels. Furthermore, these findings may lead to the development of technologies that can quantitatively evaluate AM functions, which could promote research on ecology and agricultural application of AM symbiosis.

Chapter II

Polyphosphate metabolism in arbuscular mycorrhizal fungi –Biochemical analysis of AM fungal VTC4 protein–

2.1. Introduction

Arbuscular mycorrhizal (AM) fungi accumulate polyphosphate (polyP) in their mycelia, which functions the P storage and translocation. PolyP metabolism has been extensively studied in eukaryotes. The polyphosphate kinases PPK1 and PPK2 that are widely distributed in Gram-negative bacteria catalyze polyP biosynthesis using ATP as a substrate (forward reaction) and also ATP generation using polyP as a phosphate donor (reverse reaction) (Rao *et al.*, 2009). In eukaryotes, polyP metabolic enzymes have been well documented in the budding yeast *Saccharomyces cerevisiae* (Secco *et al.*, 2012; Azevedo & Saiardi, 2017; Austin & Mayer, 2020; Denoncourt & Downey, 2021). Degradation of vacuolar polyP is mediated by the endopolyphosphatases PPN1 (Kumble & Kornberg, 1996; Shi & Kornberg, 2005) and PPN2 (Gerasimaite and Mayer, 2017) that show both exo- and endopolyphosphatase activities. The NUDIX-family hydrolase DDP1, originally identified as inositol pyrophosphate phosphatase (Safrany *et al.*, 1998), also shows endopolyphosphatase activity (Safrany *et al.*, 1998; Lonetti *et al.*, 2011). *S. cerevisiae* possesses the cytosolic exopolyphosphatase PPX1, but its function is unclear (Wurst & Kornberg, 1994; Wurst *et al.*, 1995). Despite extensive studies on polyP-degrading enzymes in the past decades, polyP-polymerizing enzymes in eukaryotes have only recently been identified in the yeast. The vacuolar transporter chaperone 4 (VTC4) is responsible for the biosynthesis of polyP by transferring the γ(gamma)-Pi of ATP to the acceptor Pi or the terminal Pi residue of polyp (Hothorn *et al.*, 2009a) VTC4 that forms a complex with VTC1 and VTC3 (VTC1/3/4 complex) is localized in the tonoplast, whereas the VTC1/2/4 complex is mainly present in the endoplasmic reticulum (Hothorn *et al.*, 2009). VTC4 contains an SYG1/Pho81/XPR1 (SPX) domain at the N-terminus, a catalytic tunnel domain, and a transmembrane domain at the C-terminus, with the first two domains facing the cytoplasm (Müller *et al.*, 2003; Wild *et al.*, 2016). VTC2 and VTC3 show a domain structure similar to that of VTC4, but their tunnel domains lack the functional active sites. VTC1 consists only of a transmembrane domain. VTC5 was identified as an accessory protein that associates with the VTC complex and enhances the polyP-polymerizing activity (Desfougères *et al.*, 2016). The VTC complex embedded in the tonoplast synthesizes polyP using ATP in the cytosol as a substrate and

simultaneously translocates the polymer into the vacuoles, which requires an electrochemical gradient generated by the vacuolar H^+-ATPase (Hothorn *et al.*, 2009; Gerasimaitė *et al.*, 2014).

VTC proteins are widely present in fungi, protozoan parasites, and green algae and play significant roles in various cellular processes (Rooney *et al.*, 2011; Gomes-vieira *et al.*, 2018; Austin & Mayer, 2020; Denoncourt & Downey, 2021; Plan *et al.*, 2021). Null mutants of yeast VTC proteins not only reduce polyP levels (Ogawa *et al.*, 2000) but also affect membrane transport and vesicular traffic (Cohen *et al.*, 1999; Murray & Johnson, 2000; Muller *et al.*, 2002; Müller *et al.*, 2003; Uttenweiler *et al.*, 2006). In the phytopathogenic fungus *Ustilago maydis*, VTC4 is involved in fungal morphogenesis and virulence in maize(Boyce *et al.*, 2006). *VTC4* knockout and knockdown mutants in protozoan parasites decrease polyP accumulation in the acidocalcisomes, which influences the infectivity of the parasites in the host (Lander *et al.*, 2013; Ulrich *et al.*, 2014; Kohl *et al.*, 2018). In the green algae *Chlamydomonas reinhardtii*, polyP polymerization by VTC proteins affects acclimation to sulfur deprivation and cellular ATP homeostasis (Aksoy *et al.*, 2014; Sanz-Luque *et al.*, 2020).

AM fungi can accumulate a massive amount of polyP (> 60% of total cellular P) without perturbation of cytosolic Pi levels, which probably provide a large P pool for supplying P to their host plants (Hijikata *et al.*, 2010). Tani *et al.* (2009) demonstrated that AM fungus *Rhizophagus clarus* possesses polyP-polymerizing activity using ATP as a direct substrate in an organelle fraction. The AM fungi *R. irregularis* and *R. clarus* possess three genes encoding VTC1, VTC2, and VTC4 (Tisserant *et al.*, 2013; Ezawa & Saito, 2018), and the transcript levels of these genes in extraradical hyphae of *R. clarus* were increased by applying Pi to the mycelia (Kikuchi *et al.*, 2014; Ezawa & Saito, 2018). These findings suggest that AM fungal VTCs are responsible for polyP synthesis, but there has been no direct evidence for their biochemical activity. In this chapter, we characterized the biochemical properties of a recombinant catalytic domain of *R. irregularis* VTC4, with emphasis on the kinetics of the forward (polyP polymerization) and reverse (polyP depolymerization) reactions.

2.2. Materials and Methods

2.2.1. Expression and Purification of Recombinant Proteins

The gene encoding the catalytic domain of *R. irregularis* VTC4 (from glycine 183 to glutamine 474, RiVTC4*) was amplified from cDNA of *R. irregularis* colonizing *Lotus japonicus* roots by PCR with the primers 5'-AACTGCAGGCCAACAACAAAATTTTGTTCG-3' and 5'-CGGAATTCCTATTGTGGAAGCCAGAAAGGA-3'. The PCR product was first inserted into pGEM-T (Promega, Madison, WI, USA) to create pGEM-RiVTC4*. The gene was then inserted into pTrcHisB (Invitrogen, Carlsbad, CA, USA), from the *Pst*I (5') to the *Eco*RI (3') site, yielding pTrc-HisB-RiVTC4*. *E. coli* ArcticExpress (DE3) RIL (Agilent Technologies, Santa Clara, CA, USA) harboring pTrc-HisB-RiVTC4* was cultured in 250 ml Terrific Broth with 50 μg ml^{-1} carbenicillin at 30°C. The culture was induced with 0.1 mM isopropylthio-β-D-galactoside at an OD_{600} of 0.5 at 18°C. After incubation for 19 h, cells were harvested by centrifugation and resuspended in 14 ml lysis buffer (50 mM Tris-HCl pH 7.4, 150 mM NaCl, 48 mM imidazole, and 0.5 mM phenylmethylsulfonyl fluoride). Bacterial cells were lysed using a sonicator and centrifuged at 15,300 × *g* for 10 min at 4°C. The supernatant was filtered through a 0.45-μm cellulose acetate membrane filter (Advantec, Tokyo, Japan). The crude extract was loaded onto a HisTrap HP column (Cytiva, Tokyo, Japan), washed with 50 column volumes of buffer A (50 mM Tris-HCl pH 7.4, 150 mM NaCl, and 70 mM imidazole), and the recombinant protein was placed on a step gradient against buffer B (50 mM Tris-HCl pH 7.4, 150 mM NaCl, and 300 mM imidazole). The buffer was changed to 50 mM Tris-HCl pH 7.4 using a PD-10 column (Cytiva). The recombinant protein was concentrated using an Amicon Ultra-4 10 K centrifugal unit (Merck, Kenilworth, NJ, USA). Protein concentrations were measured using the Qubit Protein Assay Kit (Invitrogen). Sodium dodecyl sulfate-polyacrylamide gel electrophoresis (SDS-PAGE) and staining with Oriole (Bio-Rad, Hercules, CA, USA) were performed.

2.2.2. Assays for PolyP-polymerizing Reaction

The polyP-polymerizing activity of RiVTC4* was assayed in triplicate at 24°C in a reaction mixture (10 μl) containing 50 mM PIPES-KOH pH 6.8, 150 mM NaCl, 1 mM $MnCl_2$, 0.005–7.5 mM ATP-Na (Oriental Yeast, Tokyo, Japan), and 200 nM RiVTC4*. When indicated, 5 mM sodium pyrophosphate was added to the reaction. The reaction was initiated by the addition of ATP and terminated with 1 μl of 0.15 M EDTA after 60 min. The amount of ADP generated by ATP hydrolysis during polyP polymerization was determined using the Fluorospark Kinase/ADP Multi-Assay Kit (FUJIFILM Wako Chemicals, Osaka, Japan) following the manufacturer's instructions after the reaction solution was diluted five or ten times with MilliQ H_2O. Fluorescence (excitation: 540 nm, emission: 590 nm) was

measured using a microplate reader (Corona Electric, Ibaraki, Japan). One unit of polyP-polymerizing activity was defined as the amount of enzyme required to catalyze the generation of 1 μmol of ADP equivalents per min. The kinetic parameters (V_{max} and apparent K_m) were calculated by nonlinear regression using the function drm in the add-on package drc of R version 4.0.0 (Ritz *et al.*, 2015). The enzyme kinetics at varying concentrations of disodium hydrogenphosphate, sodium pyrophosphate, sodium tripolyphosphate (Sigma-Aldrich), and short-chain polyP EXP-S (EXP-S, mean chain length 14-mer; RegeneTiss, Nagano, Japan) were also analyzed using 1 mM ATP under the same reaction conditions, since these polyP stimulate the polyP-polymerizing activity of ScVTC4, possibly by a priming effect (Hothorn *et al.*, 2009a; Lander *et al.*, 2013). To determine the optimum pH for polyP-polymerizing activity, the assay was performed at a pH range of 5.1 to 8.9. The reaction mixture contained 50 mM MES-KOH, PIPES-KOH, HEPES-KOH, or Tris-HCl buffer, 150 mM NaCl, 1 mM $MnCl_2$, 1 mM ATP, 1 mM sodium pyrophosphate, and 50 nM RiVTC4*. Assays to examine the effects of metals (1 mM $CoCl_2$, $MgCl_2$, $MnCl_2$, $NiCl_2$, and $ZnCl_2$) and 1 mM EDTA on the enzyme activity were conducted under the same reaction conditions as for the pH assay, except that PIPES-KOH pH 6.8 was added to a final concentration of 50 mM. To determine the polyP chain length produced by the polyP-polymerizing reaction, RiVTC4* proteins (1 μM final concentration) were assayed at 24°C for 1, 2, 4, and 8 h in an ATP-regenerating mixture (50 mM PIPES-KOH pH 6.8, 150 mM NaCl, 1 mM $MnCl_2$, 1 mM ATP, 40 mM creatine phosphate, and 50 IU ml^{-1} creatine kinase [Oriental Yeast]) with 1 mM sodium pyrophosphate or 0.1 mM (as Pi) of the fractionated polyP PP5 with a mean chain length of 37-mer (Ohtomo *et al.*, 2008). The synthesized polyP was analyzed by polyacrylamide gel electrophoresis (PAGE) as described below. The effects of ADP on polyP kinase activity were determined by PAGE after incubating 1 μM RiVTC4* at 24°C for 4 h in a reaction mixture containing 50 mM PIPES-KOH pH 6.8, 150 mM NaCl, 1 mM $MnCl_2$, 1 mM sodium pyrophosphate, 1 mM ATP, and the indicated concentrations of ADP (0–2 mM).

2.2.3. Assays for PolyP-depolymerizing Reaction

The polyP-depolymerizing reaction to produce ATP from polyP and ADP by RiVTC4* was determined. The reaction mixture contained 50 mM PIPES-KOH pH 6.8, 150 mM NaCl, 1 mM $MnCl_2$, 0.125–25.6 mM ADP-Na (Oriental Yeast), 0.4–500 μM (as Pi) EXP-S, and 50 or 100 nM RiVTC4* in a final volume of 10 μl. Six independent reactions were performed for each enzyme assay. The reaction was initiated by the addition of ADP at 24°C and terminated by heating at 70°C for 5 min. The reaction time was 60 min. After the reaction solution was diluted with four volumes of 250 mM Tricine-KOH pH 7.8, ATP concentration was determined using an ATP Bioluminescence Assay Kit CLS II (Roche, Mannheim, Germany) following the manufacturer's instructions. Since luciferase activity is known to be affected by pyrophosphate and tripolyphosphate (Fontes *et al.*, 2008), an ATP standard curve was

prepared for each concentration of polyP. One unit of polyP-depolymerizing activity was defined as the amount of enzyme that catalyzes the generation of 1 μmol of ATP equivalents per min. The apparent optimal pH for the polyP-depolymerizing activity was determined by incubating the enzyme in 50 mM MES-KOH, PIPES-KOH, HEPES-KOH, and Tris-HCl buffer. As substrates, 5 mM ADP and 0.5 mM (as Pi) EXP-S were included in the reactions. An assay to examine the effects of divalent metal cations (1 mM $CoCl_2$, $MgCl_2$, $MnCl_2$, $NiCl_2$, and $ZnCl_2$) and 1 mM EDTA on polyP-depolymerizing activity was performed. To monitor polyP chain length during the reaction, 1 mM (as Pi) EXP-S and 1 mM long-chain polyP EXP-L (EXP-L, mean chain length 130-mer; RegeneTiss) were incubated with 100 nM RiVTC4* at 24°C in an ADP-regenerating mixture (50 mM PIPES-KOH pH 6.8, 150 mM NaCl, 1 mM $MnCl_2$, 5 mM ADP, 50 mM glucose, and 50 IU ml^{-1} hexose kinase [Oriental Yeast]) and separated by PAGE as described below. To detect Pi, pyrophosphate, and tripolyphosphate generated during the polyP-depolymerizing reaction, these P compounds contained in solutions incubated with 10 mM (as Pi) EXP-S and 500 nM RiVTC4* in the ADP-regenerating mixture were separated by PAGE and thin-layer chromatography (TLC) as described below.

2.2.4. Effects of ATP:ADP Ratios on PolyP Polymerization and Depolymerization

EXP-S (1 mM as Pi) were incubated at 24°C for 4 h in a reaction solution containing 50 mM PIPES-KOH pH 6.8, 150 mM NaCl, 1 mM $MnCl_2$, 1 μM RiVTC4*, and the indicated concentrations of ATP (0–10 mM) and ADP (0–5 mM). Control experiments without enzyme addition were also performed in parallel. PolyP was separated by PAGE as described below.

2.2.5. Electrophoresis of PolyP

Solutions containing polyP were neutralized with a NaOH solution after adding phenolphthalein indicator, and then mixed with 5× loading dye solution (5× Tris-borate-EDTA [TBE], 15% Ficoll 400, and 0.1% bromophenol blue [BPB] or orange G). Samples and the polyP size markers PP4, PP5, and PP6 (Ohtomo *et al.*, 2008) were loaded onto polyacrylamide gels (33 or 15% acrylamide:bis-acrylamide (19:1), 1× TBE, 0.07% ammonium persulfate, 0.08% TEMED). The running buffer used was a 1× TBE. After a pre-run at 300 V for 1 h, electrophoresis was performed at 300 V until BPB migrated 4.5 cm from the top of the gel. The gel was stained with 2 μg ml^{-1} 4',6-diamidino-2-phenylindole dihydrochloride (DAPI) in a fixative solution (25% methanol, 5% glycerol, and 50 mM Tris) for 30 min and destained in the fixative solution for 15 min (Smith & Morrissey, 2007). The gels were then exposed to 360 nm light on a UV transilluminator for several minutes to induce

photobleaching, after which digital images of DAPI negative staining for polyP were captured (Smith & Morrissey, 2007).

2.2.6. TLC of PolyP

Pi, pyrophosphate, tripolyphosphate, and longer polyPs were separated by TLC according to Scott & Haight (1975). After the polyP-depolymerizing assay with 10 mM EXP-S, the solutions were neutralized with NaOH solution after adding the phenolphthalein indicator. Samples (1 µl) were spotted 2 cm from the bottom of a 7-cm PEI cellulose F 25 plastic sheet (Merck, Darmstadt, Germany). We also spotted 3.33 nmol disodium hydrogenphosphate, 1.66 nmol sodium pyrophosphate, and 1 nmol sodium tripolyphosphate as markers. Ascending chromatography was performed using a developing solvent containing 1.5 M LiCl and 1 M formic acid. After drying, the TLC sheets were sequentially sprayed with 1% ammonium heptamolybdate, 10% trichloroacetic acid, and 2% ascorbic acid. The sheets were then placed in an oven at 100°C for 3 min.

2.2.7. Gene Expression Analysis

Gene expression analysis was performed as previously described (Kobae *et al.*, 2015). Briefly, *Lotus japonicus* B-129 "Gifu" was grown in a mesh bag culture system (Kikuchi *et al.*, 2014), in which mycorrhizal and hyphal compartments were separated by a cone-shaped nylon mesh bag. Plants were inoculated with 1,000 spores of *R. irregularis* DAOM197198 and cultivated in a growth chamber at 25°C with a 16 h day/8 h night cycle for four weeks. Mycorrhizal roots and extraradical mycelia were harvested from the mycorrhizal and hyphal compartments, respectively. Total RNA was extracted using the RNeasy Plant Mini Kit (Qiagen, Hilden, Germany). Genomic DNA was digested using RNase-free DNase I (Qiagen) and Turbo DNA-*free* (Thermo Fisher Scientific, Waltham, MA, USA). First-strand cDNA was synthesized using a High Capacity cDNA Reverse Transcription Kit (Thermo Fisher Scientific). Quantitative PCR was performed using a StepOne Real-Time PCR System (Thermo Fisher Scientific) with the Power SYBR Green PCR Master Mix (Thermo Fisher Scientific) and the primers *RiVTC1* (5'-AGTACGGGGAACATTTTT-3' and 5'-GAAAATAGCAAATTGATCGAAA-3'), *RiVTC2* (5'-GGTTCGCGAGGATAATTTTGAC-3' and 5'-TTGCGACGCCACTCATCTT-3'), and *RiVTC4* (5'-CATGGTGTCGCAACACTTATGG-3' and 5'-GTGGAAGCCAGAAAGGAAAAAG-3'). Expression levels were normalized to the quantity of *R. irregularis EF1β* (Kobae *et al.*, 2015). All reactions were performed using three biological replicates. Expression of the VTC genes between intraradical and extraradical mycelia was analyzed using Welch's *t*-test.

2.2.8. Bioinformatics Analysis

Amino acid sequences of AM fungal VTC proteins were obtained by BlastP searches against AM fungal genome databases (**Table 2-1**) using *S. cerevisiae* VTC1–VTC5 as queries (https://www.yeastgenome.org). In these searches, those that showed similarity to VTC3 were not considered because *ScVTC2* and *ScVTC3* were derived by a recent duplication in the lineage, thus sharing high sequence similarity (Gomes-vieira *et al.*, 2018). InterPro (https://www.ebi.ac.uk/interpro/) was used to predict the domain of VTC proteins in *R. irregularis*. The transmembrane region was predicted using TMHMM (http://www.cbs.dtu.dk/services/TMHMM/). Amino acid sequences of AM fungal and *S. cerevisiae* VTC proteins were aligned using ClustalW with manual adjustments (**Data 2-1**). Maximum-likelihood tree inference and bootstrapping with 100 replicates were performed with RAxML-NG version 1.0.1 (Kozlov *et al.*, 2019) using the LG+I+G amino acid substitution model. The best-fitted evolutionary model was identified using ModelTest-NG version 0.1.3 (Darriba *et al.*, 2020). Trees were visualized and annotated using the iTOL platform version 5.7 (Letunic & Bork, 2019). The alignment and tree files presented were deposited in the Dryad Digital Repository (https://doi.org/10.5061/dryad.ghx3ffbp7).

Table 2-1. List of VTC protein sequences in arbuscular mycorrhizal fungi and budding yeast

Species	Database	Accession no.†			
		VTC1	VTC2/3	VTC4	VTC5
Rhizophagus cerebriforme DAOM 227022	Mycocosm	RIA88956.1	RIA93067.1	RIA98427.1	
Rhizophagus clarus HR1	GenBank	GBC02351.1	GBC06127.1	GBC09375.1	
Rhizophagus diaphanus MUCL 43196	Mycocosm	RGB33820.1	RGB27579.1	RGB31432.1	
Rhizophagus irregularis DAOM 197198	GenBank	BBB37598.1	BBB37597.1	BBB37596.1	
Diversispora epigaea IT104	GenBank	RHZ49166.1	RHZ47133.1	RHZ65141.1	
Gigaspora margarita BEG34	GenBank	KAF0514596.1 (VTC1-1) KAF0385400.1 (VTC1-2)	KAF0363282.1	KAF0486751.1	
Gigaspora rosea DAOM 194757	Mycocosm	RIB11453.1 (VTC1-1) RIB03475.1 (VTC1-2)	RIB23933.1	RIB07217.1	
Geosiphon pyriformis	Mycocosm	18051	9393	2689	
Saccharomyces cerevisiae S288C	SGD	YER072W	YFL004W (VTC2) YPL019C (VTC3)	YJL012C	YDR089W

[†]Accession no. in the GenBank (https://www.ncbi.nlm.nih.gov/genbank/) for the fungal species other than *G. pyriformis* and *S. cerevisiae*. *G. pyriformis*: protein ID in JGI Mycocosm (https://mycocosm.jgi.doe.gov/Geopyr1/Geopyr1.home.html). *S. cerevisiae*: gene name in SGD (https://www.yeastgenome.org).

Data 2-1. Amino acid sequence alignment of VTC proteins of eight AM fungal species and budding yeast *Saccharomyces cerevisiae*. Abbreviations of the species names are: Rhice, *Rhizophagus cerebriforme*; Rhicl, *R. clarus*; Rhidi, *R. diaphanus*; Rhiir, *R. irregularis*; Divep, *Diversispora epigaea*; Gigma, *Gigaspora margarita*; Gigro, *G. rosea*; Geopy, *Geosiphon pyriformis*; Sacce, *S. cerevisiae.*

1. C-terminal sequences containing Duf202 domain of VTC1, VTC2, and VTC4

```
>Rhiir_VTC1   MS-TQPLLQ---AQKRIALPTRVEPKVFFANERTFLSWLQFTVVLGGLALGLLNF-G--DK--VGKISAAIFTFVAMAIMLYALLIYHWRATKIRKRESGPYDDRYGPTVLCFFLVGAVVTNFILRFTN
>Rhicl_VTC1   MS-TQPLLQ---PQKRIALPTRVEPKVFFANERTFLSWLQFTVVLGGLGLGLLNF-G--DK--IGKISAAIFTFVAMAIMLYALSIYHWRATKIRKRESGPYDDRYGPTVLCIFLVGAVITNFILRFT-
>Rhice_VTC1   MS-TQPLLQ---QQKRIALPTRVEPKVFFANERTFLSWLHFTVVLGGLAIALLNF-G--DR--VGKISAGVFTFVAMAVMVYALYTFHWRATKIRKRETGPYDDRYGPTFLCFFLVAAVVTNFVLRFTS
>Rhidi_VTC1   MS-TQPLLQ---PQKRIALPTRVEPKVFFANERTFLSWLQFTVVLGGLALGLLNF-G--DK--VGKISAAIFTFVAMAIMLYALLIYHWRATKIRKRETGPYDDRYGPTVLCFFLVGAVITNFILRFTD
>Divep_VTC1   MS-N---QQ---SQRRIIIPVRIEPKVFFANERTFLSWLQFTVVLGGLAIGLLNF-G--DK--IGRISAGLFTLVAMSMMMYALLIYHWRASKIRKKEEGPYDDRYGPTLLCGFLFAAVITNFILRFTS
>Gigma_VTC1-1 MS-SQPLLQ----NKRIALPARVEPKVFFANERTFLSWLQFTVILGGLAIGLLNF-G--DK--VGRISAALFTSVAMLVMVYALSLYHWRAAKIRKRESGPYDDRYGPTFLCIFLIIVVITNFILRFTS
>Gigma_VTC1-2 MS-S---LQ----NKRIALPAKVEPKVFFANERTFLSWLQFTVILGGLAIGLLNF-G--DK--VGRISAALFTSVAMLVMVYALFLYHWRAAKIRKRESGPYDDRYGPTFLCIFLIIVVITNFILRFTS
>Gigro_VTC1-1 MS-SQPLLQ----SKRIALPARVEPKVFFANERTFLSWLQFTVVLGGLAIGLLNF-G--DR--VGRISAALFTSVAMLVMVYALSLYHWRAAKIRRRESGPYDDRYGPTFLCIFLIIVVITNFILRFTS
>Gigro_VTC1-2 MS--QPLLQ----NKRIALPARVEPKVFFANERTFLSWLQFTVVLGGLAIGLLNF-G--DR--VGRISAALFTSVAMLVMVYALSLYHWRAAKIRKRESGPYDDKYGPTFLCIFLIIVVITNFILRFTS
>Geopy_VTC1   MSETEPLLQERPPQKRVAIPVRVEPKVFFANERTFLSWLQFTVVLGGLAIGLLNF-G--DR--VGKISAALFTFVAMAVMIYALSIYHWRADRIRKREGGAYDDRFGPTILCIFLLAAVITNFALRFSA
>Sacce_VTC1   MS-SAPLLQ-RTPGKKIALPTRVEPKVFFANERTFLSWLNFTVMLGGLGVGLLNF-G--DK--IGRVSAGLFTFVAMGTMIYALVTYHWRAAAIRRRGSGPYDDRLGPTLLCFFLLVAVIINFILRLKY
>Rhiir_VTC2   GPEEVILPPNISMPHKIITPVRVEPKVFFANERTFFHWMRFSVLLGSFSLALFNTSG-DDR--VGYMCGFIYAIISVAALIYSLIKYNKRLTMINNREPGPYDDVLAPPLVCISLVFAIGLNFYLKYNP
>Rhicl_VTC2   GPEEVILPPNVSIPRKIITPVRVEPKVFFANERTFFHWMRFSVLLGTFSLALFNTSG-DDR--IGYMCGFIYAIISVITLIYSLVKYNKRLTMINNREPGPYDDILAPPLVCISLVLAIGLNFYLKYNP
>Rhice_VTC2   APEAVILPPNVSIPRKIITTVQVEPKVFLANERTFFSWMRFSVMLGTFSLALFNASG-DDR--VGYICGFMYAIISIVLIYSLVKYNKRLTMINNRDPGPYDDVLAPPLVCIALFFAVGINFYLKYNP
>Rhidi_VTC2   GPEEVILPPNISMPHKIITPVRVEPKVFFANERTFFHWMRFSVLLGSFSLALFNTSG-DDR--VGYMCGFIYAIISVTALIYSLIKYNKRLTMINNREPGPYDDVLAPPLVCISLVFAIGLNFYLKYNP
>Divep_VTC2   IPDRETISRILPLPPKVVGPVQVEPKVFYANERTFFSWLRFCVLLGSLALGLFNSAAADNK--LAIYCAVSYTSISVVVLFYSLFQFKKRNRMINSLHPGPYDDLIAPAAVCAAIFVAIGLNFYLKLAP
>Gigma_VTC2   RPDRVIIPYNVKEPERVVGSVKVEAKVFFANERTFFSWMKFSILLSTFALALFNASAADNE--LGMRCAIAYTGIGIGCLIYSVYKYNSRLSMINSKHPGPYDDIFAPIFVCLSLFLASGLNFYLKLHP
>Gigro_VTC2   RPDRVIIPYNVKEPERVVGSVKVEAKVFFANERTFFAWMKFSILLSTFALALFNASAADNE--LGMRCAIAYTGIGITCLIYSVYKYNSRLSMINSKHPGPYDDILAPIFVCLSLFLASGLNFYLKLHP
>Geopy_VTC2   NEPPSNLPPAVHVPQHVETPIRVEPKVYFANERTFFAWMRFSVLLGTFSLALFNA-G-NDK--IGRSFGLLYSIISLSILLYSLNQFHKRNDMINSRDPGPYDDLVFPTVVCIALVFAVYAELYFMNIY
>Sacce_VTC2   EIELPPGVKKPLNLLKNAGPVNVEAKVWLANERTFNRWLSVTSLLSVLTFSIYNSVKKAEYPTLANYMAYVYFGLTIFCALWSYSIYMKRVDIIQQRSGQHLDAPLGPVLVSIVLFVTLVVNFVMAFRN
>Sacce_VTC3   SFQLPPGVKKPVHLLKNAGPVKVEAKVWLANERTFNRWLSVTTLLSVLTFSIYNSVQKAEFPQLADLLAYVYFFLTLFCGVWAYRTYLKRLTLIKGRSGKHLDAPVGPILVAVVLIVTLVVNFSVAFKE
>Rhiir_VTC4   VTP-AGKVPKTYHGKKIAIPVRVEPKVFFANERTFLSWLNFSVVLGGFAIGLLNF-G--DK--ITVTAASFLVFVTMMVMLYALGTYLWRVKKIRKRESGPYEDRYGPTFICIMLLISVTINFWLRLHE
>Rhicl_VTC4   VTP-AGKVPKTYQGKKIAIPVRVEPKVFFANERTFLSWLNFSVTLGAVALGLLNF-G--DK--VTVTAAALLTTITMAVMLYALGTYLWRVRKIRKRESGPYEDRYGPTFVCLLLLISVIVNFMLRLRD
>Rhice_VTC4   ITP-AGKVPKTYNGKRIAVPVRIEPKVFFANERTFLSWLNFTVLVGTIAVGLLNF-G--DK--IALTAAIMFTFVTMMVMIYALVNYLLRVRKIRKRESGPYDDRYGPTILCGILLIAVLVNFWLR-WD
>Rhidi_VTC4   VTP-AGKVPKTYHGKKIAIPVRVEPKVFFANERTFLSWLNFSVVLGGFAIGLLNF-G--DK--ITVTAASFLVSVTMMVMLYSLGTYLWRVKKIRRRESGPYEDRYGPTFICILLLISVTINFWLRLHE
>Divep_VTC4   L----REVPTTYRGKRIAVPVRVEPKVYFANERTFLTWLNFTVMLSGLAVGLLNF-G--DR--IAIIAAGMFTAISMSAMLYSLIVYYWRARKIRKRDFGPYDDRIGPTFLCFALCVALMMNFKLKFRA
>Gigma_VTC4   VPL---QVPNYYKGRRVAVPVRVEPKVFFANERTFIAWLHFTIINGFALGLLNF-G-SDD--LSNIVAGTFMFVSLMIMLYALGMYLCRVYMIRKRSSGPYEDKFGPAFICGLLFVGVLVNFCFRFWD
>Gigro_VTC4   STS-TRQVPNDYKGRRVAVPVRVEPKVFFANERTFIAWLHFTIIINGFALGLLNF-G-TDD--LSNIVAGTFMFVSLVIMLYALGMYLCRVYMIRKRSSGPYEDKFGPAFICGLLFVGVLVNFCFRFWQ
>Geopy_VTC4   SSSSTSAIPSQFHGKRVAVPVRIEPKVFFANERTFFHWMRFSVLLGSFSLALFNTSGDD-R--VGYMCGFIYAIISVTALIYSLIKYNKRL
>Sacce_VTC4   KGTTFDTQIRAPPGKTICVPVRVEPKVYFATERTYLSWLSISILLGGVSTTLLTY-G---SPT-AMIGSIGFFITSLAVLIRTVMVYAKRVVNIRLKRAVDYEDKIGPGMVSVFLILSILFSFFCNLVA
```

2. Whole sequences of VTC1 and VTC2

```
>Rhiir_VTC2
MKFGSQLRVALYGEWNEYYLDYDGLKKHLKRGEK------KEGGYTEKDESEFVEKLDKELEKIYAFQNSKYEEIKGRVQHCENSVASIS
NVPSMNVPD---RYAEVEREINDITEELNELAKYARLNYTGIMKIIKKHDRRTS--YNLRAMFSVRLNACPF-YKETFEPIIVQLSRLYH
IVHQGLGD--QS-DVRPSTPNFSALSTS---WKPST--SEERALIQTNKYWVHQDNIMEVKTSILRHLPVLVYKPGT------------
----------------------------------------DSSITSIYFDNEVLELYQDKVDRKPGDQIIRLRWYGNKKNTKDIFVER
KIRE---QGEDE--VKERFLIKEKHVNAFLK-GEYAMEKAINKMKEDPSKTDEDIQQFQKLIKDIQDIIKEKNLSPVLRTYYNRMAFQIP
GDQHVRISLDTDFYMVREDNFDN---TRRRGEDEWRRNDID---GDMFSKLPSTECAKFPFAVLEVKLKLDEGEQEPA------------
---WVKELVSSHLVEEAPQFSKYVHGVATVFTS---HAPSLPYWLPNIDKDILKPPNARQSQ--EEEEDYPES--STSHVARPKRTMSGK
NVINVEVVGGRRD--RKNKGKAVD-Y----NIEEARGNEDASLL-EE----EEEEEEDEQQ-RPMGVKTIRKIFQRKKRSGPEEVILPPN
---------ISMPHKIITPVRVEPKVFFANERTFFHWMRFSVLLGSFSLALFNTSGDD-R--VGYMCGFIYAIISVAALIYSLIKYNKRL
TMINNREPGPYDDVLAPPLVCISLVFAIGLNFYLKYNPTKVEGSEDLNNDINTYNNVDTSSFYSEHSKPFVFNMQNV-------------
----------------------------------------------------------------------------------------
>Rhicl_VTC2
MKFGSQLRAALYGEWNEYYLDYDGLKKHLKRCEK------KEGGYTEKDESDFVEKLDKELEKIYAFQNSKYEEIKGRVQHCENAVASIS
NVPSMNVPD---RYAEVEREINDITEELNELAKYARLNYTGIMKIIKKHDRRTS--YILRASFSVRLNACPF-YKETFEPIVVQLSRLYH
IVHQGIGD--QS-DARPPTPNFSALSTS---WKPST--SEERALIQTNKYWVHQDNIMEVKTSILRHLPVLVYKPGT------------
----------------------------------------DSSITSIYFDNEVFELYQDKVDRKPGDQIIRLRWYGNKKNTKDIFVER
KIRE---QGEDE--VKDRFLIKEKHVDAFLK-GEYAMDKTINKMREDPSKTEEDIQQFQKLVKDIQDIIKEKNLSPALRTYYNRMAFQIP
GDQHVRISLDTDFYMIREDNFDI---IRR-GDNEWRRNDID---DDMF-KLPPTECVKFPFAILEVKLKLDEGEQEPA------------
---WIKELVSSHLVEEAPQFSKYVHGVATLFTS---HAPSLPYWLPNIDKDILKPPNARQLQ--EEEEDYPES--STS-APRSKRTMSGK
NIINVEVVGGRRD--RKNKGKAVD-Y----NIEEAGVNENTSLL-EE----EEEEDEDEQQ-RPMGVKTIRKIFQQKKRSGPEEVILPPN
---------VSIPRKIITPVRVEPKVFFANERTFFHWMRFSVLLGTFSLALFNTSGDD-R--IGYMCGFIYAIISVITLIYSLVKYNKRL
TMINNRESGPYDDILAPPLVCISLVLAIGLNFYLKYNPTKVEGREDLNNDINTYNSVDTSSFYSEHSTPSLFNVQNV-------------
----------------------------------------------------------------------------------------
>Rhice_VTC2
MKFGSQLRAALYGEWSEYYLDYDGLKKHLKRGEK------KEGGYTDKDEAEFVERLDKELEKIHAFQNTKYEEIKGRVQHCENAVESIS
NVPSMNIPD---KYAEVEREINDITEELNELARYARLNYTGIMKIIKKHDRRTR--YNLRPMFSVRLNACPF-YKETFEPIVVQLSKLYH
IVHQGLGD--QSIDVRPSTPNFSALTAASPSWKPST--SEERILCQTYKYWVHPDNLMEVKTSILRHLPVLVY-PGT------------
----------------------------------------DSSITSIYFDNELFELYQDKVDRKPGDQIIRLRWYGNKMNNKDIFLER
KIRK---QGEDE--IKDRFLIKEKHVDAFLK-GEYSMDKAIKKMKENPSKTEDDIQQFQTLIKEIQDIIRENRLEPVLRTYYNRMAFQIP
GDQHVRISLDTDFYMIREDNFEN---VHRRRDNEWRRSDID---ENSFDKLPSSESVKFPFAVLEVKLKLDEGEQEPA------------
---WVKELVSSHLVEEAPQFSKYVHGVATLFTS---HAPSLPYWLPNIDKDIIKPPSARQLQ--EEEE-YPESSTSTAHAATRKRTISGK
NIVNVEVVGGRRD--RKNKGKAVD-Y----NIEEVGGNENVSLL-EEGREEEEEEEEDEQQ-KPIGLKTFRKMFQRKKRSAPEAVILPPN
---------VSIPRKIITTVQVEPKVFLANERTFFSWMRFSVMLGTFSLALFNASGDD-R--VGYICGFMYAIISIIVLIYSLVKYNKRL
TMINNRDPGPYDDVLAPPLVCIALFFAVGINFYLKYNPTMVEGNDD-------YNVINISTIY---QKPAVFNIQNV-------------
----------------------------------------------------------------------------------------
>Rhidi_VTC2
MKFGSQLRVALYGEWNEYYLDYDGLKKHLKRGEK------KEGGYTEKDESEFVEKLDKELEKIYAFQNSKYEEIKGRVQHCENSVASIS
NVPSMNVPD---RYAEVEREINDITEELNELAKYARLNYTGIMKIIKKHDRRTS--YNLRAMFSVRLNACPF-YKETFEPIIVQLSRLYH
IVHQGLGD--QS-DVRPSTPNFSALSTS---WKPST--SEERALIQTNKYWVHQDNIMEVKTSILRHLPVLVYKPGT------------
----------------------------------------DSSITSIYFDNEVFELYQDKVDRKPGDQIIRLRWYGNKKNTKDIFVER
KIRE---QGEDE--VKERFLIKEKHVNAFLK-GEYAMEKAINKMKEDPSKTDEDIQQFQKLIKDIQDIIKEKNLSPVLRTYYNRMAFQIP
GDQHVRISLDTDFYMVREDNFDN---TRRRGEDEWRRNDID---GDMFSKLPSTECAKFPFAVLEVKLKLDEGEQEPA------------
---WVKELVSSHLVEEAPQFSKYVHGVATVFTS---HAPSLPYWLPNIDKDILKPPNARQLQ--EEEEDYPES--STSHVARPKRTMSGK
NVINVEVVGGRRD--RKNKGKAVD-Y----NIEEARGNEDASLL-EE----EEEEEEDEQQ-RPMGVKTIRKIFQRKKRSGPEEVILPPN
---------ISMPHKIITPVRVEPKVFFANERTFFHWMRFSVLLGSFSLALFNTSGDD-R--VGYMCGFIYAIISVTALIYSLIKYNKRL
TMINNREPGPYDDVLAPPLVCISLVFAIGLNFYLKYNPTKVEGSEDLNNEINTYNNVDTSSFYSEHSKSFVFNMQNV-------------
----------------------------------------------------------------------------------------
>Divep_VTC2
MKFGSQIKATLHLEWKNYYVDYDGLKKILKQGEN------REGGYTEKDETEFFEKLDKELEKVYTFQNTKYEEIKNRVQKSEKIVESVG
KDRSLNAHQ---IYSDIERQINSITEELNELAKYARLNYTGIIKIIKKHDRRTR--YFLRPMFSVRLNACPF-YKETFEPVIVNLSRLYH
IVHRGLGG---D-EISSIPPNISNIIPL---F-P----SQEKFFRQSRKFWVHPDNVVEVETTILRHLPVLIYKPGS-------------
----------------------------------------DSSVHSIYLDNNSFELYQDKVDRKPGDQLIRLRWYG-KVPANDIYVER
KVR----QEDDE--IKERFAVKEKYTNALLK-GEYSVDKKVKEMKEHPGTTEEEVQNFQTLVKEIQNTIVEKKLQPVLRTYYNRMAFQIP
GDSSVRVSFDTEFYMTREDNFGDSDDSNRRRNDDWRRRDID---DDNFNKLPPSECIKFPYAVLEVKLNLSENEQEPD------------
```

```
---WVQELASSHLVEAAPQFSKYVHGVATLFTS---QAQSLPYWLPNIDKDILKPPTLRQPSDANANEESVASSSSVLITPSLPRNINSE
DNSTTIEVNDSLDMDINKKGKAVV-Y----TSDDEDHDENAPLLGE-----EEREVVIQQQDRPIGLRTFSRIFRKR-RPIPDRETISRI
---------LPLPPKVVGPVQVEPKVYFANERTFFSWLRFCVLLGSLALGLFNSAAADNK--LAIYCAVSYTSISVVVLFYSLFQFKKRN
RMINSLHPGPYDDLIAPAAVCAAIFVAIGLNFYLKLAPKMVEDENHN-----FVIKLNLPE--------------------------
------------------------------------------------------------------------------------------

>Gigma_VTC2
MKFGSQLRAALYVDWAEYYIDYDGLKKLLKRGLK------KEGGYTGKDETEFVEKLDKELEKVYAFQNAKYEEIKSKVQRCEDTANLIS
KDSSSNGKE---RYTEIERQINAITEELNELAKYKRLNYTGIMKIIKKHNRRTK--FDLNPFISVRLKACPF-YKETFEPVVINLSQLYH
IVHQ-------A-DQSSSSLNLPSIPTT---L-P----SQERTLRQSTRYWIHPDNVMEVKTTILRHLPVLIYKPGT-------------
------------------------------------------DASITSLYFDNDAFELYQDKVDRKPGDQLIRLRWYGIKESTREIFVER
KVHE---QGEEE--SKDRFAVKEKYVDDFLK-GNYSMDKAIKKMKENPGKSEDDIKNFQTLIKEIQDTIREKKLQPVLRTYYHRMAFQIP
RDERVRISLDTEFYMIREDNFD----IKRRQEVAWRRTDID---NADFGKLSPSEYTKFPYAILEVKLNLN-GEQEPN------------
---WVKELVKSGLIEEAPQFSKYVHGVATLFTS---QAPSLPYWLPNIDKDILKPSVRQSSE--DYEEDYDEGSSSALYGISQDRSNRGK
NIIDIES-GDRRD-----KGKAVEVYKN--DDDDDQYDETAPLL-E-H---DDDEDIRE-N-KPIGLKTFRKIFRRRTRSRPDRVIIPYN
---------VKEPERVVGSVKVEAKVFFANERTFFSWMKFSILLSTFALALFNASAADNE--LGMRCAIAYTGIGIGCLIYSVYKYNSRL
SMINSKHPGPYDDIFAPIFVCLSLFLASGLNFYLKLHPKLIEGSTG-------ASTTNVTN----------------------------
------------------------------------------------------------------------------------------

>Gigro_VTC2
MKFGSQLRAALYDDWAEYYIDYDGLKKLLKRGLK------NVGGYTGKDETEFVEKLDKELEKVHAFQNAKYEEIKSKVQRCEDTVNLIS
KDSSSNGKE---RYTDIERQINAITEELNELAKYKRLNYTGIMKIIKKHNRRTK--FDLTPFISVRLKACPF-YKETFEPVVINLSQLYH
IVHQGLG----S-DQSSSSLNFSSIPTT---L-P----SQERTLRQSTRYWIHPDNVMEVKTTILRHLPVLIYKPGT-------------
------------------------------------------DASITSLYFDNDAFELYQDKVDRKPGDQLIRLRWYGSKESTREIFVER
KTRL---QGEEE--SKDRFLVKEKYVDDFLK-GTYSMDKAIKKMKENPGKTDDDIKNFQSLVKDIQDTVREKKLQPVLRTYYHRMAFQIP
RDERVRISLDTEFYMIREDNFD----KERRQDVAWRRTDID---NSDFGKLSPSECTKFPYAILEVKLNLD-GEQEPN------------
---WVKELVKSGLIEEAPQFSKYVHGVATLFTS---QAPSLPYWLPNIDKDILKPSVRQSSE--DYDEDYDEGSSSALYGIS---SNRGK
NIIDIES-GDRRD-----KGKAVEVYKN--DDDDDQFDETAPLL-D-H---DDDEDIRE-N-KPIGLKTFRKIFRKRTRSRPDRVIIPYN
---------VKEPERVVGSVKVEAKVFFANERTFFAWMKFSILLSTFALALFNASAADNE--LGMRCAIAYTGIGITCLIYSVYKYNSRL
SMINSKHPGPYDDILAPIFVCLSLFLASGLNFYLKLHPKMIETS-HN------SSTTNASSPNSM------------------------
------------------------------------------------------------------------------------------

>Geopy_VTC2
MKFGSQLEGALYKEWAEYYLDYSGLKKRLKLGEN------QDG-YTEKHESEFVERLDKELEKIYAFQNAKIEEIKDRVHHCENAVASIN
RNSPINVPD---IYAEVESEINSITEELNELAKYARLNYTGIIKIVKKHDRRTR--YMLRPMFNVRLNACPF-YKETYEPIIVQLSKLYH
IVHVGLGYD-QQ-DPKIPPSPANFSLSLSSSWKPPTLLSSQRFLRQNHKFWVHPNNIMEVKTTILRHLPVLIYKAAF------------
------------------------------------------DPSLSTIYLDNQNLELYQDKIDHKGGEQVIRLRWYGSKEVTNEVFIER
KMQR---EGDKE--IKEQFMIKEKYVNQFLN-GNYDMKKTIEKMREIP-KKEEEIKQFENLVSEIQTTILKKKLTPVLRTICNRMAFQIP
GDARCRISLDTDFVSIREDNFNH---IIRRKADEWRRTDIE---DQNLFGKTSSDVSKFPYAILEIKLKLEENEQEPS------------
---WVRELIESHLVEKAPQFSKFVHGVATLFTS---EAPSLPFWLPNVDKDILKTPNDETASNSSTLPMFIPSNGRNSSHNGRRRSSPNK
AMNYVEVIVDK-DNQRKGKGKAVDHRNGHHEDKGEDVNESTPLLGE-H---DDNSVTRF-I-SNIPTLLSKLRNIFYPTSNEPPSNLPPA
---------VHVPQHVETPIRVEPKVYFANERTFFAWMRFSVLLGTFSLALFNAGNDK----IGRSFGLLYSIISLSILLYSLNQFHKRN
DMINSRDPGPYDDLVFPTVVCIALVFAVYAELYFMNIY-----------------------------------------------------
------------------------------------------------------------------------------------------

>Sacce_VTC2
MLFGVKLANEVYPPWKGSYINYEGLKKFLKEDSVKDGSNDKKARWDDSDESKFVEELDKELEKVYGFQLKKYNNLMERLSHLEKQTDTEA
AIKALDADA-------FQRVLEELLSESTELDNFKRLNFTGFAKIVKKHDKLYPKYPSVKSLLEVRLKELPS-HSEEYSPLLYRISFLYN
ILRSNFN-------TASEPLASASKFSS-------IVSNDIDMNFRSFKFWVHNDNLMEVKTRILRHLPVLVYANVPSENDDLVNRFESD
ISNNDEI---VGSSSST-SSV-----EHGLG-------ARSFDPLINTLYFDNEHFELYNDKLLKLNSAPTLRLRWTGQLSDKPDIFLEK
KTLIEDEATGKSEFDLTKLQLKQKFINGFIFEGDKKFKEQTLKKLKESGTAGRDLERLEEDFSEIQNFIIKNELQPVFRTVYTRTAFQIP
GDDKIRVTIDSNIVFIKEDSFDR--ERPIRDPNTWHRTDIDANVANPLKFLRGGEYAKFPYSVMEIKVKSSLDSSMSASSMISNVKLPKK
HGQWLNDLTNSHLVKEIPKFSIFVQGVASLYGDDEK-LDILPFWLPDLETDIRQDPKQAYEE--EKKKLLKQKEIQKKIDGMRRLSNLKE
PQHQAAVPVSQEENERITSQGDLEAD----GSSDEETEQEPHSKRSKKVRRRKPKATFLRILAGRDPKLMGVD--SEEEE----IELPPG
------VKKPLNLLKNAGPVNVEAKVWLANERTFNRWLSVTSLLSVLTFSIYNSVKKAEYPTLANYMAYVYFGLTIFCALWSYSIYMKRV
DIIQQRSGQHLDAPLGPVLVSIVLFVTLVVNFVMAFRNAAKSRQELQIQNLEVPERIPEVLRPLQNYLFKLMGPSSD------------
------------------------------------------------------------------------------------------

>Sacce_VTC3
MLFGIKLANDVYPPWKDSYIDYERLKKLLKESVIHDGRSSVDS-WSERNESDFVEALDKELEKVYTFQISKYNAVLRKLDDLEENTKSAE
KIQKINSEQ-------FKNTLEECLDEAQRLDNFDRLNFTGFIKIVKKHDKLHPNYPSVKSLLQVRLKELPFNNSEEYSPLLYRISYLYE
FLRSNYDH----PNTVSKSLASTSKLS--------HFSNLEDASFKSYKFWVHDDNIMEVKARILRHLPALVYASVPNENDDFVDNLESD
VRVQPEARLNIGSKSNSLSSDGNSNQDVEIGKSKSVIFPQSYDPTITTLYFDNDFFDLYNNRLLKISGAPTLRLRWIGKLLDKPDIFLEK
RTFTENTETGNSSFEEIRLQMKAKFINNFIFKNDPSYKNYLINQLRERGTQKEELEKLSRDFDNIQNFIVEEKLQPVLRATYNRTAFQIP
GDQSIRVTIDSNIMYIREDSLDK--NRPIRNPENWHRDDIDSNIPNPLRFLRAGEYSKFPYSVMEIKVINQDNSQMPN------------
-YEWIKDLTNSHLVNEVPKFSLYLQGVASLFGEDDKYVNILPFWLPDLETDIRKNPQEAYEE--EKKTLQKQKSIHDKLDNMRRLSKISV
PDGKTTERQGQKDQNTRHVIADLEDH----ESSDEETQLPKKSAVKKGKKFKTNAAFLKILAGKNISENGNDPYSDDTDSASSFQLPPG
------VKKPVHLLKNAGPVKVEAKVWLANERTFNRWLSVTTLLSVLTFSIYNSVQKAEFPQLADLLAYVYFFLTLFCGVWAYRTYLKRL
TLIKGRSGKHLDAPVGPILVAVVLIVTLVVNFSVAFKEAAR--RERGLVNVSSQPSLPRTLKPIQDFIFNLVGE----------------
------------------------------------------------------------------------------------------

>Rhiir_VTC4
MKFGHHLKTSLYPEWTFYYLSYDELKRELKTRTR-------GNQWSEEDETIFFELLEKELEKVFTFQDVKSGEINRRIQNCEKEIHDIM
EANSANED----DFLAIEEELSMIIADVHDLAKFTRLNYTGFLKIIKKHDKQTR--WVLKPMFMARLNAKPF-YKENYDALIVKLSRNYD
IVRT-----------RGNPVKGNAAAGG----------QQQNFVRNTTKYWVHPDNITELKLLILKHLPVLVFNPNKE------------
---------------------------------------FEPADSAITSIYFDNDSFDLYLGRLEKSEGAEAIRLRWYG-GMDNNEIFVER
KTHREDWTGEKS--VKARFGIKEKDVNKYLR-GEY--KKTFEKLKQK-GKGDKEIESLEQLASEVQYRVLTKKLRPVVRSFYNRTAFQLP
GDARVRISLDTELSMIREDNFEN--NPRLRSGNNWRRMDIGI--DYPFSKLPDGEIERFPYAILEVKLQTQYGQEPPE------------
---WVQELVQSHLVEAVPKFSKFIHGVATLMDSR--QIPLFPFWLPQMDIDIRKPPS-----------NFRLERPSASNP-----TTPAN
ERGNPFS--GTED--IEVLVDSLEDD----ED-EEDASENTPLLS--ESS-QNTNTQ---LRSTPHISSLEELEEYLATVT--PAGKVPK
---------TYHGKKIAIPVRVEPKVFFANERTFLSWLNFSVVLGGFAIGLLNFG-DK----ITVTAASFLVFVTMMVMLYALGTYLWRV
KKIRKRESGPYEDRYGPTFICIMLLISVTINFWLRLHEKS-------------------------------------------------
------------------------------------------------------------------------------------------

>Rhicl_VTC4
MKFGHHLKTSLYPEWTFYYLAYDDLKRELKTRTR-------GNQWSEEDEVAFVELLEKELDKVFNFQDVKSGEINRRIQHCEKEINDIL
ETNAATED----DYLTIEEELSMIIADVHDLAKFTRLNYTGFLKIIKKHDKQTR--WVLKPMFMVRLNAKPF-YKENYDALIVKLSRSYD
IVRT-----------RGNPVKGNSAAGG----------QQQNFVRNTTKYWVHPDNITELKLLILKHLPVLVFNPNKE------------
---------------------------------------FESADSAITSIYFDNESFDLYLGRLEKSEGAEAIRLRWYG-GMDNNEIFVER
KTHREDWTGEKS--VKARFSIKEKDVNKYLR-GEYNMDKTFDKLKQK-GKSDKEIENLAQLASEVQYRVLTKKLRPAVRSFYNRTAFQLP
GDARVRISLDTELCMIREDNFEN--NPRLRSGNNWRRMDIGI--DYPFSKLPDEEIERFPYAILEVKLQTQYGQEPPV------------
---WVQELVQSHLVEAVPKFSKFIHGVATLMDSR--KIPLFPFWLPQMDIDIRKPPS-----------NFRLERPTASSP-----TTPAN
ERGNPFS--GTEE--IEVLVDSQEDD----EDDEEDTDENTPLLD--RSSGSATSSQ---NTSTPHISSLEQLEEYLATVT--PAGKVPK
---------TYQGKKIAIPVRVEPKVFFANERTFLSWLNFSVTLGAVALGLLNFG-DK----VTVTAAALLTTITMAVMLYALGTYLWRV
RKIRKRESGPYEDRYGPTFVCLLLLISVIVNFMLRLRDYS-------------------------------------------------
------------------------------------------------------------------------------------------

>Rhice_VTC4
MKFGHHLKTSLYPEWTFYYLGYDELKRELKTRIR-------NNQWTDDDETSFVELLENELEKVFTFQTVKSGEINRRIQHCEKEIDD-L
DTNVATEE----DYLAIEEELSMIIADVHDLAKFTRLNYTGFLKIIKKHDKQTK--WVLKPMFMARLNAKPF-YKENYDALIVKLSRLYD
IVRT-----------RGNPVKGNSSAGG----------QQQNFVRNTTKYWVHPDNITELKLLILKHLPVLVFNPNKE------------
---------------------------------------FESADSAISSIYFDNENFELYLGRLEKSEGAEAIRLRWYG-GMDVNEIFVER
KTHREDWTGEKS--VKARFQLKEKEVNKYLR-GQH--NVSFDKMRQK-GASEKEIESLTQLASEVQYRVLTKKLRPVVRTFYNRTAFQLP
GDARVRISLDTELSMIREDNFEN--NPRLRSGDNWRRMDIGI--DYPFSKLLDEEIERFPYAVLEVKLQTQLGQEPPE------------
---WVQELVQSHLVEAVPKFSKFCHGVATLMENR--RIQLLPFWLPQMDIDIRKPPS-----------NFRLQRPSASNP-----TTPAN
ESGNPFS--EIEDDNIEIYVDDQEND----DE---DASERSPLLA--HSSGSASSSQNVQLRGAPHISSLEELEEYLTAIT--PAGKVPK
---------TYNGKRIAVPVRIEPKVFFANERTFLSWLNFTVLVGTIAVGLLNFG-DK----IALTAAIMFTFVTMMVMIYALVNYLLRV
RKIRKRESGPYDDRYGPTILCGILLIAVLVNFWLR-WDYS-------------------------------------------------
------------------------------------------------------------------------------------------

>Rhidi_VTC4
MKFGHHLKTSLYPEWTFYYLSYDELKRELKTRTR-------GNQWSEEDETIFFELLEKELEKVFTFQDVKSGEINRRIQNCEKEIHDIM
EANSANED----DFLAIEEELSMIIADVHDLAKFTRLNYTGFLKIIKKHDKQTR--WVLKPMFMARLNAKPF-YKENYDALIVKLSRNYD
IVRT-----------RGNPVKGNSAAGG----------QQQNFVRNTTKYWVHPDNITELKLLILKHLPVLVFNPNKE------------
-----------------------------------FEPADSAITSIYFDNESFDLYLGRLEKSEGAEAIRLRWYG-GMDNNEIFVER
KTHREDWTGEKS--VKERFGIKEKDVNKYLR-GEY--KKTFEKLKQK-GKSDKEIESLTQLASEVQYRVLSKKLRPVVRSFYNRTAFQLP
GDARVRISLDTELSMIREDNFEN--NPRLRSGNNWRRMDIGI--DYPFSKLPDGEIERFPYAILEVKLQTQYGQEPPE------------
---WVQELVQSHLVEAVPKFSKFIHGVATLMDSR--QIPLFPFWLPQMDIDIRKPPS-----------NFRLERPTASNP-----TTPAN
ERGNPFS--GTED--IEVLVDSLDDD----ED-EEDSSENTPLLS--ESS-QNTNTQ---LRRAPHISSLEELEEYLATVT--PAGKVPK
---------TYHGKKIAIPVRVEPKVFFANERTFLSWLNFSVVLGGFAIGLLNFG-DK----ITVTAASFLVSVTMMVMLYSLGTYLWRV
KKIRRRESGPYEDRYGPTFICILLLISVTINFWLRLHEKS-------------------------------------------------
```

```
--------------------------------------------------------------------------------
>Divep_VTC4
MKFGHHLKTSLYSEWTSHYLAYDGLKSELKIRTR-------GGQWHESDEESFVELLEKDLDKVYTFQKDKSVEINRRIQNCEKEINGIK
DSETTTEE----NFVTLEEELSLIIADVHDLAKFSRLNYTGFLKIIKKHDKQTK--WHLKPQFMVRLNAKPF-YKEDYDALIVKLSRLYD
IVRT-----------RGNPVKGNSAAGG----------QQQNFVRNTSKYWVHPDNITELKLLILKHLPVLVFNPNKE------------
-------------------------------------FEKADSAISSIYYDNEAFELYLGRLEKTEGAEAIRLRWYG-GMDTREIFVER
KTHREDWTGEKS--VKERFPIKEKYVNKYLK-GEHTLEKQLAKMKAK-GKSEKEIEGTRQLSKEVQYRVITKKLQPVIRSFYNRTAFQLP
GDARVRISLDTELSLIREDNFEK--NPRNRCGDNWRRTDIGI--DYPFRQLPDKDIEKFPYAILEVKLQTQYGQEPPQ------------
---WAQELVESHLVEPVPKFSKFIHGVATLIED---KIQLLPFWLPQMGVDIRKPSS-----------SFRLQRPPSSGNLLEVLVDPSS
DTEENANEGTPLTLRNRSRPSNLDED----SDIDESADERTPLIS--------------------RSDADQSENQNTSTSN--TLREVPT
---------TYRGKRIAVPVRVEPKVYFANERTFLTWLNFTVMLSGLAVGLLNFG-DR----IAIIAAGMFTAISMSAMLYSLIVYYWRA
RKIRKRDFGPYDDRIGPTFLCFALCVALMMNFKLKFRAEQQ-----------------------------------------------
--------------------------------------------------------------------------------
>Gigma_VTC4
MKFGHHLKTSLYPEWTIYYVAYDDLKRELKTRIR-------NGQWSDDDEVSFLELLEKELDKVYGFQTSMSKDINKRVQLCEKEVNDVI
NDSEATED----RYLALEEELSLIIADVHDLAKFSRLNYSGFLKIIKKHDKQTN--REIKYTYLSRLNAKPF-FKETYDALIVKLSRLYD
IVRT-----------RGNPVKGNSASGG----------QQQNFVRNTTKYWVHPENITELKLLILKHLPVLVFNPDKQ------------
-------------------------------------FDQADSAISSIYFDNDEFDLYLGRLEKTEGAEAIRLRWYG-GMDVSEIFVER
KTHREDWTGEKS--VKERFQIKEKNVNKYLR-GEHTMADDFKKLRDK-GKSEKEIADLERLANEVQYRVLTKKLHPVLRTFYNRTAFQLP
GDARVRISLDTELTMVREDNYGN--VTR--CGNNWRRMDIGI--DYPFSQLPEEDVERFPYAVLEVKLQTQFGQEPPE------------
---WVQELVRSHLVEAVPKFSKFIHGVSTLVEEN--RVHLLPFWLPQMNVDIHKPPQG----------NYGVQRPLGALD------TPSH
EHNDPMS--SGSSGQEESITVQIDNE----DE----ITEETPLIT------DNDQESSRWLWTTPPTNVLEDETIFASTSTGQVPLQVPN
---------YYKGRRVAVPVRVEPKVFFANERTFIAWLHFTIIINGFALGLLNFGSDD----LSNIVAGTFMFVSLMIMLYALGMYLCRV
YMIRKRSSGPYEDKFGPAFICGLLFVGVLVNFCFRFWDNEQFLSIK-----------------------------------------
--------------------------------------------------------------------------------
>Gigro_VTC4
MKFGHHLKTSLYPEWTIYYLAYDDLKRELKTRIR-------NGQWSDDDEVSFLELLEKELEKVYGFQTSMSKDINRRVQLCEKEIDNVL
QDSEATED----RYLALEEELSLIIADVHDLAKFSRLNYSGFLKIIKKHDKQTN--REIKYTYLSRLNAKPF-FKETYDALIVKLSRLYD
IVRT-----------RGNPVKGNSASGG----------QQQNFVRNTTKYWVHPENITELKLLILKHLPVLVFNPDKQ------------
-------------------------------------FDQADSAISSIYFDNDEFDLYLGRLEKTEGAEAIRLRWYG-GMDVSEIFVER
KTHREDWTGEKS--VKERFQIKEKNVNKYLR-GEHDMADDFKKLRDK-GKSEKEISDLERLANEVQYRVLTKKLHPVLRTFYNRTAFQLP
GDARVRISLDTELTMVREDNFGD--VTR--CGDNWRRMDIGI--DYPFSQLPDEDVERFPYAVLEVKLQTQFGQEPPE------------
---WVQELVRSHLVEAVPKFSKFIHGVSTLVEEN--RIHLLPFWLPQMDVDIQKPPQG----------NYGVQRPLGALD------TPSH
EHNDPMS--SGSSGQEDSITVQIDNE----DE----ITEETPLIT------DNDPESSRWLWTTPPTNVLEDETVFASTST----RQVPN
---------DYKGRRVAVPVRVEPKVFFANERTFIAWLHFTIIINGFALGLLNFGTDD----LSNIVAGTFMFVSLVIMLYALGMYLCRV
YMIRKRSSGPYEDKFGPAFICGLLFVGVLVNFCFRFWQNEQFIPIRIR----------------------------------------
--------------------------------------------------------------------------------
>Geopy_VTC4
MKFGHHLKTSLYPEWTFYYLAYDDLKHELKLRTL-------KREWSEDDEVAFVELLEKELDKVFTFQTMKSGEINRRIQFCEKEITEIT
QSKTAEEE----EFIALEQELSMIIADVHDLAKFTRLNYTGFLKIIKKHDKQTK--WVLKPMYLARLNSKPF-FKENYDALIVKLSRLYD
IVRT-----------RGNPVKGNSAAGG----------QQQNFVRNTRKYWVHQDNITELKLLILQHLPVLVFNPNKE------------
-------------------------------------FEPADSAISSIYFDNEDFELYLGRLEKTEGAEALRLRWYG-DIDERVIFVER
KTHREDWTGEKS--VKARFAIKEKYVNKYLR-GEYTMDKAFEKLKIKKGKGDTEIESLKRLANEVQYTVITKKLKPVLRTFYNRTAFQLP
GDARVRISLDTELTMIREDNFEN--IPNNRSGKNWRRMDIGI--DYPFDKLPQSDISRFPYAVLEVKLQTQSGQDPPQ------------
---WVQELKDSHLVEEVHKFSKFIHGVATLMENH--RIQLLPFWLAQMDVDIRKPPS-----------RFRIQRPGSTISEGN--TTPAL
ETSKRLGDDDYGDGKIEVLVKKTDDE----PN------EGTPLLTSRHSYDRYKSVPSYQAGGGGGGTSSRSALIQDPSSS--STSAIPS
---------QFHGKRVAVPVRIEPKVFFANERTFLSWLNFTVILGGLAVGLLNFG-DK----IGRIAAAMFTTISLMVMIYSLWTYHWRA
QKIRKREPGPYDDRFGPTFLCGILLLAIIINFFLRFEEGVNHAFATRDQPLKPIRTTLLSYTDKNTSYDKSKLFFNYEATVGSVIAVMKK
TIKVSGSESGFKMVVSRKKRKEDVLAEGIDNKKVAAKALSAHSWGSETGDTTESESIDMEKECLVEEISIDYGESGAFIEGDPN
>Sacce_VTC4
MKFGEHLSKSLIRQYSYYYISYDDLKTELEDNLSK-----NNGQWTQELETDFLESLEIELDKVYTFCKVKHSEVFRRVKEVQEQVQHTV
RLLDSNNPPTQLDFEILEEELSDIIADVHDLAKFSRLNYTGFQKIIKKHDKKTG--FILKPVFQVRLDSKPF-FKENYDELVVKISQLYD
IART-----------SGRPIKGDSSAGG----------KQQNFVRQTTKYWVHPDNITELKLIILKHLPVLVFNTNKE------------
-------------------------------------FEREDSAITSIYFDNENLDLYYGRLRKDEGAEAHRLRWYG-GMSTDTIFVER
KTHREDWTGEKS--VKARFALKERHVNDFLK-GKYTVDQVFAKMRKEGKKPMNEIENLEALASEIQYVMLKKKLRPVVRSFYNRTAFQLP
GDARVRISLDTELTMVREDNFDG--VDR--THKNWRRTDIGV--DWPFKQLDDKDICRFPYAVLEVKLQTQLGQEPPE------------
---WVRELVGSHLVEPVPKFSKFIHGVATLLND---KVDSIPFWLPQMDVDIRKPPLP---------TNIEITRPGRSDNEDNDFDEDDE
DDAALVAAMTNAPGNSLDIEESVGYG----ATSAPTSNTNHVVES---ANAAYYQRKIRNAENPISKKYYEIVAFFDHYFNGDQISKIPK
GTTFDTQIRAPPGKTICVPVRVEPKVYFATERTYLSWLSISILLGGVSTTLLTYG-SP----TAMIGSIGFFITSLAVLIRTVMVYAKRV
VNIRLKRAVDYEDKIGPGMVSVFLILSILFSFFCNLVAK-----------------------------------------------
--------------------------------------------------------------------------------
```

2.3. Results

2.3.1. AM Fungal VTCs

AM fungi have homologs of *ScVTC1*, *ScVTC2*, and *ScVTC4*, but not *ScVTC5*, in their genome (**Table 2-1**). *Gigaspora margarita* and *G. rosea* possess two *ScVTC1* homologs, whereas other fungi have only one, and single homologs of *VTC2* and *VTC4* were found in all fungi. The AM fungal VTCs share structural similarities with the ScVTCs. VTC1 consists of a DUF202 domain (IPR003807) with three transmembrane regions, while VTC2 and VTC4 possess an SPX domain (IPR004331) at the N-terminal, a VTC domain (IPR018966) with the catalytic tunnel domain in the middle, and a DUF202 domain at the C-terminal (**Figure 2-1**). Maximum likelihood phylogenetic trees were drawn based on the shared C-terminal sequences, indicating that there are three clades corresponding to VTC1, VTC2, and VTC4 in the fungi (**Figure 2-2**). The tree also suggests that the two homologs of *VTC1* in the two *Gigaspora* spp. likely arose from a gene duplication event after speciation. Transcripts of *VTC1*, *VTC2*, and *VTC4* were detected in both extraradical and intraradical mycelia of *R. irregularis*, and their expression levels were not significantly different between the mycelia, confirming that all three genes were expressed in this fungus (**Figure 2-3**).

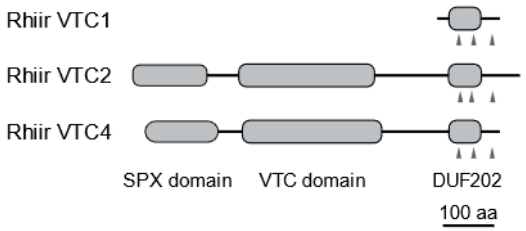

Figure 2-1. Domain structures of VTC1, VTC2, and VCT4 in *Rhizophagus irregularis*. Arrowheads show transmembrane regions predicted by TMHMM search. Scale: 100 amino acids.

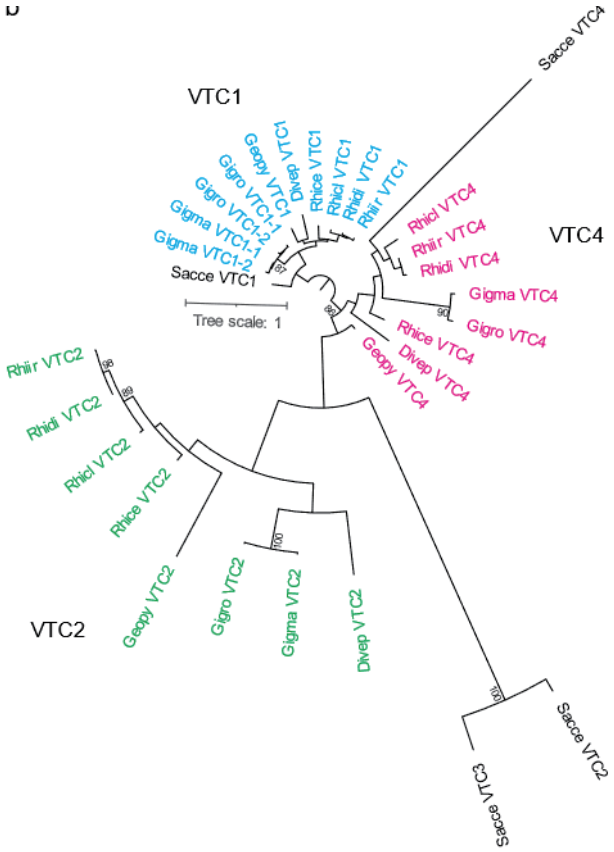

Figure 2-2. Phylogenetic analysis of VTC proteins in arbuscular mycorrhizal fungi. Maximum likelihood tree of C-terminal sequences containing DUF202 domain of VTC1, VTC2, and VTC4 in eight arbuscular mycorrhizal fungi and *Saccharomyces cerevisiae*. Bootstrap values (from 100 replicates) greater than 75% are shown next to the branches. Accession no. of VTC protein sequences used in these analyses were listed in Table 1. Abbreviations of the species names are: Rhice, *Rhizophagus cerebriforme*; Rhicl, *R. clarus*; Rhidi, *R. diaphanus*; Rhiir, *R. irregularis*; Divep, *Diversispora epigaea*; Gigma, *Gigaspora margarita*; Gigro, *G. rosea*; Geopy, *Geosiphon pyriformis*; Sacce, *S. cerevisiae*.

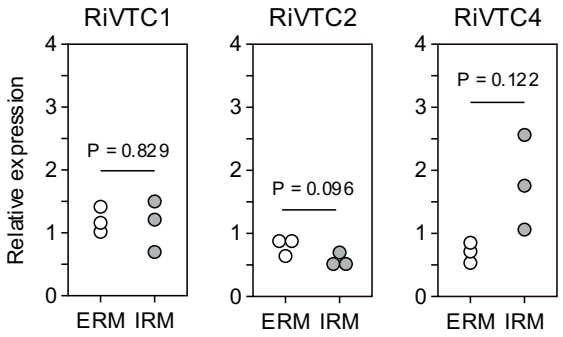

Figure 2-3. Gene expression analysis of *VTC1*, *VTC2*, and *VTC4* in extraradical mycelia (ERM) and intraradical mycelia (IRM). The *Rhizophagus irregularis EF1β* gene was used as an internal control. *P*-values are based on Welch's test (*n* = 3).

2.3.2. Isolation of Recombinant RiVTC4* Protein

To examine the biochemical properties of *R. irregularis* VTC4, we produced recombinant RiVTC4* (RiVTC4$^{183–474}$) containing the catalytic tunnel domain. Initially, we used the bacterial strain ArcticExpress which expresses chaperones at low temperatures to produce soluble RiVCT4* proteins. However, RiVTC4* was strongly bound to the chaperones, which interfered with the analysis of its biochemical properties. A strain lacking the chaperone plasmid was obtained from the ArcticExpress colonies harboring pTrc-HisB-RiVTC4*, resulting in the production of soluble protein with polyP-polymerizing activity. The RiVTC4* protein purified using an Ni^{2+}-charged affinity column showed a single band with SDS-PAGE that had a molecular mass of approximately 38.5 kDa, which is close to the predicted size (**Figure 2-4)**.

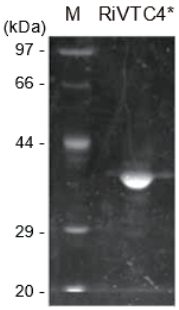

Figure 2-4. SDS-PAGE analysis of purified RiVTC4*. Standards and samples were fractionated by 10% SDS-PAGE. M: size standards.

2.3.3. PolyP-polymerizing Activity of RiVTC4

Pyrophosphate increased the activity of RiVTC4* by up to 5 mM **(Figure 2-5**). Tripolyphosphate slightly stimulated the reaction, but Pi and EXP-S had no effect. The addition of pyrophosphate resulted in the synthesis of short-chain polyP of various sizes below 35-mer within 1 h of incubation, with chain lengths of approximately 30-mer as the most abundant (**Figure 2-6**). The chain length increased with incubation duration (up to 8 h) to 40 – 50-mer with a major size range of approximately 35-mer. Longer polymers (80 – 100-mer) were synthesized in the presence of PP5, indicating the priming effect of short-chain polyP on the polyP-polymerizing activity of RiVTC4* (**Figure 2-6**).

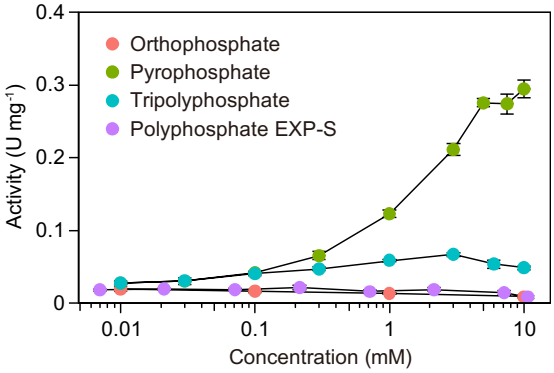

Figure 2-5. Effect of phosphate compounds on the polyP-polymerizing activity. RiVTC4* protein (200 nM) was incubated with 1 mM ATP and various concentrations of orthophosphate, pyrophosphate, tripolyphosphate, and polyP EXP-S for 60 min at pH 6.8. The molar concentration of polyP EXP-S was calculated based on its mean chain length of 14-mer. After stopping the reaction with EDTA, the concentration of ADP was determined. Other experimental conditions were as described in the "Materials and methods" section. One unit (U) is defined as 1 µmol of ADP generated per min; units mg^{-1} of protein gives the specific activity. Mean ± SD, *n* = 3.

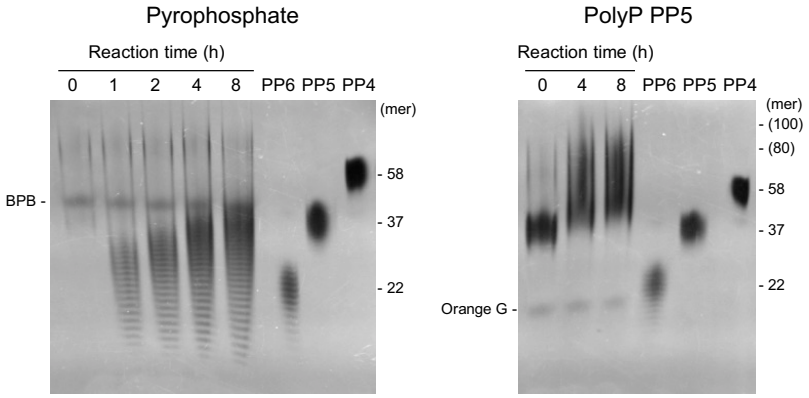

Figure 2-6. Time course of polyP polymerization by RiVTC4*. PolyP was synthesized by incubating 1 µM RiVTC4* with an ATP-regenerating system for the indicated periods. The reaction mixtures contained 1 mM pyrophosphate (left panel) or 0.1 mM (as phosphate) polyP PP5 with a mean chain length of 37-mer (right panel). The reaction mixtures were resolved on 33% polyacrylamide gels. PolyP was visualized with DAPI-negative staining. Numbers on the right side indicate chain lengths of the polyP size markers PP4, PP5, and PP6. Chain lengths in parentheses were estimated from the relative mobility of PP4–PP6 in the gel. BPB and orange G are loading dyes.

RiVTC4* exhibited higher activity in the neutral pH range of 6.5 to 7.5, with optimal activity at pH 6.9 (**Figure 2-7).** The activity was highest in the presence of Mn^{2+} and was completely inhibited by the chelating agent EDTA (**Figure 2-8**). We further investigated ATP (Pi donor)-dependence of the RiVTC4* polyP-polymerizing activity in the absence and presence of pyrophosphate. K_m values for ATP were approximately 300 µM regardless of the presence of pyrophosphate, but the catalytic potency (V_{max} and k_{cat}) of the enzyme was >10 times greater in the presence of pyrophosphate

(**Figure 2-9 and Table 2-2**). However, at 7.5 mM ATP, the activity of RiVTC4* was slightly decreased in the presence of pyrophosphate, suggesting product inhibition by the ADP generated from ATP hydrolysis. Indeed, this activity was inhibited at higher concentrations of ADP (**Figure 2-10).**

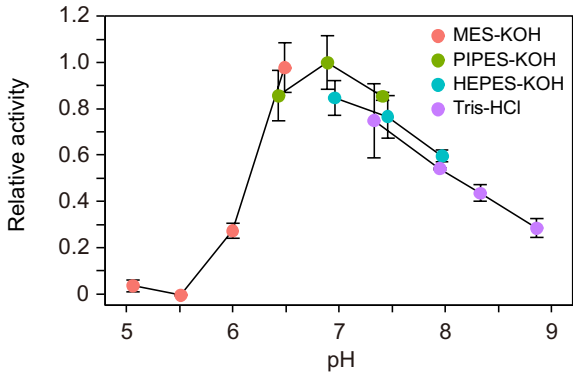

Figure 2-7. Optimum pH of the polyP-polymerizing activity. 1 mM pyrophosphate was included in all cases. Mean ± SD, *n* = 3.

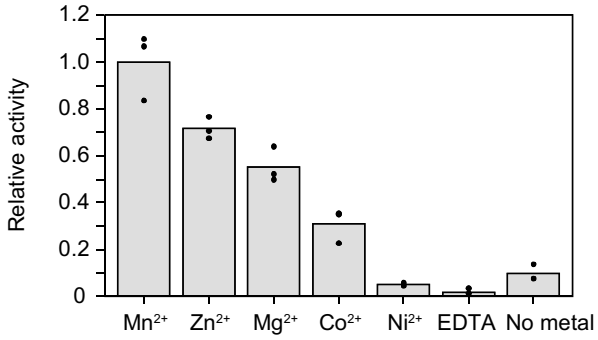

Figure 2-8. Activation of the polyP-polymerizing activity by divalent metals. The final concentration of each metal ion and EDTA was 1 mM. In all cases, 1 mM pyrophosphate was included. Bars and dots show means and data points, respectively.

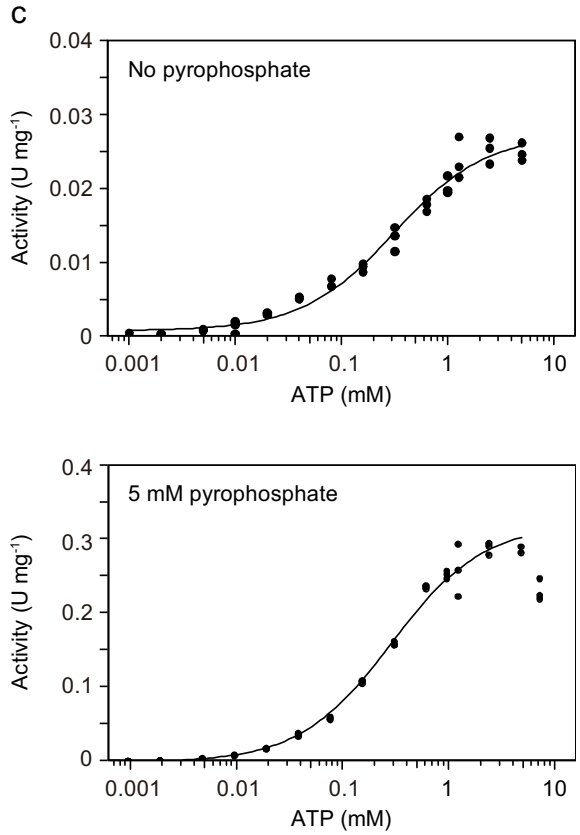

Figure 2-9. ATP dependence of the polyP-polymerizing activity in the presence or absence of pyrophosphate (5 mM). The activity was determined, and data were fitted between 0.001–7.5 mM ATP as indicated in the "Materials and methods" section.

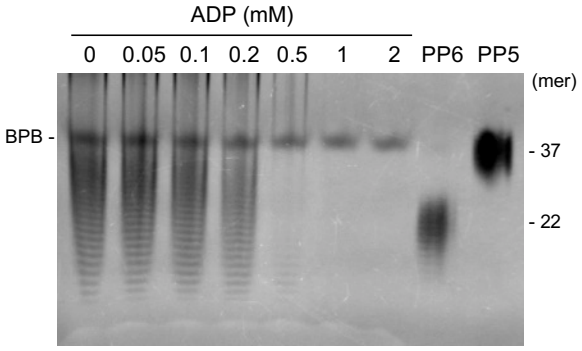

Figure 2-10. Inhibition by ADP to the polyP-polymerizing activity of RiVTC4*. RiVTC4* protein (1 μM) was incubated with various concentrations of ADP in the presence of 1 mM ATP and 1 mM pyrophosphate for 4 h. PolyP generated in the reaction mixture was analyzed by 33% polyacrylamide gels. Numbers on the right indicate the mean chain lengths of the polyP markers PP5 and PP6. BPB is a loading dye.

Table 2-2. K_m, V_{max}, and k_{cat} values of the forward (polyP polymerization) and reverse (ATP generation) reactions of *Rhizophagus irregularis* VTC4*.

Substrate				
Variable conc.	Fixed conc.	K_m (μM)	V_{max} (U mg^{-1})	k_{cat} (s^{-1})
PolyP polymerization				
ATP (0.001–5 mM)	No pyrophosphate	314.4 ± 35.4[†]	0.027 ± 0.001	0.018
ATP (0.001–5 mM)	5 mM pyrophosphate	290.3 ± 20.7	0.320 ± 0.006	0.205
ATP generation				
EXP-S[‡] (0.03–7.1 μM)	5 mM ADP	0.08 ± 0.02	0.048 ± 0.001	0.031
ADP (0.25–7.6 mM)	0.5 mM EXP-S	2,058.6 ± 378.5	0.069 ± 0.004	0.044

[†]Mean ± SE. [‡]Short-chain polyP EXP-S. Concentration as 14-mer polyphosphate.

2.3.4. PolyP-depolymerizing Activity of RiVTC4*

Both EXP-S and EXP-L were gradually depolymerized in the presence of 5 mM ADP and became undetectable by DAPI that visualizes 14-mer and longer polyPs (Smith *et al.*,2018) after 8 h of incubation with RiVTC4* (**Figures 2-11**). In the TLC analysis, the staining intensity of polyP decreased with increasing incubation time, consistent with the PAGE analysis, in which tripolyphosphate appeared after 8 h and then disappeared after 24 h (**Figure 2-12**). Because EXP-S used as a substrate originally contained a small amount of Pi and pyrophosphate, we could not determine whether the reaction newly produced Pi and pyrophosphate. In order to quantify the reverse reaction (the regeneration of ATP from polyP) by RiVTC4*, the amount of ATP produced from ADP and EXP-S was measured.

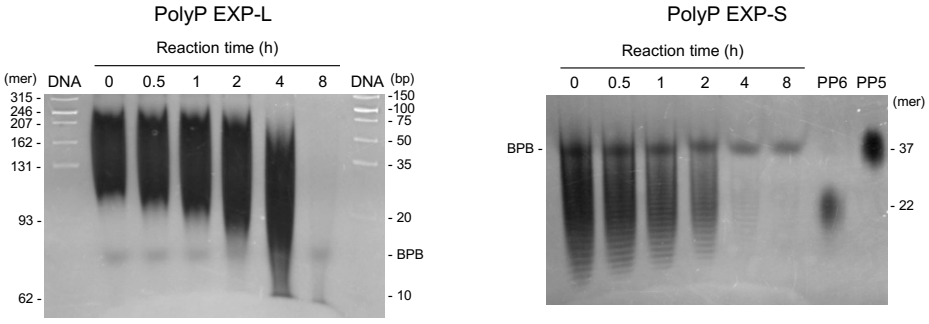

Figure 2-11. Time course of polyP depolymerization by RiVTC4*. Long-chain polyP EXP-L (left panel) and short-chain polyP EXP-S (right panel) were incubated with RiVTC4* in an ADP-regenerating mixture for the indicated periods. The concentration of polyP was 1 mM as phosphate. Other experimental conditions were as described in the "Materials and methods" section. After the reaction, polyP was resolved on 15% (EXP-L) or 33% (EXP-S) polyacrylamide gels, and visualized with DAPI-negative staining. DNA markers (DNA) were also resolved to estimate the chain length of polyP

according to Smith *et al.* (2018) Mean chain lengths of the polyP size markers PP4 and PP5 were shown on the right side of the gels. BPB is a loading dye.

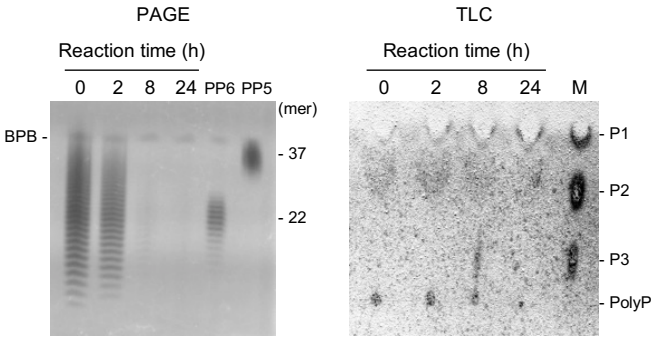

Figure 2-12. Time course of polyP depolymerization by RiVTC4*. Short-chain polyP EXP-S were incubated with RiVTC4* in an ADP-regenerating mixture for the indicated periods. The concentration of polyP was 10 mM as phosphate. Other experimental conditions were as described in the "Materials and methods" section. After the reaction, polyP was resolved on 33% polyacrylamide gels (PAGE), and visualized with DAPI-negative staining. Mean chain lengths of the polyP size markers PP4 and PP5 were shown on the right side of the gels. BPB is a loading dye. Orthophosphate (P1), pyrophosphate (P2), and tripolyphosphate (P3) were separated by thin-layer chromatography (TLC). M: P1–P3 markers.

High activity was observed in the neutral pH range of 7–8 (**Figure 2-13).** The pH profile in the alkaline range, however, could not be properly evaluated because of the very low activity in the HEPES-KOH and Tris-HCl buffer solutions. The enzyme showed the highest activity in the presence of the divalent metal cation Mn^{2+}, which is consistent with the forward (polyP-polymerizing) reaction (**Figure 2-14**). The K_m of EXP-S (in terms of 14-mer polyP) was less than 0.1 µM with a V_{max} of 0.048 U mg^{-1} protein in the presence of 5 mM ADP, whereas that of ADP was 2 mM with a V_{max} of 0.069 U mg^{-1} protein in the presence of 0.5 mM EXP-S (**Figure 2-15** and **Table 2-2**). The apparent turnover rates (k_{cat}) of the reverse reaction were 0.031 and 0.044 which were less than that of the forward reaction with 5 mM pyrophosphate, but two times higher than that without pyrophosphate (**Table 2-2).** Taken together, although the affinity of RiVTC4* for ADP in the reverse reaction is an order of magnitude lower than that for ATP in the forward reaction, the apparent turnover rates of the reverse reaction are within the range of those in the forward reaction, suggesting that the reverse reaction could proceed at certain ATP:ADP ratios in the cell. This issue is further addressed subsequently.

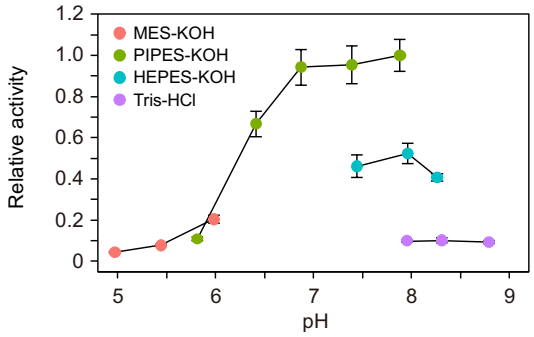

Figure 2-13. Optimum pH of the reverse reaction. RiVTC4* protein (100 nM) was incubated with 5 mM ADP and 1 mM polyP EXP-S at various pH levels. After stopping the reaction by heating, the concentration of ATP generated was determined. Other experimental conditions were as described in the "Materials and methods" section. Mean ± SD, *n* = 6.

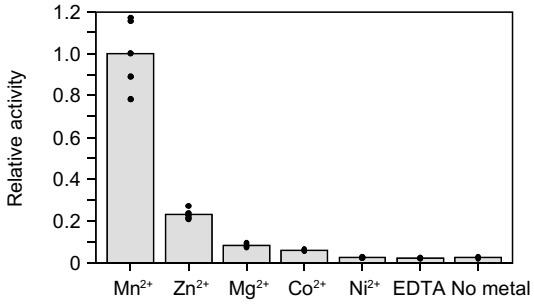

Figure 2-14. Activation of the reverse reaction by divalent metals. The final concentration of each metal ion and EDTA was 1 mM. In all cases, 5 mM ADP and 1 mM polyP EXP-S were included. Bars and dots show means and data points, respectively.

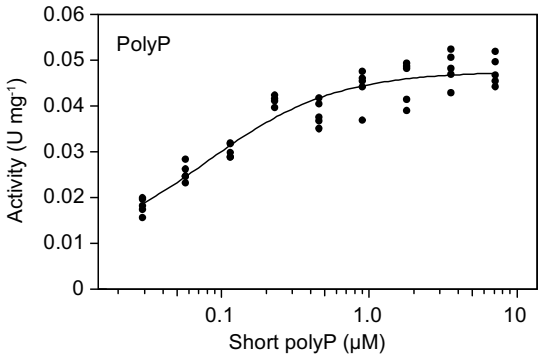

Figure 2-15. PolyP (EXP-S) dependence of the reverse reaction in the presence of 5 mM ADP. One unit (U) is defined as 1 µmol of ATP generated per min; units mg^{-1} of protein denotes the specific activity. The activity was determined, and data were fitted as indicated in the "Materials and methods" section.

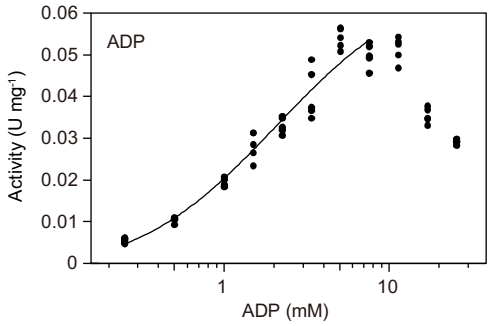

Figure 2-16. ADP dependence of the reverse reaction in the presence of 1 mM polyP EXP-S. Data were fitted between 0.25–7.59 mM ADP.

2.3.5 ATP:ADP ratio drives reaction direction

At 0 and 0.2 mM ADP, no polyP depolymerization was observed, and apparent polyP polymerization, that is, shifts in the chain length distribution of the products from those of the substrate EXP-S to higher molecular weights, were observed in the presence of 1 mM and higher ATP concentrations **(Figure 2-17**). At 1 and 5 mM ADP, polyP polymerization occurred in the presence of 2 mM and higher and 10 mM ATP, respectively, but below these ATP concentrations, polyP depolymerization was observed. These results implied that the direction of the reaction was switched at ATP:ADP ratios of 2:1 – 5:1.

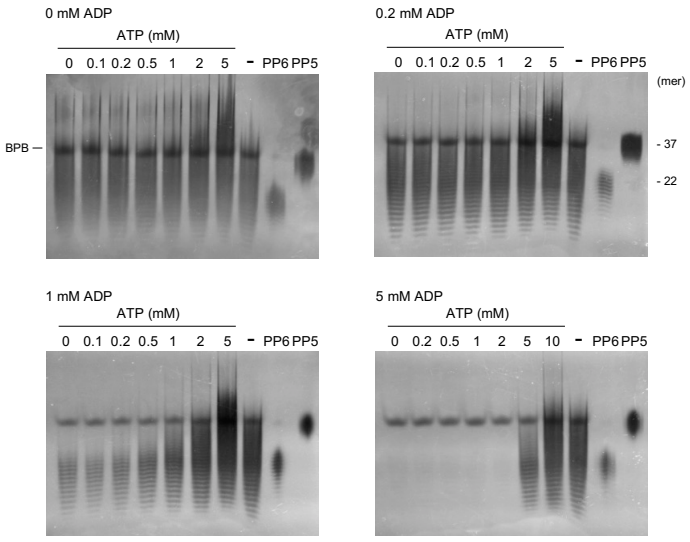

Figure 2-17. Effects of ATP and ADP ratios on polyphosphate (polyP) polymerizing and depolymerizing activity of RiVTC4*. RiVTC4* proteins (1 μM) were incubated with various combinations of ATP and ADP in the presence of 1 mM polyP EXP-S for 4 h. Control experiments without enzyme addition (-) were also performed in parallel. PolyP generated in the reaction mixture and the polyP markers PP5 and PP6 were analyzed by 33% polyacrylamide gels. Numbers on the

right indicate the mean chain lengths of PP5 and PP6. BPB is a loading dye. Representative gels of three independent experiments are shown.

2.4 Discussion

Our experiments demonstrate that the catalytic domain of *R. irregularis* VTC4 is capable of synthesizing polyP using ATP as the phosphoryl donor and also of generating ATP using polyP as the phosphoryl donor; the VTC4 catalyzes both the forward and reverse reactions as the bacterial PPKs (Rao *et al.*, 2009). PolyP is the major form of P storage and translocation in AM fungi (Saito & Ezawa, 2016). PolyP polymerization is prominent in extraradical mycelia (Ezawa *et al.*, 2004; Tani *et al.*, 2009), while depolymerization of polyP is observed in intraradical mycelia (Solaiman *et al.*, 1999; Viereck *et al.*, 2004; Ohtomo & Saito, 2005; Takanishi *et al.*, 2009). Our study suggests the involvement of VTC4 in both polymerization and depolymerization.

As expected, the enzymatic properties of RiVTC4* were similar to those of *S. cerevisiae* VTC4. RiVTC4* is likely to synthesize polyP in a non-processive manner because various chain lengths of polyP were generated during the reaction, which is consistent with ScVTC4 (Hothorn *et al.*, 2009a; Lander *et al.*, 2013), but in contrast to the bacterial PPKs that act in a processive mode (Robinson & Wood, 1986; Ishige *et al.*, 2002; Zhang *et al.*, 2002). The other properties, including the acceleration of the forward reaction by pyrophosphate (i.e., the priming effect), the optimal pH in the neutral range, and the requirement of Mn^{2+} were also in agreement with those of ScVTC4 (Hothorn *et al.*, 2009a; Lander *et al.*, 2013).

We demonstrated for the first time that VTC4 catalyzes the reverse reaction (the regeneration of ATP from polyP) by using AM fungal VTC4. Given that the nucleotide substrate ATP is supplied in the cytosol in the forward reaction in *S. cerevisiae* (Müller *et al.*, 2003; Hothorn *et al.*, 2009a), it is highly likely that the catalytic domain of RiVTC4 also faces the cytosol, which is indirectly supported by our result of an optimum pH between 7 and 8, which is the cytosolic pH range of the fungi (Jolicoeur *et al.*, 1998; Funamoto *et al.*, 2014). Therefore, we consider that the direction of the reactions is dependent on the ATP:ADP concentration ratios in the cytosol. In *S. cerevisiae*, intracellular ATP ranges from submillimolar to millimolar concentrations and is only several-fold higher than that of ADP, and the ATP:ADP ratios vary, mainly depending on the availability of the carbon source (Walther *et al.*, 2010; Ozalp *et al*., 2010;Takaine, Nguyen *et al*., 2019; Takaine *et al*., 2019). Although there is no information about cytosolic ADP levels in AM fungi, ATP levels in the extraradical mycelia of *R. clarus* were estimated to be 10–20 nmol mg^{-1} protein, which was maintained even during polyP accumulation, suggesting that ATP homeostasis is tightly regulated in the mycelia (Kikuchi *et al.*, 2016). Given that the polyP levels in extraradical mycelia are likely to be

dynamically regulated by the balance between synthesis and degradation during translocation (Ezawa *et al.*, 2001), the reverse reaction (i.e., ATP regeneration from polyP) by VTC4 could provide an energetically more favorable mechanism for polyP turnover than simple degradation by hydrolases such as PPN/PPX. The *in vivo* occurrence of the reverse reaction in AM fungi should be investigated in the future.

The absence of the SPX domain in the truncated RiVTC4 (i.e., RiVTC4*) that consists only of the catalytic domain may alter the kinetic parameters. SPX domains occur not only in VTCs but also in Pi transporters and Pi-signaling proteins and act as sensors for the regulation of cellular Pi homeostasis via interaction with transcription factors and inositol polyphosphates (InsPs), through which the function of the SPX-containing proteins is modulated (Wild *et al.*, 2016). In *S. cerevisiae* VTCs, the binding of InsP to the SPX domains enhanced polyP-polymerizing activity and thus polyP accumulation in the vacuoles (Wild *et al.*, 2016; Gerasimaite and Mayer, 2017). Therefore, it is possible that the kinetic parameters estimated using RiVTC4* are likely underestimated compared with those of the native protein in the presence of InsP in vivo. Modulation of the kinetic/enzymatic properties by SPX-InsP interactions should be assessed by different approaches, for example, heterologous expression of intact RiVTC4 in yeast.

Chapter III

Transfer of P at the arbuscular interface –Polyphosphate localization in arbuscules formed in the *ha1-1* mutant–

3.1. Introduction

The molecular mechanisms underlying plant's uptake of Pi released from arbuscules are well documented. Plant Pi transporter genes that are upregulated during AM symbiosis have been identified in many plant species (reviewed in Chiu & Paszkowski, 2019). In particular, the AM-specific transporter genes of the *Medicago truncatula PT4*/*Oryza sativa PT11* clade are conserved in all AM vascular plants (Yang *et al.*, 2012b; Delaux *et al.*, 2015) and are strongly expressed in arbuscule-containing cortical cells (Harrison *et al.*, 2002; Glassop *et al.*, 2005; Nagy *et al.*, 2005; Yang *et al.*, 2012b). Arbuscules are surrounded by host-derived periarbuscular membrane (PAM) (Smith & Smith , 1990; Harrison, 1999; Smith & Smith, 2011) with localized MtPT4/OsPT11 proteins (Harrison *et al.*, 2002; Kobae & Hata, 2010; Pumplin *et al.*, 2012). Mutation of *MtPT4*, *OsPT11*, and their orthologs severely impairs symbiotic Pi uptake, indicating that AM-specific Pi transporters play a central role in the mycorrhizal pathway (Javot *et al.*, 2007; Yang *et al.*, 2012; Xie *et al.*, 2013; William *et al.*, 2013; Watts-Williams *et al.*, 2015). These Pi transporters are classified as H^+/Pi symporters and require H^+ electrochemical potential gradient across the PAM for Pi uptake from an apoplastic interface between the plant and fungus, the periarbuscular space (PAS), into a plant cell. PAS is an acidified compartment (Guttenberger, 2000) in which H^+-ATPase activity has been observed (Marx *et al.*, 1982; Gianinazzi-Pearson *et al.*, 1991). The *Medicago* HA1, rice HA1, and tomato HA8 proteins have been identified as AM-specific H^+-ATPases that are responsible for generating the H^+ gradient across PAS, contributing to symbiotic Pi uptake by AM-specific Pi transporters (Krajinski *et al.*, 2014; Wang *et al.*, 2014; Liu *et al.*, 2020).

P release from AM fungus to PAS in arbuscule-containing cortical cells is a critical step in the mycorrhizal pathway. Mathematical modeling of AM fungus-plant nutrient exchange dynamics predicts that P is exported as Pi by fungal H^+-coupled Pi transporters localized in the plasma membrane of arbuscules (Schott *et al.*, 2016; Dreyer *et al.*, 2018). H^+-coupled Pi transporters expressed in intraradical hyphae have indeed been identified in AM fungi (Balestrini *et al.*, 2007; Fiorilli *et al.*, 2013; Xie *et al.*, 2016a). However, no evidence was found for Pi efflux into the PAS via these transporters. Ezawa & Saito (2018) postulated the involvement of the AM fungal SYG proteins (named after suppressor of yeast gpa1) in P release from arbuscules based on evidence that animal and plant SYG homologs mediate Pi export (Arpat *et al.*, 2012; Giovannini *et al.*, 2013). An alternative

hypothesis is that polyP is directly exported to interfacial apoplasts around arbuscules (Saito & Ezawa, 2016). This hypothesis is supported by the observation that polyP is distributed in the cell walls of germ tubes and extraradical hyphae of AM fungi (Werner *et al.*, 2007; Kuga *et al.*, 2008). However, the precise distribution of polyP in arbuscules remains unclear. In this chapter, the subcellular localization of polyP in arbuscules was determined using 4',6-diamidino-2-phenylindole (DAPI) staining (Tijssen *et al.*, 1982) and by enzyme-affinity labeling with the polyP binding domain (PPBD) of *E. coli* exopolyphosphatase PPX1 (Saito *et al.*, 2005) to elucidate the role of polyP in P transfer at the symbiotic interface. In this analysis, *Lotus japonicus* with an AM-specific H^+-ATPase *HA1* mutation was used to analyze P dynamics in mature arbuscules. *Medicago*, rice, and tomato *ha1* mutants, similar to the *pt4*/*pt11* mutants, show a decrease in mature arbuscules due to degeneration of premature arbuscules (Krajinski *et al.*, 2014; Wang *et al.*, 2014; Liu *et al.*, 2020). However, there is considerable variation in phenotype depending on the plant species and mutant alleles. Here, polyP distribution in the *L. japonicus ha1-1* mutant that shows a relatively mild defect in arbuscule formation was analyzed.

3.2. Materials and Methods

3.2.1. Biological Materials and Growth Conditions

The *L. japonicus* homozygous *ha1-1* mutant line with a *LORE1* insertion in the *HA1* gene (gene ID: LotjaGi3g1v0066100.1 in the Lotus Base Gifu v1.2) and the wild-type segregant were selected from a heterozygous *LORE1* insertion line (plant ID: 30006854) that was obtained from Lotus Base (https://lotus.au.dk/). Genotyping was performed using *HA1*-specific primers (**Table 3-1**) combined with the P2 internal *LORE1* primer (Fukai *et al.*, 2012; Urbański *et al.*, 2012). A two-compartment culture system consisting of root-hyphal (RHC) and hyphal (HC) compartments was used to cultivate plants (**Figure 3-1**). The two-compartments were separated by a three-layered barrier (Kobae *et al.*, 2014) comprising the RHC filter (57 µm opening), a medial mesh (1 mm in thickness; 2 mm opening), and the HC filter (32 µm opening), which prevented plant roots from passing through but allowed AM fungal hyphae to pass through. The compartments were filled with autoclaved river sand (particle size, 0.5–2.0 mm). *L. japonicus* seeds were surface sterilized with a hypochlorite solution, sown on a wetted filter paper in a Petri dish, and germinated at 26°C for two days in dark and three days in light. Seedlings were transplanted to RHC and inoculated with 500 spores of *Rhizophagus irregularis* DAOM 197198 (Mycorise, Premier Tech, Rivière-du-Loup, Canada) per plant. The inoculated and non-inoculated plants were grown in a growth chamber (photoperiod: 16 h, temperature: 26°C, photosynthetic photon flux density: 150 µmol m^{-2} s^{-1}) for four weeks. RHC was supplied with a half-strength Hoagland's solution containing a low concentration of KH_2PO_4 (100 µM) every two days to promote AM colonization. HC was provided with a high-nutrient solution with 500 µM KH_2PO_4 to enhance P translocation from the HC via AM fungal hyphae. The amount of applied fertilizer that did not flow from the HC into the RHC was determined before cultivation.

Table 3-1. Primers used for screening of *LORE1* insertion mutants.

Gene name	Primer sequence (5' 3')	Reference
HA1 (plant ID: 30006854)	TTTCATTGTGGAACTGGACATTTTGA	This study
	TGGTTCACATAGGCTGTCTCAGCA	
P2 primer	ACCTTGTTGCTTCAGCCATGG	Urbanski *et al.* 2012.

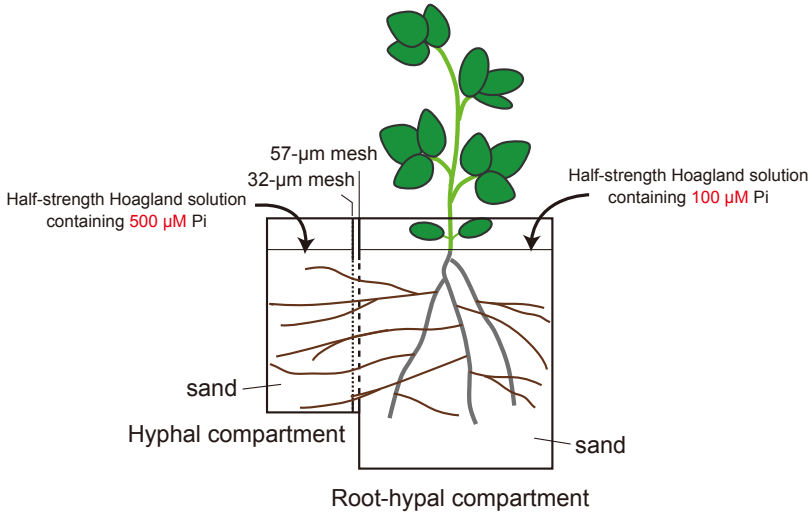

Figure 3-1. The two-compartment system. The root-hyphal (RHC) and hyphal (HC) compartments were separated by nylon meshes, allowing only hyphae of arbuscular mycorrhizal fungi to pass into the HC. The compartments were supplied with a half-strength Hoagland solution containing a low phosphate (Pi) concentration. HC was supplied with a nutrient solution with a high concentration of Pi.

3.2.2. Cryostat Sectioning

Fresh mycorrhizal roots from at least three independent plants were cut into 5–10 mm fragments, placed in plastic molds, and covered with the O.C.T. compound (Sakura Finetek, Tokyo, Japan). The roots were frozen in dry ice-isopentane and stored at −80°C. The frozen roots were sectioned longitudinally at a thickness of 25–30 µm using a cryostat (Leica, Wetzlar, Germany). Cryosections were placed on an adhesive glass slide (Frontier, Matsunami, Osaka, Japan) and dried at room temperature for 60 min. These sections were used for DAPI staining and enzyme cytochemistry of phosphatase activity.

3.2.3. High-Pressure Freezing and Freeze-Substitution

Mycorrhizal roots from at least three independent plants of each genotype were cut into 5-mm fragments using a razor blade in a Petri dish on ice. The root fragments were placed in aluminum specimen carriers with 0.05 M sucrose as a cryoprotectant and then frozen using a Leica EM PACT2 high-pressure freezer. The frozen samples were temporarily maintained in liquid nitrogen and transferred into vials containing 1% glutaraldehyde in anhydrous acetone that was precooled to −80°C. The samples were freeze-substituted at −80°C for 48 h and gradually warmed to 4°C over a period of 21 h using a Leica EM AFS2. Roots were washed twice with anhydrous acetone for 15 min and twice with propylene oxide for 5 min at room temperature. The samples were infiltrated with

Spurr's resin:propylene oxide mixture of ratios 1:2, 1:1, 2:1, 3:1, and 4:1 for 1 h in each mixture sequentially (Spurr's resin from Polysciences, PA, USA). Final soak was thrice in pure resin for 3 h, and samples were polymerized at 70°C for 12 h. The embedded roots were trimmed and sectioned longitudinally using an ultramicrotome. For fluorescence microscopy, semithin sections, approximately 200 nm thick, were cut with a knife (XAC, SYNTEC, Yokohama, Japan) and placed on an adhesive glass slide. For TEM, ultrathin sections of approximately 90 nm thickness were cut with a diamond knife (DiATOME, PA, USA) and picked up on nickel grids. These sections were immediately processed for polyP labeling.

3.2.4. PolyP Detection by DAPI Staining

Cryosections of fresh roots and semithin sections of resin-embedded roots were used for DAPI staining. Cryosections were washed gently with 70% ethanol, 25% ethanol, and distilled water (DW) sequentially for 3 min in each solution. Semi-thin sections were etched with 0.2% sodium ethoxide in ethanol for 5 min and then washed twice with 100% ethanol, 70% ethanol, and 25% ethanol sequentially for 3 min in each solution. Root samples were stained with 80 µg ml^{-1} DAPI in 70% ethanol for 60 min at room temperature in the dark. After washing with 70% ethanol and DW, the sections were mounted in DW and observed within 1 h. Fluorescence microscopy was performed using an Axio Imager D1 microscope (Carl Zeiss, Jena, Germany). DAPI-polyP fluorescence was excited with UV light, and the emitted fluorescence was detected using a long-pass filter, LP420. Digital images were captured with a digital CCD camera (AxioCam MRc5, Carl Zeiss) operated with AxioVision (Carl Zeiss). After randomly selecting images of mature arbuscules, the areas showing the DAPI-polyP signal in the arbuscules were measured using ImageJ software (Schneider *et al.*, 2012).

3.2.5. PolyP Detection by Enzyme Affinity Labeling with PPBD

PolyP labeling using *E. coli* PPBD was performed according to the method described by Saito *et al.* 2005 and Kuga *et al.* 2008 with some modifications. For fluorescence microscopy, semithin sections of the resin-embedded roots were etched with 0.2% sodium ethoxide in ethanol for 5 min and then washed with 0.05% sodium ethoxide followed by 100% ethanol, 50% ethanol, and DW wash. The sections were blocked with 1% bovine serum albumin (BSA) in Tris-buffered saline (TBS) containing low concentrations of salts (TBS-low salt; 25 mM Tris-HCl pH 7.4, 13.7 mM sodium chloride, and 0.27 mM potassium chloride) for 10 min. Sections were first incubated in a mixture of 20 µg ml^{-1} PPBD, 10 µg ml^{-1} mouse anti-Xpress epitope antibody (#R910-25, Thermo Fisher Scientific, MA, USA), TBS-low salt, and 1% BSA for 2 h at room temperature. The sections were then washed with TBS-low salt

buffer containing 0.05% Triton X-100, followed by TBS-low salt. Samples were incubated with a goat anti-mouse IgG antibody conjugated with Alexa Fluor 488 (#A28175, Thermo Fisher Scientific) diluted to ratio 1:100 in TBS-low salt containing 1% BSA for 1 h at room temperature. The sections were washed with TBS-low salt containing 0.05% Triton X-100, followed by TBS-low salt and DW. Alexa Fluor 488 fluorescence was excited with a band-pass filter BP470/40, and the emitted fluorescence was detected with BP525/50 using an epifluorescence microscope Axio Imager D1. Digital images were captured with a digital CCD camera (AxioCam MRm, Carl Zeiss) operated with AxioVision.

For TEM observation, ultrathin sections of the resin-embedded roots were etched with 0.2% sodium ethoxide in ethanol for 5 min. They were then washed with 0.02% sodium ethoxide, followed by 100% ethanol, 50% ethanol, and DW wash. Specimens were blocked with 1% BSA in phosphate-buffered saline (PBS) containing low concentrations of salts (PBS-low salt; 10 mM phosphate buffer pH 8.4, 13.7 mM sodium chloride, and 0.27 mM potassium chloride). They were then incubated in a mixture of 20 μg ml^{-1} PPBD, 10 μg ml^{-1} mouse anti-Xpress epitope antibody, PBS-low salt, and 1% BSA, and washed with PBS-low salt buffer containing 0.05% Triton X-100, followed by PBS-low salt. Samples were incubated with a goat anti-mouse IgG antibody conjugated with 6 nm colloidal gold (#115-195-146, Jackson ImmunoResearch Laboratories, PA, USA) diluted 1:20 in PBS-low salt buffer containing 1% BSA for 1 h at room temperature. The samples were washed with PBS-low salt containing 0.05% Triton X-100, followed by PBS-low salt and DW wash. Specimens were stained with 50% TI-Blue (Nisshin EM, Tokyo, Japan) for 10 min, followed by lead citrate staining for 5 min, and observed using a TEM (JEOL, Tokyo, Japan) at an accelerating voltage of 80 kV. Negative controls were prepared by incubating sections without PPBD. Another negative control was prepared by incubating sections with an excessive competitor (100 mM tripolyphosphate) during the first reaction.

3.2.6. Enzyme Cytochemistry of Phosphatase Activity

Acid or neutral phosphatase activity was detected using TEM with a cerium-based method (Dreyer *et al.*, 2008) with some modifications. Root fragments (5–10 mm) were pre-fixed with 2.5% glutaraldehyde in 100 mM cacodylate buffer (pH 7.0) for 2 h on ice. The fragments were washed twice with cacodylate buffer for 30 min. Roots were further cut into 0.5 mm fragments. The fragments were sequentially incubated in a pre-incubation buffer (2 mM $CeCl_3$ in 100 mM acetate buffer (pH 4.6) and 100 mM Tris-HCl buffer (pH 7.4) for acid and neutral phosphatase activity, respectively) for 1 h, a reaction buffer (1 mM β-glycerophosphate and 2 mM $CeCl_3$ in acetate or Tris-

HCl buffer) for 30 min, a pre-incubation buffer for 15 min, and an acetate or Tris-HCl buffer for 15 min at 37°C. Samples were post-fixed with 1% OsO_4 in cacodylate buffer for 2 h on ice, followed by washing with DW thrice for 5 min. Roots were dehydrated with an ethanol series (20%, 50%, 70%, 90%, and 95% once and 100% thrice) for 20 min each at 4°C and incubated twice with propylene oxide for 5 min at room temperature. The samples were infiltrated with Spurr's resin:propylene oxide (1:2, 1:1, 2:1, 3:1, and 4:1) for 1 h in each step and thrice with pure resin for 3 h, and polymerized at 70°C for 12 h. Ultrathin sections on copper grids were stained with gadolinium acetate (Nakakoshi *et al.*, 2011) and lead citrate and observed using a TEM at an accelerating voltage of 80 kV. Controls were prepared by incubating sections without β-glycerophosphate in the reaction buffer and without 2 mM $CeCl_3$ in the pre-incubation and reaction buffers.

The localization of phosphatase activity was also analyzed by fluorescence microscopy. Cryosections of mycorrhizal roots were fixed with 0.25% glutaraldehyde in PBS (pH 7.4) for 8 min at 4°C. They were then permeabilized by immersion in 25% ethanol in 100 mM acetate buffer (pH 4.6) and 100 mM Tris-HCl buffer (pH 7.4) for several seconds for acid and neutral phosphatase activity, respectively, and washed twice with the same buffer. The sections were incubated with 25 µM ELF97 phosphatase substrate (Thermo Fisher Scientific) in either acetate or Tris-HCl buffer for 30 min at room temperature in the dark and washed with the same buffer without the substrate. Fluorescence of the ELF97 reaction product was excited with UV, and the emitted fluorescence was detected with a long-pass filter, LP420, using an epifluorescence microscope Axio Imager D1 microscope.

For dual labeling of polyP accumulation and phosphatase activity, cryosections of mycorrhizal roots were sequentially washed with 70% ethanol, 25% ethanol, and DW. First, sections were labeled with 80 µg ml^{-1} DAPI in either 100 mM acetate buffer (pH 4.6) or 100 mM Tris-HCl buffer (pH 7.4) for 60 min at room temperature in the dark. The samples were then gently washed in either acetate buffer or Tris-HCl buffer. Subsequently, sections were incubated with 25 µM ELF97 in acetate buffer or Tris-HCl buffer for 30 min at room temperature in the dark. After the second labeling, the sections were mounted in DW, covered with a glass coverslip, and observed within 30 min. The fluorescence of the DAPI-polyP complex and the ELF97 reaction product was excited with UV, and the emitted fluorescence was detected with a long-pass filter, LP420, using the Axio Imager D1 microscope. Digital images were captured using an AxioCam MRc5 operated with AxioVision.

3.2.7. AM Fungal Colonization

Roots were cleared in a 10% (w/v) KOH solution at 90°C for 10 min, acidified with a 2% (v/v) HCl solution for 5 min, and then stained with 0.05% trypan blue in lactic acid at 90°C for 10 min. AM colonization was assessed using the method described by Trouvelot *et al.* (1986) with some modifications. Approximately ten root fragments per plant were mounted on a slide and observed under a light microscope. The intensity of AM fungal colonization and arbuscule abundance in a field of view (diameter: 1.28 mm) was categorized into six and three classes, respectively. AM colonization parameters (F%, M%, m%, A%, and a%) were calculated based on the scores in 100 fields of view. To visualize the fine structure of AM fungal colonization, roots were also stained with wheat germ agglutinin (WGA) conjugated with Oregon Green 488 (Kojima *et al.*, 2014). Fluorescent images of the mycorrhizal roots were captured using an Axio Imager D1 microscope equipped with a digital CCD camera AxioCam MRc5. The length of the major axis of arbuscules was measured with the AxioVision software.

3.2.8. Plant P Analysis

The plants were divided into shoots and roots and dried at 70°C for 48 h and were weighed after cooling in a desiccator. Dried samples were digested with sulfuric acid and hydrogen peroxide at 200°C for 2 h. P concentrations in the samples were determined using the acid-molybdate blue method (Watanabe & Olsen, 1965). The P content was calculated by multiplying each sample's dry weight by their P concentrations.

3.2.9. Gene Expression Analysis

Total RNA was isolated from roots using RNAiso Plus (Takara Bio, Shiga, Japan) combined with Fruit-mate (Takara Bio) according to the manufacturer's instructions. Contaminating genomic DNA was eliminated using a TURBO DNA-*free* kit (Thermo Fisher Scientific). cDNA was synthesized using a ReverTra Ace qPCR RT Kit (Toyobo, Osaka, Japan). Quantitative PCR was conducted using a StepOne Real-Time PCR System (Thermo Fisher Scientific) with a THUNDERBIRD SYBR qPCR Mix (TOYOBO). The primers used for qRT-PCR are listed in Table 3-2. The *L. japonicus* elongation factor 2 (*EF2*) gene and *R. irregularis EF1β* (Kobae *et al.*, 2015) genes were used as internal controls for the expression analysis of plant and AM fungal genes, respectively. Melting curve analysis confirmed the presence of single peaks. Relative expression levels were calculated using the $2^{-\Delta Ct}$ method (Schmittgen & Livak, 2008). All the reactions were performed using three biological replicates. RT-PCR was performed using *HA1*-specific primers (**Table 3-2**) and 10 ng of cDNA template to confirm

homozygous *LORE1* insertion lines at the transcript level, and the amplified products were sequenced.

Table 3-2. Primers used for gene expression analysis.

Gene name	Primer sequence (5' 3')	Reference
Lotus japonicus		
EF2	GGTGGCTGCTGCTGGAATTA	This study
	ACGGGTATCAGTCATACGGACAT	
PT1	TGCCGGCCGAGATTTTC	This study
	GCAGCTGAGATTCCATGACAAG	
PT2	GGGCCTAATGCCACCACAT	This study
	CGGAATCTAGCCGGGAAAA	
PT3	CCTCACGCGGAGGAAATG	This study
	GTTGATGCTCTTGCAACCTTGTA	
PT4	TCCGGGCTCTCCTTTGG	Kojima *et al.* 2014.
	AGAAGCATAGCGTTCCCATCA	
AMT2;2	ACACATGCTTGCACTGCTACC	Guether *et al.* 2009.
	CTGCCCATCCTTGAACAACCC	
RAM2	GCCCGTAGCCATGGTGAA	This study
	CCCTCTTGCAGTGGTTCCA	
Rhizophagus irregularis		
EF1β	CCCATGCAGCTCGATGGTA	Kobae *et al.* 2015.
	TGCCAGGAAGTGAAGAAAATGA	
VTC1	GAGAATCAGGTCCTTATGATGATAGGT	This study
	CACCCACGAGGAAAAAGCA	
VTC2	GCACGACAGACGTACAAGTTACAA	This study
	AATGGGCACGCGTTCAAA	
VTC4	CATGGTGTCGCAACACTTATGG	This study
	GTGGAAGCCAGAAAGGAAAAAG	
PPN1	GAAAGATTTAACAATACCGAGTTGGAT	This study
	TGCGCTATTAAGTCCATCATTAACA	
PPN2	TCGACCACCTAATGCTTTTGG	This study
	ATCGCAATTATATTCTCCCCATTTT	
PPN3	CCGAATAGTGACCCATCCAAA	This study
	CATTCCGATTGTGGAGTTCCA	

3.2.10. Statistical analyses

All statistical analyses were performed using the software R (version 4.0.0). The mycorrhizal colonization rate and relative gene expression values were logit-transformed (ln[p/1−p]) and log-transformed, respectively, to avoid violating normality and homoscedasticity assumptions. To test the differences in mycorrhizal colonization and gene expression between wild-type and *ha1-1* mutants, data were analyzed using the Student's *t*-test. Tukey's HSD test was performed for multiple

comparisons of P contents of plants. Relative frequency densities of arbuscule size and the percentage of arbuscule area showing DAPI-polyP signal were calculated using the MASS package in the software. The size distributions of wild-type and *ha1-1* mutants were compared using a two-sample Kolmogorov–Smirnov test. The proportion of mature and collapsed arbuscules in wild-type and *ha1-1* was analyzed using Fisher's exact test.

3.3. Results

3.3.1. AM Phenotype of the *ha1-1* Mutant in *L. japonicus*

First, the effect of the mutation of *HA1* on the P acquisition through mycorrhizal pathway was investigated. The *L. japonicus HA1* gene was highly expressed in roots colonized by *R. irregularis* **(Figure 3-2**), as seen in a previous study (Xue *et al.*, 2018). A *L. japonicus* homozygous line carrying a *LORE1* insertion in exon 8 of the *HA1* gene was selected to obtain a *ha1* mutant, *ha1-1* (**Figure 3-3a**). RT-PCR analysis revealed that although *HA1* transcripts were observed in AM roots of the *ha1-1* mutant (**Figure 3-3b**), they had indels caused by putative abnormal splicing that created a frameshift and a premature stop codon 13 amino acids after the insertion (**Figure 3-3c**).

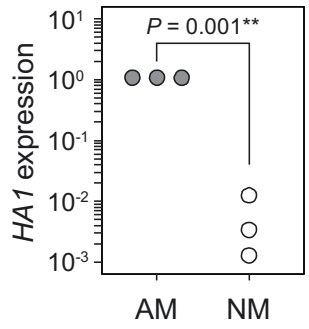

Figure 3-2. Gene expression of *HA1* in roots. *Lotus japonicus* B-129 "Gifu" was inoculated with *Rhizophagus irregularis* and grown for four weeks. Expression levels of the *HA1* gene in arbuscular mycorrhizal (AM) and non-mycorrhizal (NM) roots were normalized based on the amount of the *L. japonicus* elongation factor *EF2*. The *P*-value is based on Student's *t*-tests (**, $P < 0.01$; $n = 3$).

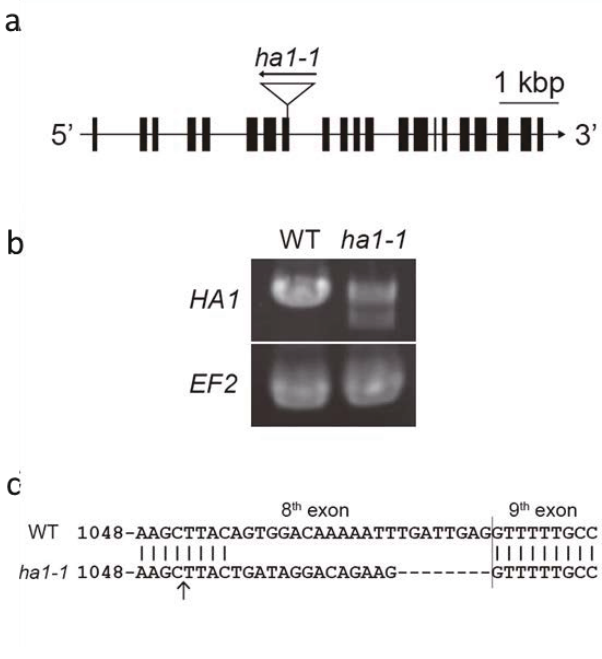

Figure 3-3. The *ha1-1* mutant. (a) Exon-intron structure of the *HA1* gene, including the *ha1-1 LORE1* insertion site. (b) RT-PCR analysis of *HA1* in wild-type (WT) and *ha1-1* arbuscular mycorrhizal roots.

The *EF2* gene was amplified as the loading control. PCR was performed using 10 ng of cDNA as a template with 35 cycles. (c) Sequence comparison between WT and the *ha1-1 HA1* cDNAs showing frameshift indels in the *ha1-1* mutant transcript. The arrow indicates the *LORE1* insertion site.

To determine whether *HA1* mutation affects P acquisition via the mycorrhizal pathway, the growth and P nutrition of the *ha1-1* mutant was examined using a two-compartment system consisting of RHC and HC (**Figure 3-1**). RHC and HC were supplied with low and high concentrations of Pi for four weeks, respectively; this setup avoided the inhibition of AM colonization and reinforced the mycorrhizal pathway. Under uninoculated conditions, plant growth and P nutrition did not differ between wild type and *ha1-1* (**Figure 3-4a-c**). In the presence of AM fungi, shoot biomass, P concentration, and P content increased in both genotypes. However, the positive effects on shoot biomass and shoot P content were lower in the *ha1-1* mutant (average increases of 188% and 268% in shoot biomass and shoot P content, respectively) than in the wild type (average increases of 300% and 492% in shoot biomass and shoot P content, respectively). In contrast, P concentration was higher in mutant roots (**Figure 3-4b**), implying that P flow from *R. irregularis* to the host was stacked in the roots. Together, these data demonstrate that P transfer from the AM fungus to the host via the mycorrhizal pathway was partially impaired in the *ha1-1* mutant.

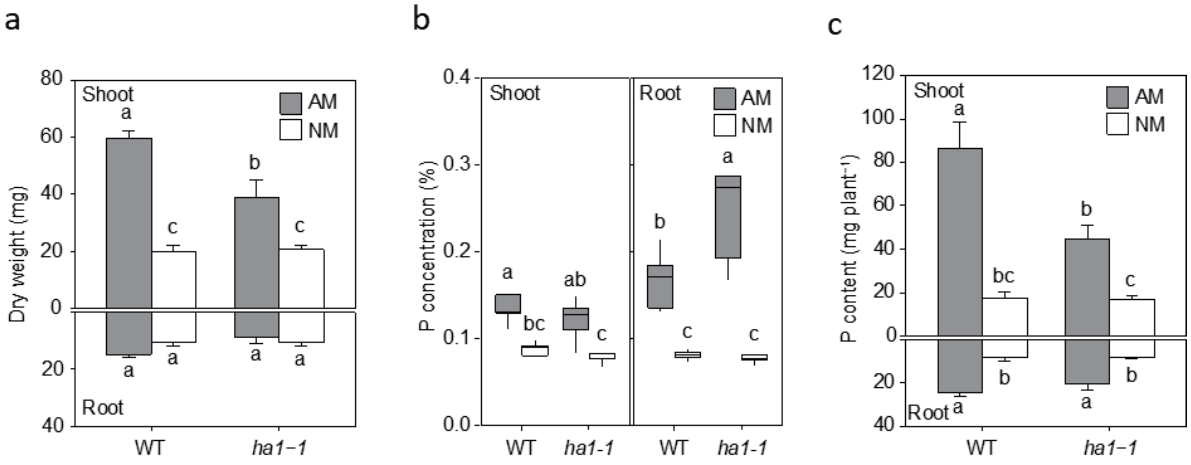

Figure 3-4. Phenotype of the *ha1-1* mutant cultivated in the two-compartment system. Dry weight (a), P concentration (b), and P content (c) in arbuscular mycorrhizal (AM) and non-mycorrhizal (NM) shoots and roots four weeks after inoculation. For each plant part, bars or boxes topped by the same letter do not differ significantly at $P < 0.05$ on Tukey's multiple comparisons test. Error bars in (a) and (c) show SE ($n = 5$). The boxes in (b) show the first quartile, the median, and the third quartile; the whiskers reach 1.5 times the interquartile range ($n = 5$).

3.3.2. AM Fungal Structures in the *ha1-1* Mutant

To examine the effects of *ha1-1* on hyphal development within roots, AM fungal colonization was assessed by staining mycorrhizal roots with trypan blue or WGA–Oregon Green 488. Microscopic

examination showed that both mutant and wild-type roots were heavily colonized by *R. irregularis* and had similar colonization patterns (**Figure 3-5**). However, quantitative analysis revealed that arbuscule densities (A% and a%) were moderately reduced in the mutant relative to wild type four weeks post-inoculation (**Figure 3-6**). Moreover, the distribution of arbuscules formed in *ha1-1* mutant roots shifted towards smaller sizes compared to wild-type roots (**Figure 3-7**). However, the range of arbuscule sizes almost overlapped between the two genotypes. Septa formed in branches of fully developed arbuscules in *ha1-1* cortical cells were sometimes observed (**Figure 3-5**). These results suggest that the *HA1* mutation induced a phase transition of the arbuscule life cycle from the mature to the degrading stage.

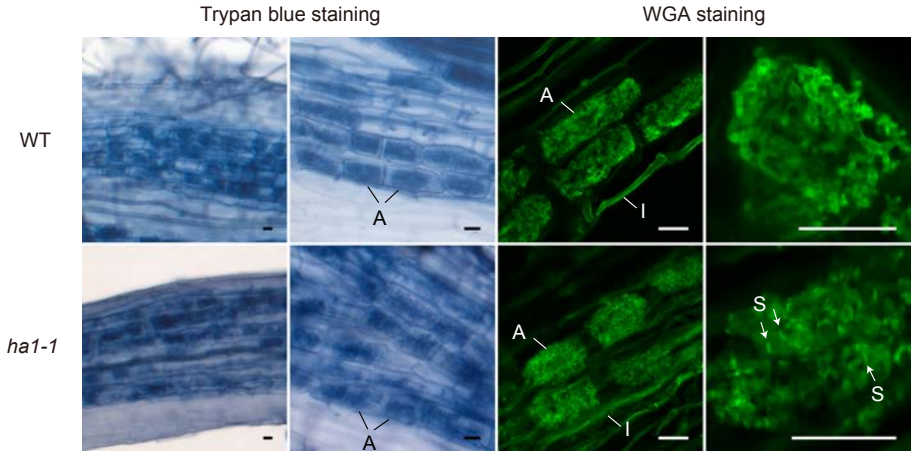

Figure 3-5. Arbuscular mycorrhizal colonization in wild-type (WT) and *ha1-1* roots. Fungal structures of *Rhizophagus irregularis* colonizing *Lotus japonicus* roots stained with trypan blue or wheat germ agglutinin (WGA) conjugated with Oregon Green 488. Optical sections of WGA-stained samples were captured using a confocal laser scanning microscope. Septa (S) were sometimes observed in fine branches of arbuscules formed in the *ha1-1* mutant. A: arbuscule, IH: intraradical hypha. Bar = 20 µm.

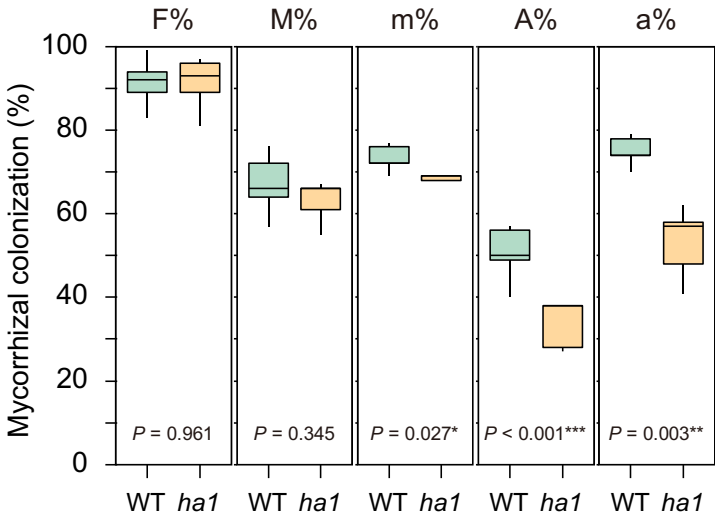

Figure 3-6. Arbuscular mycorrhizal fungal colonization in *Lotus japonicus* wild-type (WT) and *ha1-1* roots cultivated in the two-compartment system four weeks after inoculation of *Rhizophagus irregularis*. The root-hyphal and hyphal compartments were supplied with low and high phosphate concentrations, respectively. Mycorrhizal colonization was assessed according to Trouvelot *et al.* (1986) after trypan blue staining. F%, frequency of mycorrhiza in the root system; M%, intensity of mycorrhizal colonization in the root system; m%, intensity of mycorrhizal colonization in the root fragments; A%, arbuscule abundance in the root system; a%, arbuscule abundance in mycorrhizal parts of root fragments. The boxes show the first quartile, the median, and the third quartile; the whiskers reach 1.5 times the interquartile range (n = 5). P-values are based on Student's t-tests (*, P < 0.05; **, P < 0.01; ***, P < 0.001).

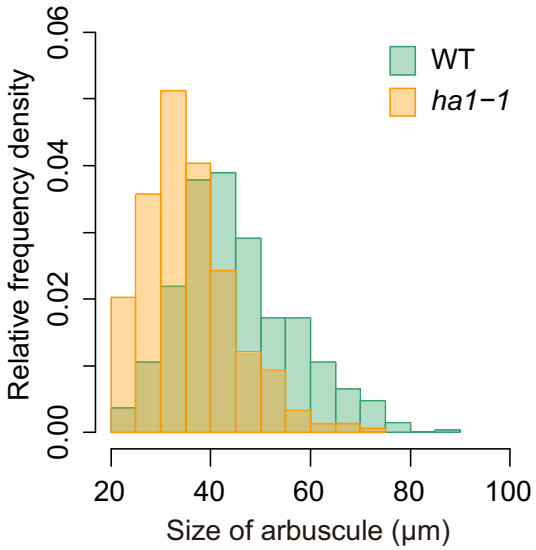

Figure 3-7. Relative frequency density of arbuscule size of *Rhizophagus irregularis* colonizing in *Lotus japonicus*. The lengths of the major axis of 549 wild-type (WT) and 297 *ha1-1* arbuscules randomly selected from >20 μm-long arbuscules stained with wheat germ agglutinin conjugated with Oregon Green 488 were measured. According to the two-sample Kolmogorov-Smirnov test, the size distribution was significantly different between the plant genotypes (P < 0.001).

3.3.3. PolyP Localization in Arbuscules –DAPI Staining–

PolyP accumulation in arbuscules was analyzed by DAPI staining. Once DAPI binds to polyP, the complex emits yellow fluorescence under UV irradiation (Tijssen *et al.*, 1982). Mycorrhizal root cryosections were DAPI-stained after polyP fixation and cell permeabilization with ethanol. Arrays of fully-developed arbuscules (mature arbuscules) and the patchy colonization of degenerating arbuscules which are small arbuscules with shrunken fine branches were observed (**Figure 3-8**). In most mature arbuscules formed in cortical cells, the fluorescent DAPI-polyP complex signal was confined to the central region, irrespective of the plant's genotype. The other region within the arbuscules, containing fine branches, exhibited non-specific blue fluorescence. In contrast, the entire hyphae of the degenerating arbuscules were stained with DAPI and fluoresced yellow. This type of

arbuscules accounted for 57% of the total arbuscules formed in *ha1-1* mutants, which was 1.4-fold higher than that in the wild-type (**Figure 3-9**). This result prompted to examine whether the shift in size distribution towards small arbuscules in the mutant, as observed by WGA staining was due to the increased number of degenerating arbuscules. The size of mature and degenerating arbuscules distinguished by the DAPI staining pattern was measured. Overall, WGA staining reduced arbuscule size relative to DAPI, possibly due to cell shrinkage caused by fixation with Farmer's solution which contained ethanol and acetic acid (**Figure 3-7** and **Figure 3-10**). In both arbuscule types, the size distribution almost overlapped between the wild-type and the *ha1-1* mutant, but the median length was 5–8 µm shorter in the mutant (**Figure 3-10**). The DAPI staining data also suggested that *HA1* mutations caused early arbuscule degeneration.

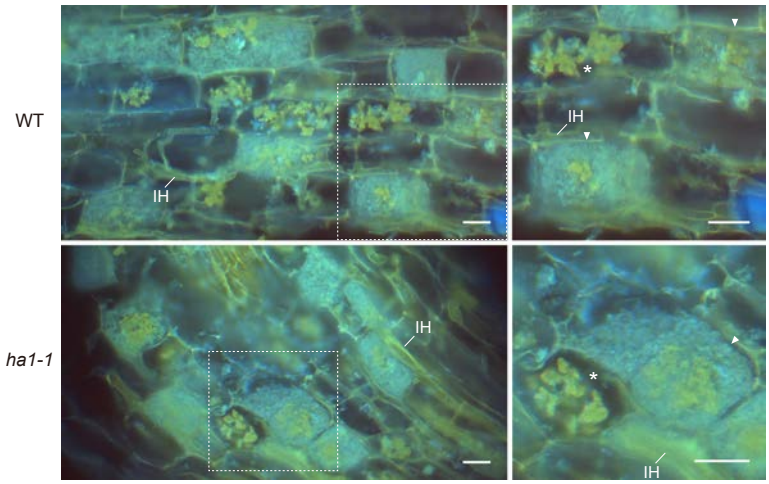

Figure 3-8. Mature and degenerating arbuscules stained with DAPI. DAPI staining of arbuscules in wild-type (WT) and *ha1-1* roots of *Lotus japonicus*. Mycorrhizal roots were harvested four weeks after inoculation with *Rhizophagus irregularis*. Cryosections of fresh roots were stained with DAPI and observed using an epifluorescence microscope. The DAPI-polyP complex emits yellow fluorescence under UV irradiation. Blue fluorescence suggests non-specific DNA binding to fungal hyphae. Right panels show the magnified images of dotted areas in the left panels. Mature arbuscules (arrowheads) and degenerating arbuscules (asterisks) are visible. IH: intraradical hypha. Scale bar = 20 µm.

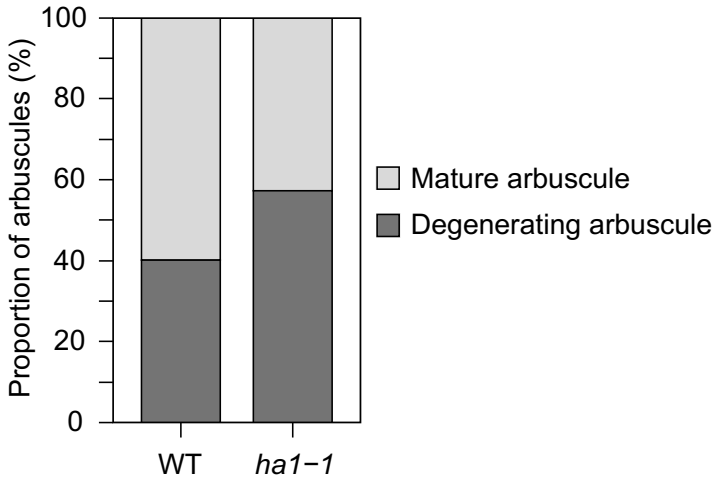

Figure 3-9. Proportion of mature and degenerating arbuscules of *Rhizophagus irregularis* in *Lotus japonicus* wild-type (WT) and the *ha1-1* mutant. Small, shrunk arbuscules that entirely show intense yellow fluorescence by DAPI staining were considered as degenerating arbuscules. Mature arbuscules fully occupy plant cortical cells. The proportion was significantly different based on Fisher's exact test ($P < 0.001$, $n = 499$ and 562 in WT and *ha1-1*, respectively).

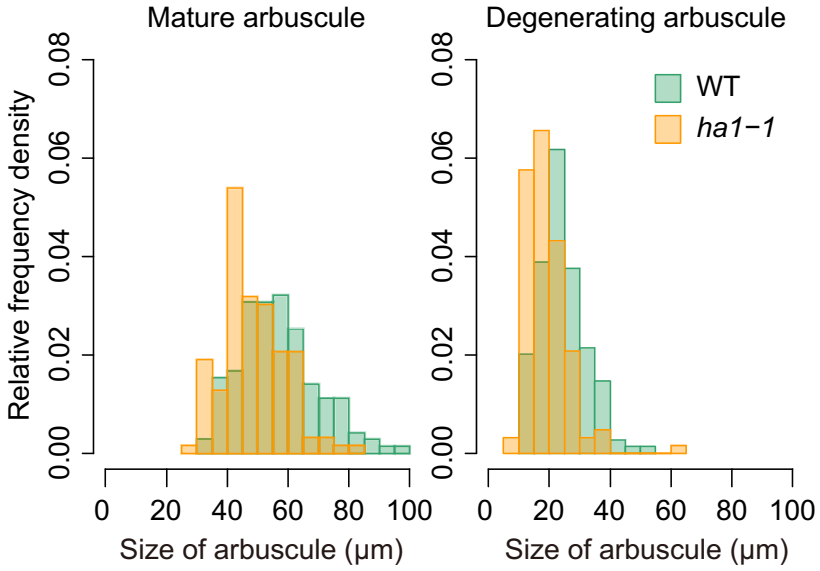

Figure 3-10. Relative frequency density of the size of mature and degenerating arbuscules of *Rhizophagus irregularis* formed in *Lotus japonicus* wild-type (WT) and *ha1-1*. The lengths of the major axis of arbuscules stained with DAPI were measured. The size distribution was significantly different between the plant genotypes according to the two-sample Kolmogorov-Smirnov test in each arbuscule type ($P < 0.001$). Mature arbuscule: $n = 143$ and 146; degenerating arbuscule: $n = 149$ and 125 in WT and *ha1-1*, respectively.

Next, the distribution of polyP in mature arbuscules was analyzed. It should be noted that the size of the DAPI-stained region in the arbuscules varied (**Figure 3-11**). Quantitative analysis revealed that the distribution of the yellow fluorescent area relative to the entire mature arbuscule

significantly differed between the wild-type and *ha1-1* (**Figure 3-12**). In the wild-type, the most abundant size class was 0%–5%; arbuscules with large DAPI-stained regions were infrequent. In contrast, the size distribution in the *ha1-1* mutant peaked at 10%–15% with a higher right tail than the wild-type, indicating an expansion of the DAPI-polyP positive region.

To obtain more precise polyP localization in mature arbuscules, semi-thin sections of resin-embedded AM roots were analyzed. Arbuscules develop with repeated branching and narrowing of hyphal diameter from a thick trunk hypha to fine branches. Here, we define the fine branch module as a set of connected branches (**Figure 3-13**). For arbuscules generated in wild-type roots, yellow fluorescence was detected in some fine branch modules located in the vicinity of the trunk hyphae (**Figure 3-14**). The fluorescent signal was also visible around the periphery of the trunk hyphae where the cell wall was localized, but not inside these hyphae. Similarly, the *ha1-1* mutant displayed DAPI-polyP signals in fine branch modules in the central region of the arbuscule and cell walls of the trunk hyphae.

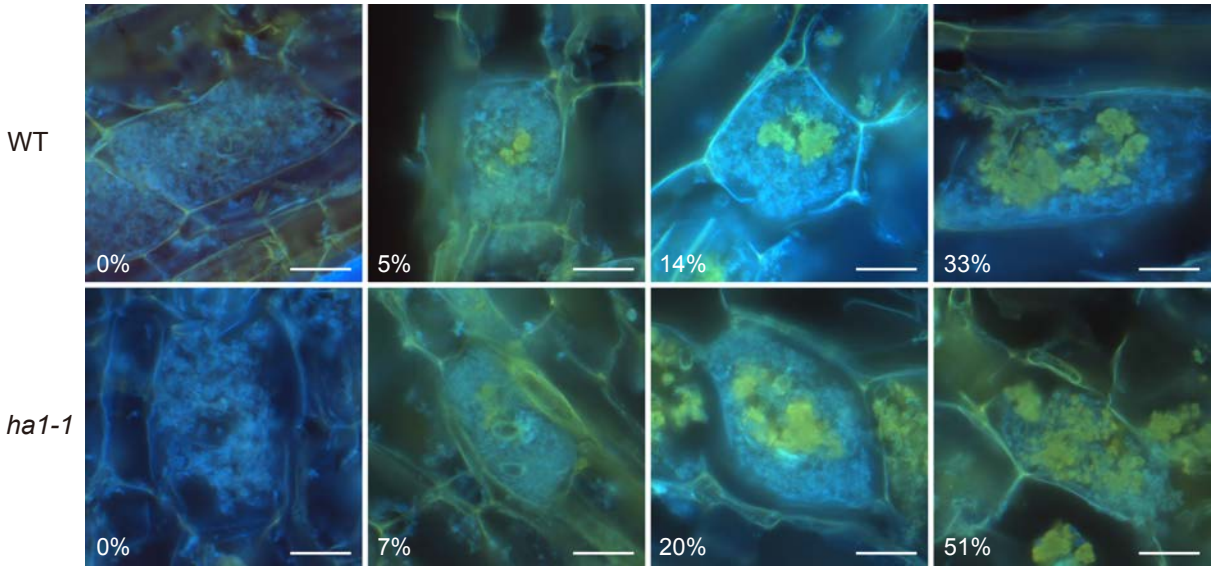

Figure 3-11. Localization of polyphosphate (polyP) by DAPI staining. Representative types of mature arbuscules stained with DAPI. Mycorrhizal roots of *Lotus japonicus* were harvested four weeks after inoculation with *Rhizophagus irregularis*. Yellow fluorescence is observed in the central part of arbuscules. Percentages of arbuscule area showing yellow fluorescence signals are shown. Scale bars = 20 µm.

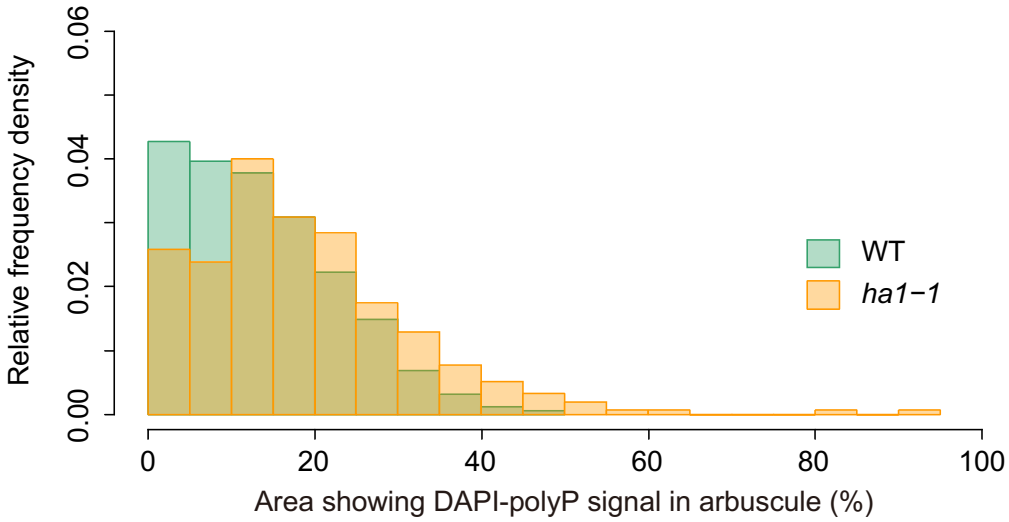

Figure 3-12. Relative frequency density of the area showing DAPI-polyphosphate signal. The percentage of arbuscule area with signal was calculated. In total, 323 and 310 mature arbuscules were measured for *Lotus japonicus* wild-type (WT) and *ha1-1*, respectively. According to the two-sample Kolmogorov–Smirnov test, the size distribution was significantly different between the plant genotypes ($P < 0.001$).

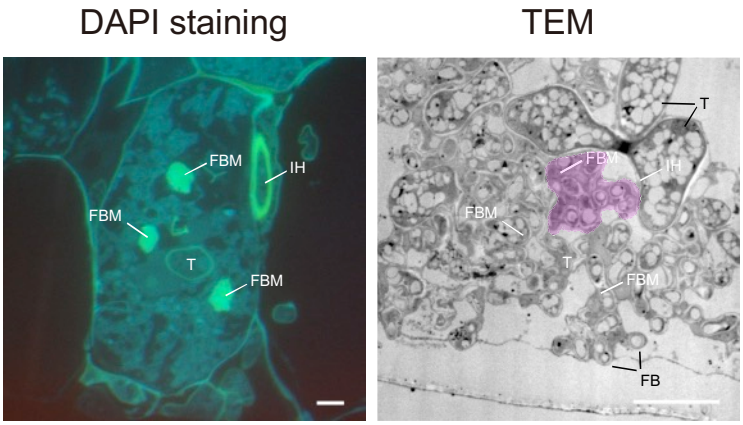

Figure 3-13. Fine branch modules in arbuscules of *Rhizophagus irregularis*. Semithin sections of mature arbuscules in resin-embedded wild-type roots of *Lotus japonicus* were stained with DAPI and observed using an epifluorescence microscope (left panel). Strong yellow fluorescence was observed in several fine branch modules, a set of connected fine branches. A transmission electron microscopy (TEM) micrograph of fine branches and trunk hyphae of an arbuscule colonized in a wild-type cortical cell (right panel). Acid phosphatase activity was detected by electron microscopic enzyme cytochemistry as black precipitates of the reaction product (cerium phosphate). The region colored in magenta is a putative FBM in which fine branches form a cluster. FB: fine branch, FBM: fine branch module, IH: intraradical hypha, T: trunk hypha. Scale bars = 5 µm.

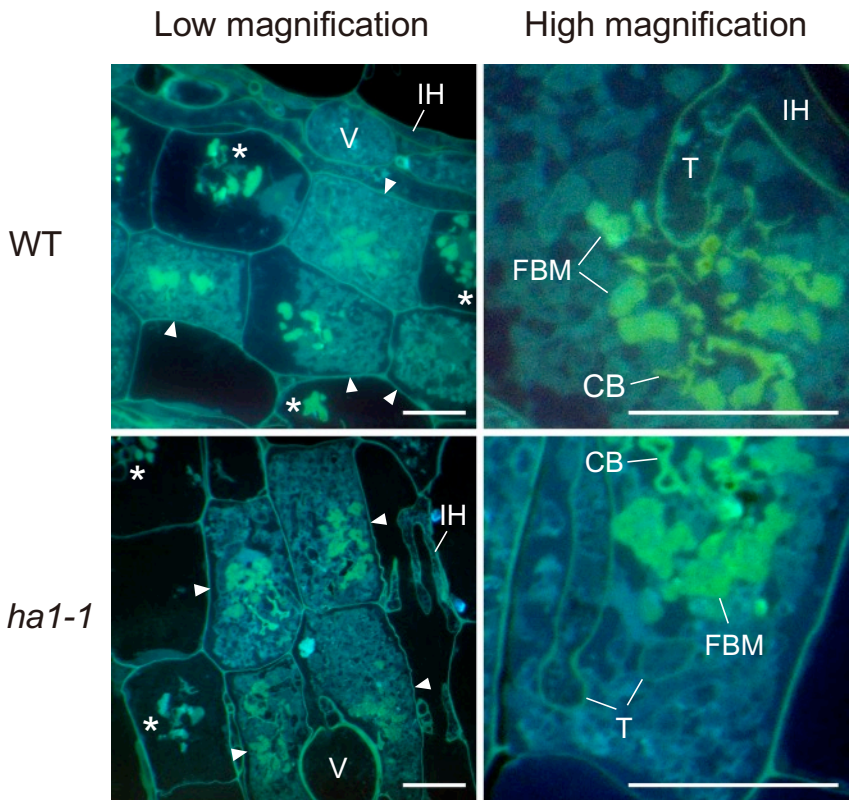

Figure 3-14. DAPI staining of semithin sections of resin-embedded mycorrhizal roots of *Lotus japonicus*. Mature arbuscules (arrowheads) and degenerating arbuscules (asterisks) of *Rhizophagus irregularis* are shown. Fine branch modules (clusters of connected branches), trunk hyphae cell walls, and collapsed branches display yellow fluorescence. CB: collapsed branch, FBM: fine branch module, IH: intraradical hypha, T: trunk hypha, V: vesicle. Scale bars = 20 µm.

3.3.4. PolyP Localization in Arbuscules –PPBD Affinity Labeling–

The subcellular localization of polyP was further analysed using enzyme-affinity labeling with PPBD, which binds specifically to long-chain polyp (Saito *et al.*, 2005) because the yellow fluorescence of DAPI is not specific only to polyP. PolyP was labeled in semithin sections of mycorrhizal roots with recombinant PPBD containing an epitope tag. The tag was then detected by indirect immunocytochemistry with an Alexa Fluor 488-conjugated secondary antibody and observed under a fluorescence microscope. In arbuscules formed in wild-type roots, a strong polyP signal was observed at the cell periphery of the trunk hyphae, possibly at the cell wall (**Figure 3-15**). Weak fluorescence was detected in plant and fungal nuclei, likely due to the low-affinity DNA-binding capability of PPBD (Saito *et al.*, 2005). There was no or very weak polyP signal in the fine branches throughout the cortical cells harboring arbuscules. This localization differed from the DAPI-polyP signal, which was associated with fine branch modules in the central region of arbuscules. These contradictory observations may result from a difference in polyP binding properties as DAPI can bind to short-chain polyP with at least 14 residues (Smith *et al.,* 2018), but PPBD has an extremely low

affinity for polyP shorter than 35 residues (Saito *et al.*, 2005). In addition, polyP detected by DAPI was immobilized in ethanol. Conversely, the PPBD enzyme-affinity method included incubation in an aqueous solution that might have eluted some polyP from the sections. In the *ha1-1* mutant, the labeling pattern of fungal polyP was similar to that of the wild-type, in which the cell periphery of trunk hyphae was labeled (**Figure 3-15**). However, polyP signals were occasionally present at the cell periphery of some fine branches.

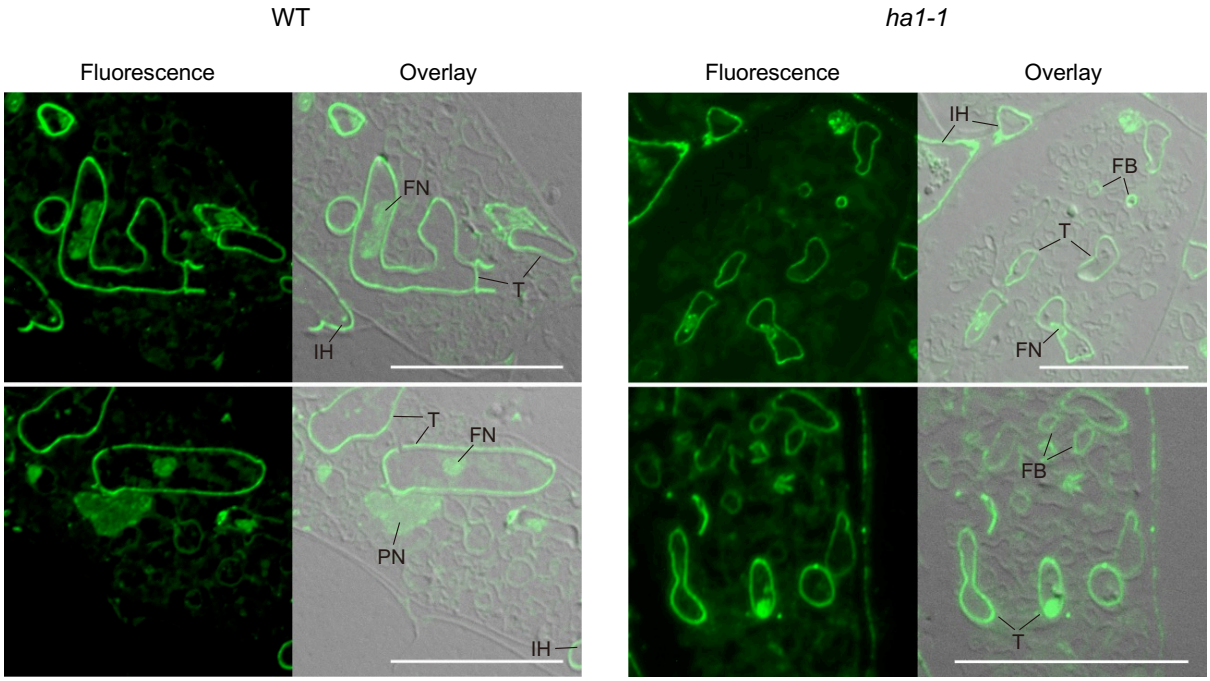

Figure 3-15. Subcellular localization of polyphosphate (polyP) using polyP binding domain (PPBD) affinity labeling. Representative fluorescence images of polyP localization (left panels) and superimposed differential interference contrast images (right panels) of arbuscule-containing cortical cells in wild-type (WT) and *ha1-1*. Sections were incubated with a PPBD-anti-Xpress antibody complex and, subsequently, an anti-mouse IgG antibody conjugated with Alexa Fluor 488. An intense fluorescence signal was observed in cell walls of trunk hyphae and intraradical hyphae in both genotypes. Signals were sometimes detected in fine branches in the mutant. FB: fine branch, FN: fungal nucleus, IH: intraradical hypha, PN: plant nucleus, T: trunk hypha. Scale bars = 20 µm.

PolyP localization was visualized by transmission electron microscopy (TEM) using the enzyme-affinity method with gold-coupled secondary antibodies. In arbuscules formed in wild-type, the polyP signal was evenly distributed in the trunk cell wall, as observed with fluorescence microscopy (**Figure 3-16a–c**. Sparse labeling was observed sporadically within vacuoles of trunk hyphae (**Figure 3-16d**). However, there was no polyP signal in the fine branches (**Figure 3-16e–f**). In *ha1-1* roots, polyP localization was similar to that in the wild-type, with presence in the trunk

hyphae fungal cell wall (**Figure 3-16g–h**). Interestingly, polyP signals were sometimes observed on the fine branch cell walls (**Figure 3-16i–j**). In particular, fine branches cut obliquely against the longitudinal axis showed prominent signals in their cell walls or their surrounding PAS (**Figure 3-16k–l**). In the negative controls, where sections of mycorrhizal roots were incubated in a reaction mixture without PPBD, no polyP signals were detected (**Figure 3-17**). There was also no polyP signal when the PPBD polyP-binding site was masked with a high concentration of tripolyphosphate. In summary, enzyme-affinity labeling using PPBD revealed that in the wild-type, relatively long-chain polyP was mainly distributed in the trunk hyphae cell walls and absent in the fine branches. However, the *HA1* mutation led to polyP accumulation in some fine branch cell walls.

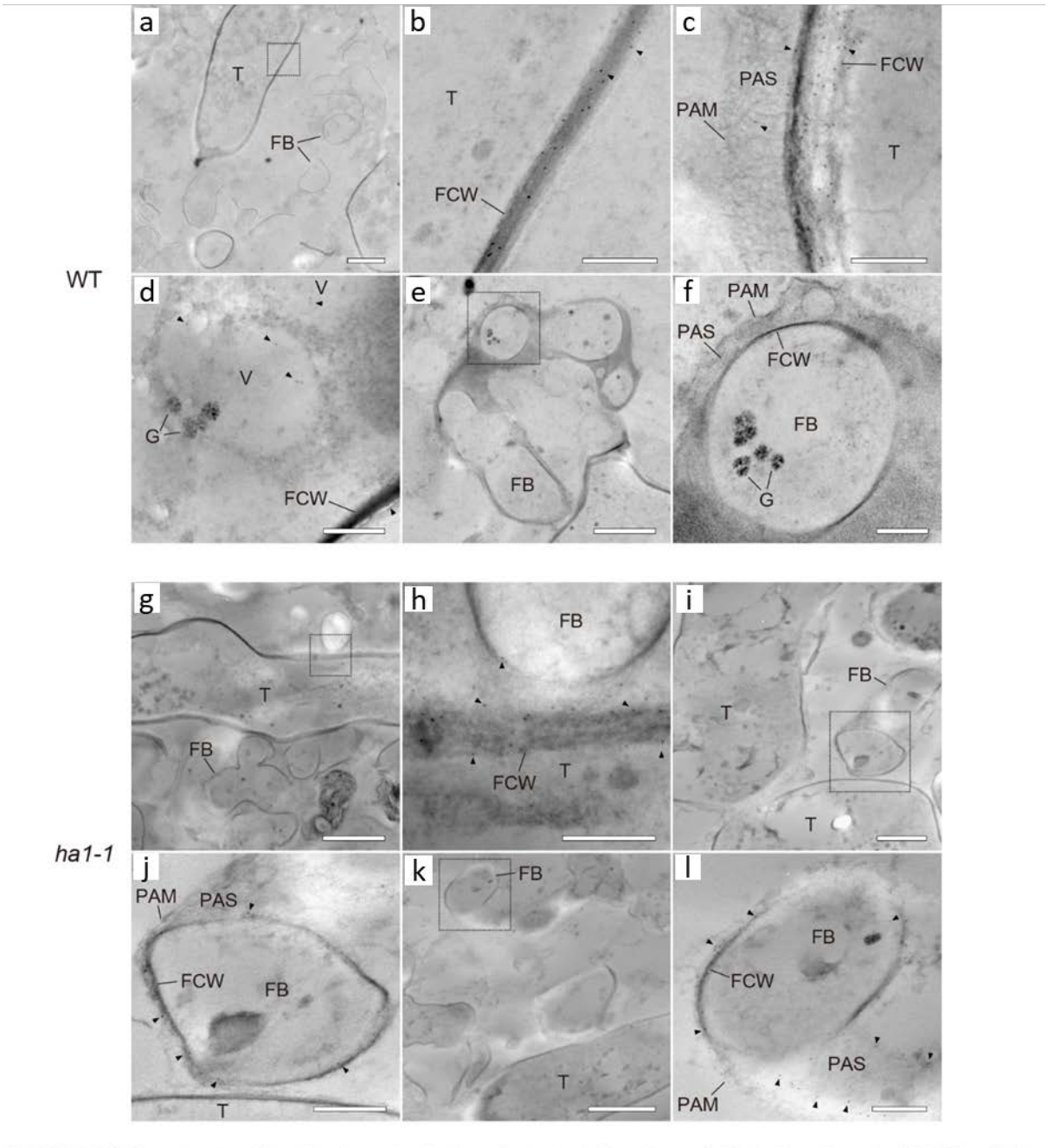

Figure 3-16. Ultrastructural localization of polyphosphate (polyP) using polyP binding domain (PPBD) affinity labeling. Representative transmission electron micrographs showing polyP distribution (gold particle) in mycorrhizal roots of wild-type (WT) (a–f) and *ha1-1* (g–l). Sections were incubated with a PPBD-anti-Xpress antibody complex and, subsequently, an anti-mouse IgG conjugated with 6-nm colloidal gold. Triangles show representative gold particles. (a–c) PolyP present in the trunk hyphae cell wall. (d) Occasional labeling in fungal vacuoles. (e–f) Fine branches lacking signal. (g and h) Signals were often detected in the trunk hyphae cell walls in the *ha1-1* roots. (i–l) Fine branch cell walls were sometimes labeled in *ha1-1*. Panels b, f, h, j, and l show the magnified images of dotted areas in the previous panels. FB: fine branch, FCW: fungal cell wall, G: glycogen granule, PAM: periarbuscular membrane, PAS: periarbuscular space, T: trunk hypha, V: vacuole. Scale bars = 500 nm.

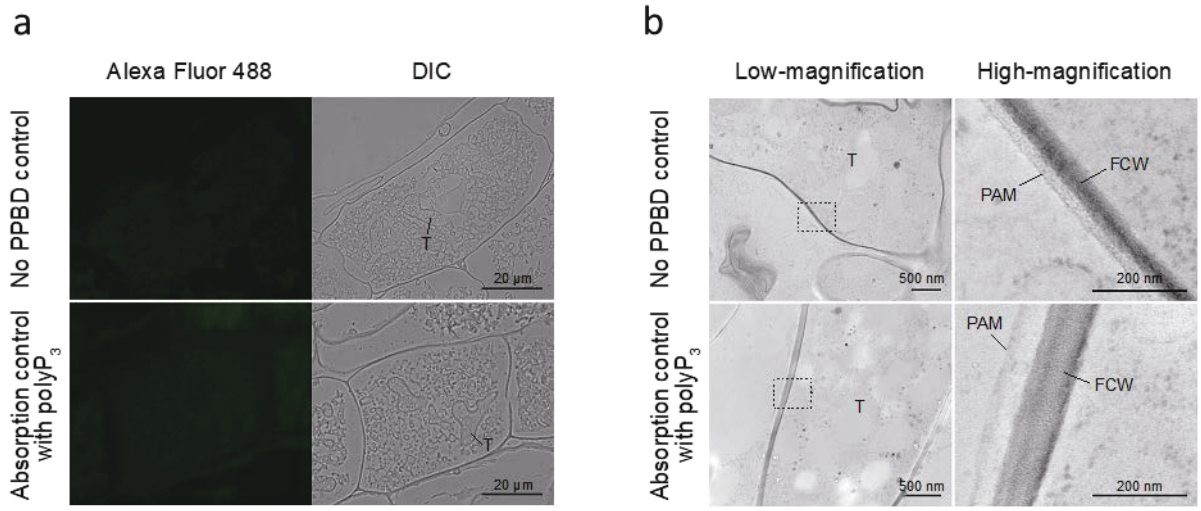

Figure 3-17. Negative controls for polyphosphate (polyP) labeling using the polyP binding domain (PPBD) affinity method. Sections of wild-type (WT) *Lotus japonicus* roots colonized by *Rhizophagus irregularis* were incubated without PPBD (no PPBD control) or with an excess of tripolyphosphate (absorption control with $polyP_3$) during the PPBD-anti-Xpress antibody incubation. (a) Fluorescence microscopy images of Alexa Fluor 488, a secondary antibody conjugate, and differential interference contrast (DIC) images of arbuscules. (b) Micrographs of transmission electron microscopy. The right panels show magnified images of the dotted areas in the left panels. FCW: fungal cell wall, PAM: periarbuscular membrane, T: trunk hypha.

3.3.5. Localization of Phosphatase Activity in Arbuscule-Containing Cortical Cells

An interesting feature of polyP localization was its almost complete absence from fine branches at the periphery of cortical cells in wild-type and *ha1-1* (**Figure 3-14**). Dreyer *et al.* (2008) reported that acid phosphatase (ACP) activity localizes at the interface between fungal cell walls and PAM. Generally, ACPs have broad substrate specificities for phosphate esters. To elucidate the spatial relationship between polyP and ACP in cells with arbuscules, the localization of ACP activity at the ultrastructural level was investigated (**Figure 3-18**). ACP activity was detected by incubating mycorrhizal roots in an acidic buffer containing the reaction substrate (β-glycerophosphate) and the

co-precipitant (cerium salt) and observing the black precipitates of the reaction product (cerium phosphate) with TEM. High ACP activity was frequently detected in PAS around the fine branches in both wild-type and *ha1-1*, which was consistent with previous observations (Dreyer *et al.*, 2008). Notably, most of the dense precipitates localized along the host-derived PAM and in small vesicles resembling the intramatrix compartment type I (IMC-I) or apoplastic vesicular structures (AVS) (Ivanov *et al.*, 2019; Roth *et al.*, 2019). In contrast, only a few signals were associated with PAS around the trunk hyphae in both wild-type and *ha1-1* cells. ACP activity was sometimes observed in fungal vacuoles. No dense cerium phosphate precipitate was observed in the control experiment lacking cerium salt (**Figure 3-19**). In the control reaction without β-glycerophosphate, a few precipitates were observed in the fungal vacuoles, possibly due to a reaction with endogenous vacuole substrates. Next, the localization of neutral phosphatase (NTP) activity in the *ha1-1* mutant was investigated because the acidification around arbuscules diminishes in *ha1* cortical cells (Krajinski *et al.*, 2014; Liu *et al.*, 2020). NTP activity localization was similar to ACP activity with signals along the PAM and in small vesicles present in the PAS surrounding fine branches (**Figure 3-20**), as previously reported (Jeanmaire *et al.*, 1985).

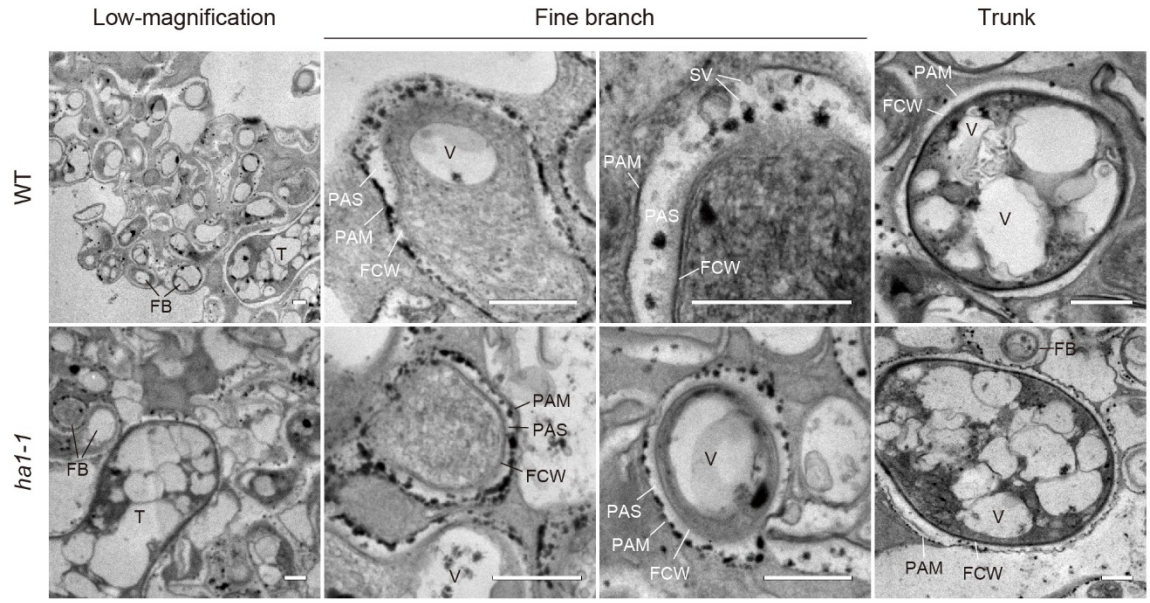

Figure 3-18. Electron microscopic enzyme cytochemistry of acid phosphatase (ACP) activity in arbuscule-containing cortical cells. Representative transmission electron micrographs showing ACP activity in arbuscule-containing cortical cells of wild-type (WT) and *ha1-1* roots colonized by *Rhizophagus irregularis*. Fine branches and trunk hyphae of an arbuscule colonized in a cortical cell are shown. ACP activity was detected as black precipitates of the reaction product (cerium phosphate) by incubating mycorrhizal roots in acetate buffer (pH 4.6) containing β-glycerophosphate and cerium chloride. FB: fine branch, FCW: fungal cell wall, PAM: periarbuscular membrane, PAS: periarbuscular space, SV: small vesicle, T: trunk hypha, V: vacuole. Scale bars = 500 nm.

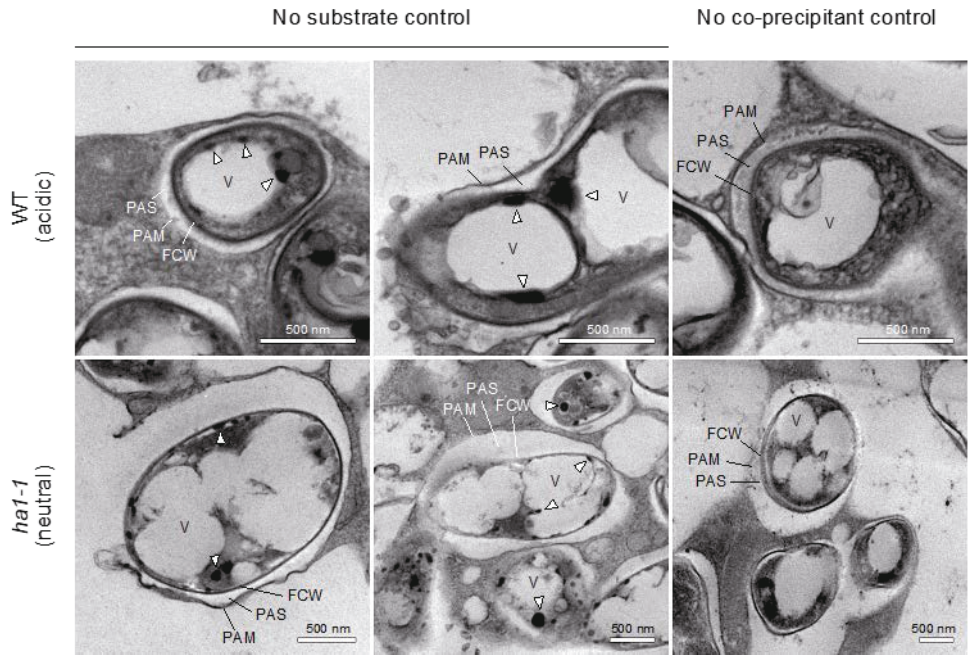

Figure 3-19. Negative controls for enzyme cytochemistry of phosphatase activity. Transmission electron micrographs show acid and neutral phosphatase activity in arbuscule-containing cortical cells of wild-type (WT) and *ha1-1*, respectively. Mycorrhizal roots were incubated in the absence of β-glycerophosphate (no substrate control) or cerium salt (no co-precipitant control) in the reaction buffer. In the no substrate control, a few precipitates (white triangles) were observed in fungal vacuoles. FCW: fungal cell wall, PAM: periarbuscular membrane, PAS: periarbuscular space, V: vacuole.

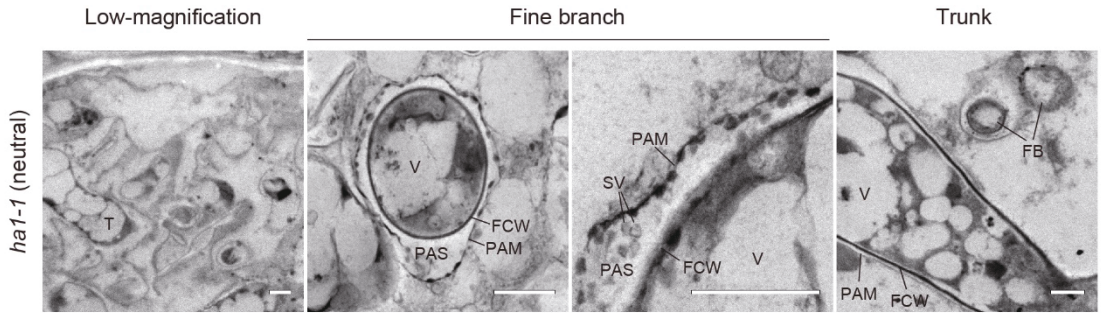

Figure 3-20. Electron microscopic enzyme cytochemistry of neutral phosphatase activity. Transmission electron micrographs showing neutral phosphatase activity in arbuscule-containing cortical cells of the *ha1-1* roots colonized by *Rhizophagus irregularis*. Neutral phosphatase activity was detected as black precipitates of the reaction product (cerium phosphate) by incubating mycorrhizal roots in Tris-HCl buffer (pH 7.4) containing β-glycerophosphate and cerium chloride. Fine branches and trunk hyphae of an arbuscule colonized in a cortical cell are shown. FB: fine branch, FCW: fungal cell wall, PAM: periarbuscular membrane, PAS: periarbuscular space, SV: small vesicle, T: trunk hypha, V: vacuole. Scale bars = 500 nm.

To further study the relationship between phosphatase activity and polyP accumulation, phosphatase activity and polyP signals simultaneously were detected by enzyme cytochemistry using the ELF97 phosphatase substrate and DAPI staining, respectively. ELF97 forms fine precipitates after hydrolysis of its phosphate ester bond by non-specific phosphatases, emitting yellow-green fluorescence at the site of phosphatase activity (Haugland, 2005). First, ACP and NTP activities were visualized in a typical mature arbuscule by single ELF97 staining in wild-type and *ha1-1* roots, respectively (**Figure 3-21a**). In the wild-type, ACP activity was present throughout the arbuscule but was excluded from its central region. Similarly, NTP activity was detected in arbuscules in the mutant but the central region without phosphatase activity was larger than that in the wild-type. Next, double labeling of phosphatase activity and polyP was performed. The localization of phosphatase activity (green) and polyP (yellow) was distinct based on different emission colors using a long-pass filter, albeit showing weak and different color signals compared to the single staining (**Figure 3-21b**). Double labeling showed that polyP was present in the center of arbuscules, and phosphatase activity localized in the surrounding regions. Thus, polyP and phosphatase activity showed opposite localization in both wild-type and *ha1-1* cells.

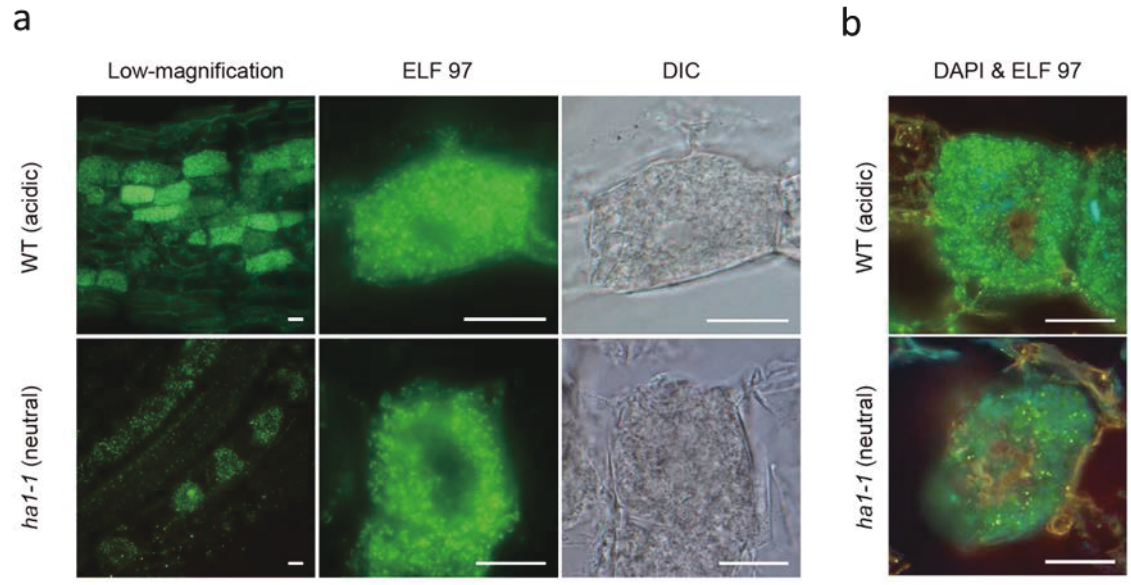

Figure 3-21. Enzyme cytochemistry of phosphatase activity in arbuscule-containing cortical cells using ELF97. (a) Representative fluorescence images of acid and neutral phosphatase activity in wild-type (WT) and *ha1-1*, respectively. Green fluorescence of the ELF97 reaction product indicates phosphatase activity. Arbuscule structure was observed under a differential interference contrast (DIC) microscope. (b) Double labeling using DAPI and ELF97 of WT and *ha1-1* under acidic and neutral conditions, respectively. The color balance was adjusted to discriminate between DAPI-polyP complex and the ELF97 reaction product fluorescence. Yellow-orange and green fluorescence indicate polyphosphate and phosphatase activity, respectively. Scale bars = 20 µm.

3.3.6. Gene Expression Analysis

Whether the *HA1* mutation affected gene expression related to plant Pi uptake and fungal polyP metabolism during AM symbiosis were investigated. The levels of the phosphate transporter *PT1*, likely to function in the direct pathway due to its downregulation during mycorrhization (Maeda *et al.*, 2006), were slightly elevated in *ha1-1* roots compared to the wild-type (**Figure 3-22**), which may reflect a partial block in P translocation via the mycorrhizal pathway. Transcripts of other phosphate transporters, including AM-specific *PT4* (Guether *et al.*, 2009; Takeda *et al.*, 2009) accumulated equally in the mycorrhizal roots of both genotypes. Similarly, the *ha1-1* mutation did not affect the expression of AM marker genes, AM-specific ammonium transporter *AMT2;2* (Guether *et al.*, 2009) and glycerol-3-phosphate acyltransferase *RAM2* (Wang *et al.*, 2012). Fungal endopolyphosphatase genes *PPN1*, *PPN2*, and *PPN3* were downregulated in AM fungi colonizing the mutant, whereas the VTC genes involved in polyP synthesis were not affected (**Figure 3-22**).

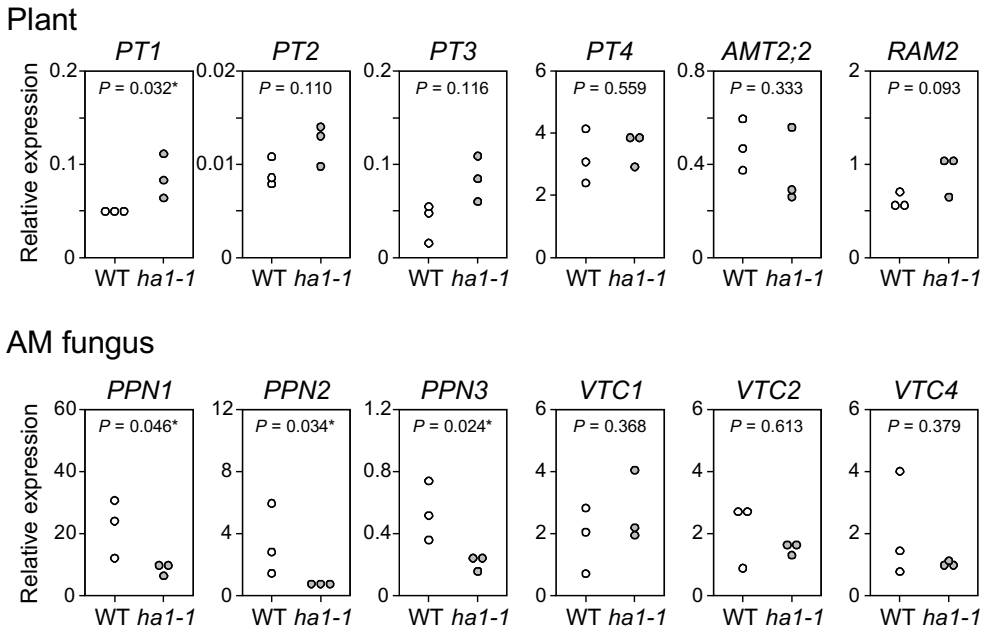

Figure 3-22. Gene expression analysis. Expression of *Lotus japonicus* genes encoding phosphate transporters (*PT1*–*PT4*), ammonium transporter (*AMT2;2*), and AM-specific glycerol-3-phosphate acyltransferase *RAM2* gene in mycorrhizal roots of the wild-type (WT) and *ha1-1* four weeks after inoculation with *Rhizophagus irregularis*. Expression levels were normalized based on the amount of *L. japonicus EF2*. Expression of *R. irregularis* genes encoding endopolyphosphatases (*PPN1*–*PPN3*) and vacuolar transporter chaperones (*VTC1*, *VTC2*, and *VTC4*) in mycorrhizal roots. The *R. irregularis EF1β* gene was used as an internal control. *P*-values are based on Student's *t*-test (*, $P < 0.05$).

3.4. Discussion

P transfer across the symbiotic interface is an important process in the mycorrhizal pathway. However, it has been challenging to elucidate this process, possibly due to rapid P movement from the AM fungus to the host. This study was conducted to clarify the intermediate process of P transfer by visualizing polyP localization in arbuscules of *R. irregularis* formed in *L. japonicus* wild-type and the *ha1-1* mutant.

PPBD affinity-labeling for specifically detecting long-chain polyP demonstrated that polyP was predominantly distributed in cell walls of trunk hyphae in arbuscules formed in wild-type, but fine branch cell walls lacked a polyP signal. Since intense ACP activities were found in PAS around fine branches, the absence of polyP in the fine branch cell walls could be explained by the degradation of polyP in fungal cell walls by apoplastic ACP. Supporting this idea, the *ha1-1* mutant, in which the mycorrhizal pathway was partially suppressed, showed polyP localization in some cell walls of the fine branches. Based on the observations, a hypothesis for P transfer at AM fungus-host interface is proposed, in which polyP is released into the cell walls of fine branches and then immediately subjected to hydrolysis by ACP located in the PAS. The liberated Pi is delivered to host cells by symbiotic Pi transporters driven by the H^+ gradient generated across the PAM by the HA1 H^+-ATPase (Javot *et al.*, 2007; Willmann *et al.*, 2013; Xie *et al.*, 2013; Krajinski *et al.*, 2014; Wang *et al.*, 2014; Watts-Williams *et al.*, 2015; Liu *et al.*, 2020) (**Figure 3-23**). However, because the mechanism of polyP release into the fungal cell wall is unknown and it remains unclear whether the apoplastic ACP can catalyze polyP hydrolysis, it cannot be ruled out the possibility that polyP is hydrolyzed in AM fungal hyphae and the liberated Pi is exported to the PAS via an unidentified Pi exporter.

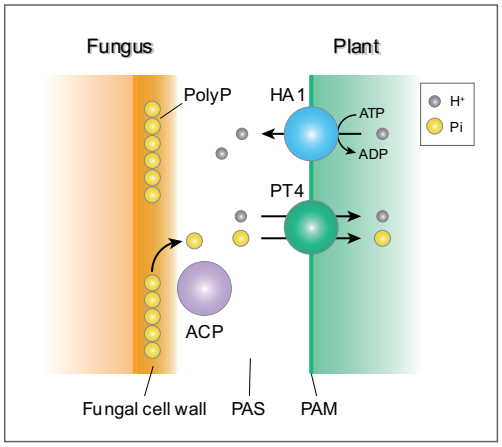

Figure 3-23. Hypothetical model for P transfer at the fungus-plant interface. The model illustrates that polyP is released into the cell walls of fine branches and then subject to hydrolysis by acid phosphatase (ACP) activity located at the periarbuscular space (PAS). The liberated Pi is delivered into the plant cell by the symbiotic Pi transporter, PT4, driven by a H^+ gradient generated across the periarbuscular membrane (PAM) by the H^+-ATPase HA1.

Moreover, polyP signals were observed within several fine branch modules close to the trunk hyphae by DAPI staining. The fine branch modules with polyP were slightly expanded in the *ha1-1* mutant. Around these fine branch modules, no phosphatase activity was observed by double staining with ELF97 and DAPI. It might be anticipated that P metabolism and export are suppressed in these fine branch modules, leading to the accumulation of polyP. This is consistent with the finding that the expression levels of endopolyphosphatase genes were reduced in AM fungi colonizing the *ha1-1* mutant, although whether polyphosphatase activity is decreased in DAPI-stained fine branch modules stained is unknown.

A remarkable feature of arbuscule polyP is its localization in the fungal cell walls. The polyP chain appears to be relatively long, as detected by the PPBD enzyme affinity method. PolyP distribution in cell walls has also been observed in germ tubes and extraradical hyphae of AM fungi and mycelia of a wide range of fungal species (Mucoromycota, Dikarya, and Chytridiomyceta) (Werner *et al.*, 2007; Kuga *et al.*, 2008). However, little is known about the molecular mechanisms underlying polyP accumulation in fungal cell walls. A possible mechanism is that polyP might be loaded into intracellular vesicles and released into the extracellular space via exocytosis. Alternatively, the VTC complex might be redistributed to the plasma membrane and then synthesize polyP. The yeast VTC2, a subunit of VTC complexes, is observed at the cell periphery along the plasma membrane under high Pi conditions, although it is localized in vacuoles in a low-Pi medium (Hothorn *et al.*, 2009a). How polyP is released across the fungal plasma membrane and the role of cell wall polyP in fungal physiology are important questions to be explored in future studies.

Extensive polyP accumulation in arbuscules has been observed in plant mutants of Pi transporter genes related to symbiotic P uptake. Arbuscules formed in *M. truncatula PT4* mutant and RNAi lines (Javot *et al.*, 2007) and in *L. japonicus PT3* RNAi lines (Funamoto *et al.*, 2007) were almost entirely stained with toluidine blue and DAPI, respectively, indicating that polyP accumulation extended to fine branches in the marginal regions of the arbuscule. However, the *ha1-1* mutant had DAPI-polyP signals in only some fine branch modules located at the arbuscule center. Similarly, *ha1-1* phenotypes in P uptake through the mycorrhizal pathway and early arbuscule degradation were not as severe as in *pt* or other *ha1* mutants (Javot *et al.*, 2007; Krajinski *et al.*, 2014; Wang *et al.*, 2014; Liu *et al.*, 2020). The *ha1-1* mutation may have partial ATPase activity. In both *ha1-1* and wild-type roots, arbuscule fine branch modules close to a trunk hypha displayed strong DAPI-polyP fluorescent signals but were not labeled with PPBD. Considering the differences in polyP chain length affinity between DAPI and PPBD (Saito *et al.*, 2005; Smith *et al*., 2018), relatively

short-chain polyPs are likely to accumulate in that region. In the *ha1-1* mutant, fine branch modules stained with DAPI were increased and expanded to the periphery of arbuscules. A similar pattern of polyP accumulation was observed in RNAi lines of the AM-inducible Pi transporter *PT3* (Funamoto *et al.*, 2007). The P flow in arbuscules appear to be initially disrupted in the fine branches close to the trunk hypha, which is observed as polyP accumulation. Subsequently, the disruption of the P flow may be extended to fine branches in other regions.

ACP activity and polyP had opposite localization in mature arbuscules. Funamoto *et al.* (2007) observed a similar spatial relationship between alkaline phosphatase (ALP) activity and polyP distribution. ALPs in AM fungi (Gianinazzi-Pearson *et al.*, 1979; Kojima *et al.*, 1998; Aono *et al.*, 2004) can hydrolyze monophosphate esters but not pyrophosphate bonds in polyp (Ezawa *et al.*, 1999; Xie *et al.*, 2013). Therefore, the reduced accumulation of polyP at sites of intense ALP activity could result from a change in P metabolism indirectly mediated by fungal ALPs (Saito & Ezawa, 2016). ACP has a broad substrate specificity for various phosphate compounds. Some plant ACPs can potentially hydrolyze polyp (Ezawa & Yoshida, 1994; Ezawa *et al.*, 2005; Huang *et al.*, 2018). Enzyme histochemical analyses have demonstrated intense ACP activity in arbuscules, particularly in PAM (van Aarle *et al.*, 2005; Dreyer *et al.*, 2008). In this study, ACP activity detected in PAS was often associated with host-derived PAM and small vesicles resembling IMC-I or AVS, possibly due to PAM outgrowth (Ivanov *et al*., 2019; Roth *et al.*, 2019). This observation suggests that ACP in the apoplastic region originates from the plant cells. However, the corresponding proteins have not been identified in the host plants. Several AM-inducible phosphatase genes are candidates for encoding ACPs present in PAS. In soybean, 2 out of 35 purple acid phosphatase genes are upregulated in AM roots (Li *et al.*, 2012). The AM-inducible soybean purple acid phosphatase gene, *GmPAP33*, is expressed in arbuscule-containing cortical cells and is involved in arbuscule degeneration via phospholipid hydrolysis (Li *et al.*, 2019). The AM-inducible marigold purple acid phosphatase TpPAP1, which differs from GmPAP33 in subclass, displays a broad substrate specificity and can catalyze polyP degradation (Ezawa & Yoshida, 1994; Ezawa *et al.*, 2005). Further research, including mutant analysis, is needed to clarify whether these purple acid phosphatases are responsible for ACP activity in PAS.

Chapter IV

Conclusions

PolyP is a crucial molecule in the symbiotic P transport system during AM fungal symbiosis. However, the polyP synthesis and metabolism in AM fungi remain poorly understood due to the difficulties of genetic and molecular analyses of AM fungi and the limited analytical techniques available for polyP. Here, we focused on polyP metabolism of AM fungi. Our findings provide insights into P transfer at the symbiotic interface.

In Chapter II, the biochemical properties of a recombinant catalytic domain of the *Rhizophagus irregularis* VTC4 (VTC4*) were examined. VTC4* synthesized polyP using ATP as a substrate. Interestingly, the reverse reaction by VTC4 was found, in which ATP was generated from polyP in the presence of high ADP concentration. This novel finding, i.e., VTC4 catalyzes the reverse reaction, implies that energy would be conserved in polyP metabolism via the VTC-mediated regulation of polyP accumulation and ATP regeneration. Although whether the VTC complex catalyzes both reactions in vivo remain unknown, the VTC complex might be important in integrating P homeostasis with energy regulation and polyP metabolism. In Chapter III, polyP metabolism in AM fungi was investigated histochemically. In arbuscules of *R. irregularis* colonizing *L. japonicus*, polyP was primarily found in the cell walls of the trunk hyphae but rarely in fine branches. However, in the *L. japonicus* H^+-ATPase *ha1* mutant defective in symbiotic P uptake, polyP was found in the cell walls of some fine branches. Double staining revealed a contrasting distribution of polyP and ACP activity in arbuscules. The ACP activity was observed in the PA space around the fine branches. These findings indicate that the relationship between polyP localized in the cell wall and apoplastic ACP activity is important for P transfer at the arbuscule interface.

Based on these findings and literature, the model of P transfer from the AM fungi to the host plant cell was proposed (Figure 4-1). Pi is absorbed through fungal Pi transporters (Harrison & van Buuren, 1995; Maldonado-Mendoza *et al.*, 2001; Benedetto *et al.*, 2005; Fiorilli *et al.*, 2013; Xie *et al.*, 2016), incorporated to ATP in the mitochondrion, polymerized by the VTC complex on the tonoplast (Hothorn *et al.*, 2009b), accumulated in the tubular vacuoles in extraradical hyphae, and translocated toward intraradical hyphae by the water flow (Kikuchi *et al.*, 2016). PolyP is then depolymerized by the VTC complex and endopolyphosphatases to short-chain polyPs, which are then released into the cell wall of fine branches by unknown mechanisms. PolyP localized in the

fungal cell wall is hydrolyzed to Pi by plant-derived ACPs that are secreted into the PA space. The liberated Pi is delivered to host cells by symbiotic Pi transporters driven by the H^+ gradient generated across the PA membrane of the HA1 H^+-ATPase (Javot *et al.*, 2007; Yang *et al.*, 2012b; Krajinski *et al.*, 2014; Watts-Williams *et al.*, 2015; Liu *et al.*, 2020). However, many factors still need to be elucidated in this model. Thus, future research is necessary to determine whether the AM fungal VTC complex catalyzes forward and reverse reactions in vivo. In addition, it is necessary to identify which ACPs are active in the PA space and how polyP is incorporated into the fungal cell wall. Notably, our model is one of the several hypotheses for P release from AM fungi, and others, such as P efflux by fungal Pi transporters and the involvement of vesicle trafficking mediated by the SYG protein, have recently been proposed (Ezawa and Saito 2018; Xie *et al.* 2022). However, definitive evidence for these models is still lacking. Thus, it is necessary to examine the possibility that the P efflux pathways depicted in these models exist independently or are interconnected.

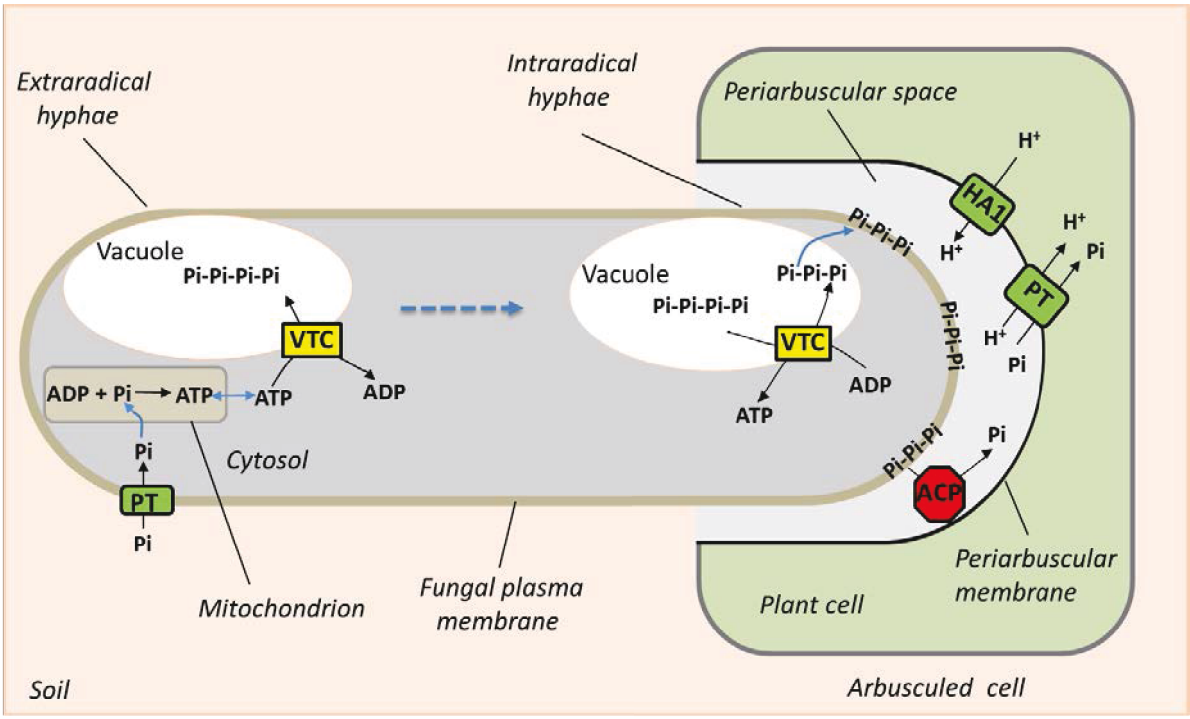

Figure 4-1. Hypothetical model for P transfer from AM fungi to the host plant. Pi is absorbed by fungal Pi transporters, incorporated to ATP in the mitochondrion, polymerized by the VTC complex on the tonoplast, accumulated in the tubular vacuoles in extraradical hyphae, and translocated toward intraradical hyphae by the water flow. PolyP is then depolymerized by the VTC complex to short-chain polyP, released into the cell wall of fine branches by unknown mechanisms, and hydrolyzed to Pi by acid phosphatases located on the periarbuscular space. The liberated Pi is delivered to host cells by symbiotic Pi transporters driven by the H^+ gradient generated across the periarbuscular membrane of the HA1 H^+-ATPase. The VTC complex can catalyze forward and reverse reactions: $polyP_n + ATP \leftrightarrow polyP_{n+1} + ADP$.

In this thesis, the P transfer model was proposed at the arbuscular interface; however, several works remain to be investigated to determine whether the VTC complex is responsible for polyP polymerization and depolymerization in vivo, what gene is responsible for ACP activity localized in the PA space, and whether the ACP is involved in symbiotic P transfer. In the future, these questions must be addressed to clarify the mechanism of P transport in AM symbiosis. Future works based on the P transfer model will facilitate the production of P-efficient crops and reduce the application of P fertilizer in sustainable agriculture by developing molecular diagnostic tools such as polyP, VTC4, and ACP for the evaluation of AM functions.

Acknowledgements

It is my great pleasure to write the messages to all those have contributed and supported me to complete this research work for fulfilment of the degree of Doctor of Philosophy.

I would like to express my sincere gratitude, appreciation and respect to my honorable advisor Dr. Katsuharu Saito, Associate Professor, Laboratory of Soil Biology, Faculty of Agriculture, Shinshu University for his kindness, competent guidance, valuable support and enthusiastic encouragement at all stages of my study and stay in Japan.

My gratitude to co-supervisor Dr. Shinpei Kato, Associate Professor, Laboratory of Plant Pathology, Faculty of Agriculture, Shinshu University for his deep concern, encouragement and constructive comments have been of great value in this study.

I am grateful to co-supervisor Dr. Akiyoshi Yamada, Associate Professor, Laboratory of Mycorrhiza, Faculty of Agriculture, Shinshu University for his valuable comments and suggestion about this study.

I appreciate Dr. Tatsuhiro Ezawa, Associate Professor, Hokkaido University for his valuable advices and comments about this study, especially construction and writing papers.

I would like to thank Dr. Hiroki Irieda, Associate Professor, Laboratory of Microbe-Plant Interactions, Faculty of Agriculture, Shinshu University for his contribution in the part of lab study.

I appreciate Dr. Ken-ichi Matsushima, Professor, Laboratory of Plant Genetics and Breeding, Faculty of Agriculture, Shinshu University for his valuable advices and comments about this study.

I appreciate Dr. Ryo Ohtomo, Senior Researcher, National Agriculture and Food Research Organization for his valuable advices and comments about this study, especially construction and writing papers.

I wish express thanks to assistance researchers in my lab Reika Oguchi for her great help to conduct the experiments in this research and Rieko Okita for her assistance in case of laboratory work and personal works as well.

I also want to thank members of the lab mates, past and present (Yusaku Sugimura, Kaori Akamatsu, Kaho Taguchi, Hidemi Mizuno, Yuta Sugiura, Rei Akiyama, Yeh Tzu Jui, Minori Kamiya, Koji Ino, Mika Ohashi) for their help, collaborate in lab works and discussion in this research.

I would also like to acknowledges to the "Japanese Government Monbukagakusho: MEXT Scholarship" authority for the financial support to accomplish this study.

My deepest thanks to Emeritus Professor Kayahara Hiroshi, Faculty of Agriculture, Shinshu University who have supported and directed me to the way to study in Japan.

I would kindly like to extend my gratitude to Dr. Nguyen Van Ket, Associate Professor, Faculty of Agriculture and Forestry, Emeritus Deputy Principal, Dalat University who have teach and given me opportunities to science research pathways.

Finally, I express heartfelt and deepest appreciation to my sweet family, my beloved father and mother, especially, my cherished husband and daughters for their love, blessing, encouragement and great sacrifice in the long process of academic career and moral support during the hardest study period in my life.

Nguyen Thi Cuc

Shinshu University

References

Aksoy M, Pootakham W, Grossman AR. **2014**. Critical function of a *Chlamydomonas reinhardtii* putative polyphosphate polymerase subunit during nutrient deprivation. **26**: 4214–4229.

Aono T, Maldonado-Mendoza IE, Dewbre GR, Harrison MJ, Saito M. **2004**. Expression of alkaline phosphatase genes in arbuscular mycorrhizas. *New Phytologist* **162**: 525–534.

Arpat AB, Magliano P, Wege S, Rouached H, Stefanovic A, Poirier Y. **2012**. Functional expression of PHO1 to the Golgi and trans-Golgi network and its role in export of inorganic phosphate. *The Plant Journal* **71**: 479–491.

Austin S, Mayer A. **2020**. Phosphate homeostasis − A vital metabolic equilibrium maintained through the INPHORS signaling pathway. *Frontiers in Microbiology* **11**: 1–21.

Azaizeh H. Marschner H, Romheld V, Wittenmayer L. **1995**. Effects of a vesicular-arbuscular mycorrhizal fungus and other soil microorganisms on growth , mineral nutrient acquisition and root exudation of soil-grown maize plants. *Mycorrhiza*: 321–327.

Azevedo C, Saiardi A. **2017**. Eukaryotic phosphate homeostasis: The inositol pyrophosphate perspective. *Trends in Biochemical Sciences* **42**: 219–231.

Balestrini R, Gómez-ariza J, Lanfranco L, Bonfante P, Piante IP, Vegetale B, Torino U, Mattioli V. **2007**. Laser microdissection reveals that transcripts for five plant and one fungal phosphate transporter genes are contemporaneously present in arbusculated cells. *Molecular Plant-Microbe Interactions* **20**: 1055–1062.

Benedetto A, Magurno F, Bonfante P, Lanfranco L. **2005**. Expression profiles of a phosphate transporter gene (*GmosPT*) from the endomycorrhizal fungus *Glomus mosseae*. *Mycorrhiza* **15**: 620–627.

Boyce KJ, Kretschmer M, Kronstad JW, Al BET. **2006**. The vtc4 gene influences polyphosphate storage, morphogenesis, and virulence in the maize pathogen *Ustilago maydis. Eukaryotic Cell* **5**: 1399–1409.

Brundrett MC, Tedersoo L. **2018**. Evolutionary history of mycorrhizal symbioses and global host plant diversity. *New Phytologist* **220**: 1108–1115.

Chiu CH, Paszkowski U. **2019**. Mechanisms and impact of symbiotic phosphate acquisition. *Cold Spring Harbor Perspectives in Biology* **11**: a034603 1.

Clark RB, Zeto SK. **2008**. Mineral acquisition by arbuscular mycorrhizal plants. *Journal of Plant Nutrition* **23** : 37–41.

Cohen A, Perzov N, Nelson H, Nelson N. **1999**. A novel family of yeast chaperons involved in the distribution of V-ATPase and other membrane proteins. *Journal of Biological Chemistry* **274**: 26885–26893.

Cooper J, Carliell-marquet C. **2013**. A substance flow analysis of phosphorus in the UK food production and consumption system. *Resources, Conservation & Recycling* **74**: 82–100.

Daniel PS, Reid RJ, Ayling SM. 1998. Update on phosphorus uptake phosphorus uptake by plants: From soil to cell. *Plant Physiology* **116**: 447–453.

Darriba D, Posada D, Flouri T, Kozlov AM, Stamatakis A, Morel B. **2020**. ModelTest-NG: A new and scalable tool for the selection of DNA and protein evolutionary models. *Molecular Biology and Evolution* **37**: 291–294.

Delaux PM, Radhakrishnan G V., Jayaraman D, Cheema J, Malbreil M, Volkening JD, Sekimoto H, Nishiyama T, Melkonian M, Pokorny L, *et al.* 2015. Algal ancestor of land plants was preadapted for symbiosis. *Proceedings of the National Academy of Sciences of the United States of America* **112**: 13390–13395.

Denoncourt A, Downey M. **2021**. Model systems for studying polyphosphate biology: a focus on microorganisms. *Current Genetics* **67**: 331–346.

Desfougères Y, Gerasimaitė R, Jessen HJ, Mayer A. **2016**. Vtc5, a novel subunit of the vacuolar transporter chaperone complex, regulates polyphosphate synthesis and phosphate homeostasis in yeast. *Journal of Biological Chemistry* **291**: 22262–22275.

Dfaz G, Honrubia M. **1996**. Influence of arbuscular mycorrhizae on heavy metal (Zn and Pb) uptake and growth of *Lygeum spartum* and *Anthyllis cytisoides*. *Plant and Soil* **180**: 241–249.

Dreyer B, Pérez-Gilabert M, Olmos E, Honrubia M, Morte A. **2008**. Ultrastructural localization of acid phosphatase in arbusculate coils of mycorrhizal Phoenix canariensis roots. *Physiologia Plantarum* **132**: 503–513.

Dreyer I, Spitz O, Kanonenberg K, Montag K, Handrich MR, Ahmad S, Schott-verdugo S, Navarro-retamal C, Rubio- E, Molina-montenegro MA, *et al.* 2018. Nutrient exchange in arbuscular mycorrhizal symbiosis from a thermodynamic point of view. *New Phytologist* **222**: 1043–1053.

Ezawa T, Shin-ya K, Sakamoto K, Yoshida T, Saito M. **1999**. Specific inhibitor and substrate specificity of alkaline phosphatase expressed in the symbiotic phase of the arbuscular mycorrhizal fungus, *Glomus etunicatum*. Mycologia **91**: 636–641.

Ezawa T, Cavagnaro TR, Smith SE, Smith FA, Ohtomo R. **2004**. Rapid accumulation of polyphosphate in extraradical hyphae of an arbuscular mycorrhizal fungus as revealed by histochemistry and a polyphosphate kinase/luciferase system. *New Phytologist* **161**: 387–392.

Ezawa T, Hayatsu M, Saito M. **2005**. A new hypothesis on the strategy for acquisition of phosphorus in arbuscular mycorrhiza: Up-regulation of secreted acid phosphatase gene in the host plant. *Molecular Plant-Microbe Interactions* **18**: 1046–1053.

Ezawa T, Saito K. **2018**. How do arbuscular mycorrhizal fungi handle phosphate? New insight into fine-tuning of phosphate metabolism. *New Phytologist* **220**: 1116–1121.

Ezawa T, Smith SE, Smith FA. 2001. Differentiation of polyphosphate metabolism between the extra- and intraradical hyphae of arbuscular mycorrhizal fungi. *New Phytologist* **149**: 555–563.

Ezawa T, Yoshida T. **1994**. Acid phosphatase specific to arbuscular mycorrhizal infection in marigold and possible role in symbiosis. *Soil Science and Plant Nutrition* **40**: 655–665.

Fiorilli V, Lanfranco L, Bonfante P. **2013**. The expression of *GintPT*, the phosphate transporter of *Rhizophagus irregularis*, depends on the symbiotic status and phosphate availability. *Planta* **237**:

1267–1277.

Fontes R, Fernandes D, Peralta F, Fraga H, Malo I, da Silva JCGE. **2008**. Pyrophosphate and tripolyphosphate affect firefly luciferase luminescence because they act as substrates and not as allosteric effectors. *FEBS journal* **275**: 1500–1509.

Fukai E, Soyano T, Umehara Y, Nakayama S, Hirakawa H, Tabata S, Sato S, Hayashi M. **2012**. Establishment of a Lotus japonicus gene tagging population using the exon-targeting endogenous retrotransposon LORE1. *The Plant Journal* **69**: 720–730.

Funamoto R, Saito K, Oyaizu H, Aono T, Saito M. **2014**. pH measurement of tubular vacuoles of an arbuscular mycorrhizal fungus, *Gigaspora margarita*. *Mycorrhiza* **25**: 55–60.

Funamoto R, Saito K, Oyaizu H, Saito M, Aono T. **2007**. Simultaneous in situ detection of alkaline phosphatase activity and polyphosphate in arbuscules within arbuscular mycorrhizal roots. *Functional Plant Biology* **34**: 803–810.

Gerasimaite and Mayer A. **2017**. Ppn2, a novel Zn^{2+}-dependent polyphosphatase in the acidocalcisome-like yeast vacuole. *Journal of Cell Science* **130** : 1625–1636.

Gerasimaitė R, Sharma S, Desfougères Y, Schmidt A, Mayer A. 2014. Coupled synthesis and translocation restrains polyphosphate to acidocalcisome-like vacuoles and prevents its toxicity. *Journal of Cell Science* **127**: 5039–5104.

Gianinazzi-Pearson V, Smith SE, Gianinazzi S, Smith FA. **1991**. Enzymatic studies on the metabolism of vesicular arbuscular mycorrhizas V. is H^+-ATPase a component of ATP-hydrolyzing enzyme-activities in plant fungus interfaces. *New Phytologist* **117**: 61–74.

Gianinazzi S, Gianinazzi-Perason V, Dexheimer J. 1979. Enzymatic studies on the metabolism of vesicular-arbuscular mycorrhiza. iii. ultrastructural localization of acid and alkaline phosphatase in onion roots infected by *Glomus mosseae* (Nicol. & Gerd.). *New Phytologist* **82**: 127–132.

Gildon A, Tinder PB. **2016**. Interactions of vesicular-arbuscular mycorrhizal infections and heavy metals in plants. II. The effects of infection on uptake of copper. *New Phytologist* **95**: 263–268.

Giovannini D, Touhami J, Charnet P, Sitbon M, Battini JL. **2013**. Inorganic phosphate xport by the retrovirus receptor XPR1 in metazoans. *Cell Reports* **3**: 1866–1873.

Glassop D, Smith SE, Smith FW. **2005**. Cereal phosphate transporters associated with the mycorrhizal pathway of phosphate uptake into roots. *Planta* **222**: 688–698.

Gomes-vieira AL, Wideman JG, Paes-vieira L, Gomes SL, Richards TA, Meyer-fernandes JR. **2018**. Evolutionary conservation of a core fungal phosphate homeostasis pathway coupled to development in Blastocladiella emersonii. *Fungal Genetics and Biology* **115**: 20–32.

Guether M, Balestrini R, Hannah M, He J, Udvardi MK, Bonfante P. **2009**. Genome wide reprogramming of regulatory networks, transport, cell wall and membrane biogenesis during arbuscular mycorrhizal symbiosis in *Lotus japonicus. New Phytologist* **182**: 200–212.

Guttenberger M. **2000**. Arbuscules of vesicular-arbuscular mycorrhizal fungi inhabit an acidic compartment within plant roots. *Planta* **211**: 299–304.

Harrison MJ, Dewbre GR, Liu JY. **2002**. A phosphate transporter from *Medicago truncatula* involved

in the acquisiton of phosphate released by arbuscular mycorrhizal fungi. *Plant Cell* **14**: 2413–2429.

Harrison MJ, Harrison MJ. **1999**. Molecular and cellular aspects of the arbuscular mycorrhizal symbiosis. *Annual review of plant physiology and plant molecular biology* **50**: 361–389.

Haugland RP. 2005. *The Handbook - A Guide to Fluorescent Probes and Labeling Technologies.* USA: Invitrogen.

Heijden MGA Van Der, Martin FM, Sanders IR. **2015**. Tansley review mycorrhizal ecology and evolution: the past, the present, and the future. *New Phytologist* **205** : 1406–1423.

Hijikata N, Murase M, Tani C, Ohtomo R, Osaki M, Ezawa T. **2010**. Polyphosphate has a central role in the rapid and massive accumulation of phosphorus in extraradical mycelium of an arbuscular mycorrhizal fungus. *New Phytologist* **186**: 285–289.

Hodge A, Campbell CD, Fitter AH. **2001**. An arbuscular mycorrhizal fungus accelerates decomposition and acquires nitrogen directly from organic material. *Nature* **413** : 297–299.

Hothorn M, Neumann H, Lenherr ED, Wehner M, Rybin V, Hassa PO, Uttenweiler A, Reinhard M, Schmidt A, Seiler J, *et al.* 2009a. Catalytic core of amembrane-associated eukaryotic polyphosphate polymerase. *Science* **324**: 513–516.

Huang R, Wan B, Hultz M, Diaz JM, Tang Y. **2018**. Phosphatase-mediated hydrolysis of linear polyphosphates. *Environmental Science & Technology* **52**: 1183-1190.

Ishige K, Zhang H, Kornberg A. **2002**. Polyphosphate kinase (PPK2), a potent, polyphosphate-driven generator of GTP. *Procedding of the National Academy of Science* **99**: 16684–16688.

Ivanov S, , Jotham Austin RHB and MJH. **2019**. Extensive membrane systems at the host–arbuscular mycorrhizal fungus interface. *Nature Plants* **5**: 194–203.

Javot H, Penmetsa RV, Terzaghi N, Cook DR, Harrison MJ. **2007**. A *Medicago truncatula* phosphate transporter indispensable for the arbuscular mycorrhizal symbiosis. *Proceedings of the National Academy of Sciences* **104**: 1720–1725.

Jeanmaire C, Dexheimer J, Marx C, Gianinazzi S. **1985**. Effect of vesicular-arbuscular mycorrhizal infection on the distribution of neutral phosphatase activities in root cortical cells. *Journal of Plant Physiology* **119**: 285–293.

Jolicoeur M, Germette S, Gaudette M, Perrier M, Be G. **1998**. Intracellular pH in arbuscular mycorrhizal fungi. *Plant Physiology* **116**: 1279–1288.

Kikuchi Y, Hijikata N, Ohtomo R, Handa Y, Kawaguchi M, Saito K, Masuta C, Ezawa T. **2016**. Aquaporin-mediated long-distance polyphosphate translocation directed towards the host in arbuscular mycorrhizal symbiosis: application of virus-induced gene silencing. *New Phytologist* **211**: 1202–1208.

Kikuchi Y, Hijikata N, Yokoyama K, Ohtomo R, Handa Y, Kawaguchi M, Saito K, Ezawa T. **2014**. Polyphosphate accumulation is driven by transcriptome alterations that lead to near-synchronous and near-equivalent uptake of inorganic cations in an arbuscular mycorrhizal fungus. *New Phytologist* **204**: 638–649.

Kobae Y, Hata S. **2010**. Dynamics of periarbuscular membranes visualized with a fluorescent

phosphate transporter in arbuscular mycorrhizal roots of rice. *Plant and Cell Physiology* **51**: 341–353.

Kobae Y, Kawachi M, Saito K, Kikuchi Y. **2015**. Up-regulation of genes involved in N -acetylglucosamine uptake and metabolism suggests a recycling mode of chitin in intraradical mycelium of arbuscular mycorrhizal fungi. *Mycorrhiza* **25**: 411–417.

Kobae Y, Tomioka R, Tanoi K, Kobayashi NI, Ohmori Y. **2014**. Selective induction of putative iron transporters , OPT8a and OPT8b , in maize by mycorrhizal colonization Selective induction of putative iron transporters , OPT8a and OPT8b , in maize by mycorrhizal colonization. *Soli Science and Plant Nutrition* **60**: 37–41.

Kohl K, Zangger H, Rossi M, Isorce N, Lye L, Owens KL, Stephen M, Mayer A, Fasel N. **2018**. Importance of polyphosphate in the *Leishmania* life cycle. *Microbial Cell* **5**: 371–384.

Kojima T, Hayatsu M, Saito M. **1998**. Intraradical hyphae phosphatase of the arbuscular mycorrhizal fungus, *Gigaspora margarita*. *Biology and Fertility of Soils* **26**: 331–335.

Kojima T, Oka N, Karasawa T, Okazaki K, Ando S, Takebe M. **2014**. Community of arbuscular mycorrhizal fungi in soybean roots after cultivation with different cropping systems. *Japan Agricultural Research Quarterly* **48**: 279–290.

Kozlov AM, Darriba D, Stamatakis A. **2019**. RAxML-NG : a fast, scalable and user-friendly tool for maximum likelihood phylogenetic inference. *Bioinformatics* **35**: 1–3.

Krajinski F, Courty P-E, Sieh D, Franken P, Zhang H, Bucher M, Gerlach N, Kryvoruchko I, Zoeller D, Udvardi M, *et al.* 2014. The H^+-ATPase HA1 of *Medicago truncatula* is essential for phosphate transport and plant growth during arbuscular mycorrhizal symbiosis. *The Plant Cell* **26**: 1808–1817.

Kuga Y, Saito K, Nayuki K, Peterson RL, Saito M. **2008**. Ultrastructure of rapidly frozen and freeze-substituted germ tubes of an arbuscular mycorrhizal fungus and localization of polyphosphate. *New Phytologist* **178**: 189–200.

Kumble KD, Kornberg A. **1996**. Endopolyphosphatases for long chain inorganic polyphosphate in yeast and mammals. *Journal of Biological Chemistry* **271**: 27146–27151.

Lander N, Ulrich PN, Docampo R. **2013**. Trypanosoma brucei vacuolar transporter chaperone 4 (TbVtc4) is an acidocalcisome polyphosphate kinase required for *in vivo* infection. *Journal of Biological Chemistry* **288**: 34205–34216.

Letunic I, Bork P. **2019**. Interactive Tree Of Life (iTOL) v4 : recent updates and new developments. *Nucleic Acid Research* **47**: 256–259.

Li B, Boiarkina I, Young B, Yu W, Singhal N. **2016**. Prediction of future phosphate rock: A demand based model. *Journal of Environmental Informatics* **31**: 41–53.

Li XL, Marschner H, Gearge E. **1991**. Acquisition of phosphorus and copper by VA-mycorrhizal hyphae and root-to-shoot transport in white clover. *Plant and soil **136***: 49–57.

Li C, Gui S, Yang T, Walk T, Wang X, Liao H. **2012**. Identification of soybean purple acid phosphatase genes and their expression responses to phosphorus availability and symbiosis. *Annals of Botany* **109**: 275–285.

Li C, Zhou J, Wang X, Liao H. **2019**. A purple acid phosphatase, GmPAP33, participates in arbuscule

degeneration during arbuscular mycorrhizal symbiosis in soybean. *Plant Cell and Environment* **42**: 2015–2027.

Liu J, Chen J, Xie K, Tian Y, Yan A, Liu J, Huang Y, Wang S, Zhu Y, Chen A, *et al.* 2020. A mycorrhiza-specific H^+-ATPase is essential for arbuscule development and symbiotic phosphate and nitrogen uptake. *Plant, Cell & Environment* **43**: 1069–1083.

Lonetti A, Szijgyarto Z, Bosch D, Loss O, Azevedo C, Saiardi A. **2011**. Identification of an evolutionarily conserved family of inorganic polyphosphate endopolyphosphatases. *Journal of Biological Chemistry* **286**: 31966–31974.

Maeda D, Ashida K, Iguchi K, Chechetka SA, Hijikata A, Okusako Y, Deguchi Y, Izui K, Hata S. **2006**. Knockdown of an arbuscular mycorrhiza-inducible phosphate transporter gene of *Lotus japonicus* suppresses mutualistic symbiosis. *Plant and Cell Physiology* **47**: 807–817.

Maldonado-Mendoza IE, Dewbre GR, Harrison MJ. **2001**. A Phosphate transporter gene from the extra-radical mycelium of an arbuscular mycorrhizal fungus *Glomus intraradices* is regulated in Response to Phosphate in the Environment. *Molecular Plant-Microbe Interactions* **14**: 1140–1148.

Maria J. Harrison & L.van Buuren. **1995**. A phosphate transporter from the mycorrhizal fungus *Glomus versiforme*. *Nature* **378**: 703–706.

Martin FM,Uroz S, Baker DG. **2017**. Ancestral alliances: Plant mutualistic symbioses with fungi and bacteria. *Science* **356**: 819.

Martin Willmann , Nina Gerlach BB, Polatajko A, , Réka Nagy , Eva Koebke , Jan Jansa , René Flisch4 and Marcel Bucher. **2013**. Mycorrhizal phosphate uptake pathway in maize: vital for growth and cob development on nutrient poor agricultural and greenhouse soils. *International Journal of Special Education* **30**: 137–149.

Marx C, Dexheimer J, Gianinazzi-Pearson V, Gianinazzi S. 1982. Enzymatic studies on the metabolism of vesicular–arbuscular mycorrhizas: IV. Ultracytoenzymological evidence (ATPase) for active transfer processes in the host-arbuscule interface. *New Phytologist* **90**: 37–43.

Miller RM, Jastrow JD. **2000**. Mycorrhizal fungi influence soil structure. In: *Arbuscular Mycorrhizas*: *Physiology and Function*. *Springer* p.3–18.

Muller O, Bayer MJ, Peters C, Andersen JS, Mann M, Mayer A. **2002**. The Vtc proteins in vacuole fusion : coupling NSF activity to V_0 *trans* -complex formation. *EMBO Journal* **21**: 259–269.

Müller O, Neumann H, Bayer MJ, Mayer A. **2003**. Role of the Vtc proteins in V-ATPase stability and membrane trafficking. *Journal of Cell Science* **116** : 1107–1115.

Murray JM, Johnson DI. **2000**. Isolation and cheracterization of Nrf1p, a novel negative regulator of the Cdc42p GTPase in *Schizosaccharomyces pombe*. *Genetics* **154**: 155–156.

Nagy R, Karandashov V, Chague V, Kalinkevich K, Tamasloukht M, Xu G, Jakobsen I, Levy AA, Amrhein N, Bucher M. **2005**. The characterization of novel mycorrhiza-specific phosphate transporters from *Lycopersicon esculentum* and *Solanum tuberosum* uncovers functional redundancy in symbiotic phosphate transport in solanaceous species. *Plant Journal* **42**: 236–250.

Nakakoshi M, Nishioka H, Katayama E. **2011**. New versatile staining reagents for biological transmission electron microscopy that substitute for uranyl acetate. *Journal of Electron Microscopy*

60: 401–407.

Nayuki K, Chen B, Ohtomo R, Kuga Y. **2014**. Cellular imaging of cadmium in resin sections of arbuscular mycorrhizas using synchrotron micro X-ray fluorescence. *Microbes and Environments* **29**: 60–66.

Newsham KK, Fitter AH, Watkinson AR. **1995**. Multi-functionality and biodiversity in arbuscular mycorrhizas. *Trends in Ecology & Evolution* **10**: 407–411.

Nielsen JS, Joner EJ, Declerck S, Olsson S, Jakobsen I. **2002**. Phospho-imaging as a tool for visualization and noninvasive measurement of P transport dynamics in arbuscular mycorrhizas. *New Phytologist* **154**: 809–819.

Ogawa N, Derisi J, Brown PO. **2000**. New components of a system for phosphate accumulation and polyphosphate metabolism in *Saccharomyces cerevisiae* revealed by genomic expression analysis. *Molecular Biology of the Cell* **11**: 4309–4321.

Ohtomo R, Saito M. **2005**. Polyphosphate dynamics in mycorrhizal roots during colonization of an arbuscular mycorrhizal fungus. *New Phytologist* **167**: 571–578.

Ohtomo R, Sekiguchi Y, Kojima T, Saito M. **2008**. Different chain length specificity among three polyphosphate quantification methods. *Analytical Biochemistry* **383**: 210–216.

Ozalp VC, Pedersen TR, Nielsen LJ, Olsen LF. 2010. Time-resolved measurements of intracellular ATP in the yeast *Saccharomyces cerevisiae* using a new type of nanobiosensor. *Journal of BIological Chemistry* **285**: 37579–37588.

Pao SS, Paulsen IANT, Saier MH. **1998**. Major facilitator superfamily. *Microbiology and Molecular Biology Review* **62**: 1–34.

Pumplin N, Zhang X, Noar RD, Harrison MJ. **2012**. Polar localization of a symbiosis-specific phosphate transporter is mediated by a transient reorientation of secretion. *Proceedings of the National Academy of Sciences* **109**: E665–E672.

Rao NN, G R. **2009**. Inorganic polyphosphate: Essential for growth and survival. *Annual Review of Biochemistry* **78**: 605–647.

Rasmussen N, Lloyd DC, Ratcliffe RG, Hansen PE, Jakobsen I. **2000**. ^{31}P NMR for the study of P metabolism and translocation in arbuscular mycorrhizal fungi. *Plant and Soil* **226**: 245–253.

Richardson AE, Lynch JP, Ryan PR, Delhaize E, Smith FA, Smith SE, Harvey PR, Ryan MH, Veneklaas EJ, Lambers H, *et al.* 2011. Plant and microbial strategies to improve the phosphorus efficiency of agriculture. *Plant and Soil* **349**: 121–156.

Ritz C, Baty F, Streibig JC, Gerhard D. **2015**. Dose-Response Analysis Using R. *PLOS ONE* **10**: 1–13.

Robinson NA, Wood HG. **1986**. Polyphosphate kinase from *Propionibacterium shermanii*. *Journal of Biological Chemistry* **261**: 4481–4485.

Rooney PJ, Ayong L, Tobin CM, Moreno SNJ, Knoll LJ. **2011**. TgVTC2 is involved in polyphosphate accumulation in *Toxoplasma gondii*. *Molecular & Biochemical Parasitology* **176**: 121–126.

Rooney DC, Killham K, Bending GD, Baggs E, Weih M, Hodge A. **2009**. Mycorrhizas and biomass

crops : opportunities for future sustainable development. *Trends in Plant Science* **14**: 542–549

Roth R, Hillmer S, Funaya C, Chiapello M, Schumacher K, Presti L Lo, Kahmann R, Paszkowski U. **2019**. Arbuscular cell invasion coincides with extracellular vesicles and membrane tubules. *Nature Plants* **5**: 204–211.

Safrany ST, Caffrey JJ, Yang X, Bembenek ME, Moyer MB, Burkhart WA, Shears SB. **1998**. A novel context for the 'MutT' module, a guardian of cell integrity, in a diphosphoinositol polyphosphate phosphohydrolase. *EMBO Journal* **17**: 6599–6607.

Saito K, Ezawa T. **2016**. Phosphorus metabolism and transport in arbuscular mycorrhizal symbiosis. *Molecular Mycorrhizal Symbiosis*: John Wiley & Sons, New Jersey. p.197–216.

Saito K, Ohtomo R, Kuga-Uetake Y, Aono T, Saito M. **2005**. Direct labeling of polyphosphate at the ultrastructural level in *Saccharomyces cerevisiae* by using the affinity of the polyphosphate binding domain of *Escherichia coli* exopolyphosphatase. *Applied and Environmental Microbiology* **71**: 5692–5701.

Sanz-Luque E, Saroussi S, Huang W, Akkawi N .2020. Metabolic control of acclimation to nutrient deprivation dependent on polyphosphate synthesis. *Science Advances* **6** : eabb5351

Schmittgen TD, Livak KJ. **2008**. Analyzing real-time PCR data by the comparative C_T method. *Nature Protocol* **3**: 1101–1108.

Schneider CA, Rasband WS, Eliceiri KW. **2012**. NIH Image to ImageJ : 25 years of image analysis. *Nature Methods* **9**: 671–675.

Schott S, Valdebenito B, Bustos D, Gomez-Porras JL, Sharma T, Dreyer I. **2016**. Cooperation through competition—dynamics and microeconomics of a minimal nutrient trade system in arbuscular mycorrhizal symbiosis. *Frontiers in Plant Science* **7**: 1–13.

Scott RA, Haight GP. **1975**. Separation and Detection of ortho- , pyro- , and tripolyphosphate by anion exchange thin layer chromatography. *Analytical Chemicstry* **47**: 2439–2441.

Secco D, Wang C, Shou H, Whelan J. **2012**. Phosphate homeostasis in the yeast *Saccharomyces* cerevisiae, the key role of the SPX domain-containing proteins. *FEBS Letters* **586**: 289–295.

Shi X, Kornberg A. **2005**. Endopolyphosphatase in *Saccharomyces cerevisiae* undergoes post-translational activations to produce short-chain polyphosphates. *FEBS Letters* **579**: 2014–2018.

Smith SA, Morrissey JH. **2007**. Sensitive fluorescence detection of polyphosphate in polyacrylamide gels using 4',6-diamidino-2-phenylindol. *Electrophoresis* **28** : 3461–3465.

Smith SA, **Wang Y, Morrissey JH**. **2018**. DNA ladders can be used to size polyphosphate resolved by polyacrylamide gel electrophoresis. *Electrophoresis* **39** : 1–16.

Smith SE and Read DJ. **2008**. *Mycorrhizal symbiosis*. Academic Press, London.

Smith SE, Smith FA. 1990. Structure and function of the interfaces in biotrophic symbioses as they relate to nutrient transport. *New Phytologist* **114**: 1–38.

Smith SE, Smith FA. **2011**. Roles of arbuscular mycorrhizas in plant nutrition and growth: New paradigms from cellular to ecosystem scales. *Annual Review of Plant Biology* **62**: 227–250.

Smith SE, Smith SA, Jacobsen I. 2003. Mycorrhizal fungi can dominate phosphate supply to plant irrespective of growth responses. *Plant Physiology* **133**: 1–13.

Smith SE, Smith FA, Jakobsen I. **2004**. Functional diversity in arbuscular mycorrhizal (AM) symbioses: The contribution of the mycorrhizal P uptake pathway is not correlated with mycorrhizal responses in growth or total P uptake. *New Phytologist* **162**: 511–524.

Solaiman MZ, Ezawa T, Kojima T, Saito M. **1999**. Polyphosphates in intraradical and extraradical hyphae of an arbuscular mycorrhizal fungus, *Gigaspora margarita. Applied and Environmental Microbiology* **65**: 5604–5606.

Solaiman MZ, Saito M. **2001**. Phosphate efflux from intraradical hyphae of *Gigaspora margarita in vitro* and its implication for phosphorus translocation. *New Phytologist* **151**: 525–533.

Strullu-derrien C, Selosse MA, Kenrick P, Martin FM. **2018**.The origin and evolution of mycorrhizal symbioses : from palaeomycology to phylogenomics. *New Phytologist* **220**: 1012–1030

Takanishi I, Ohtomo R, Hayatsu M, Saito M. **2009**. Short-chain polyphosphate in arbuscular mycorrhizal roots colonized by *Glomus* spp.: A possible phosphate pool for host plants. *Soil Biology and Biochemistry* **41**: 1571–1573.

Takeda N, Sato S, Asamizu E, Tabata S, Parniske M. **2009**. Apoplastic plant subtilases support arbuscular mycorrhiza development in *Lotus japonicus*. *Plant Journal* **58**: 766–777.

Tani C, Ohtomo R, Osaki M, Kuga Y, Ezawa T. **2009**. ATP-dependent but proton gradient-independent polyphosphate-synthesizing activity in extraradical hyphae of an arbuscular mycorrhizal fungus. *Applied and Environmental Microbiology* **75**: 7044–7050.

Thi P, Nguyen M, Ishiwata-kimata Y, Kimata Y. **2019**. Monitoring ADP/ATP ratio in yeast cells using the fluorescent-protein reporter percevalHR. *Bioscience, Biotechnology, and Biochemistry* **83**: 824–828.

Tijssen JPF, Beekes HW, Van Steveninck J. **1982**. S*accharomyces fragilis. Yeast* **721**: 394–398.

Tisserant E, Kohler A, Dozolme-Seddas P, Balestrini R, Benabdellah K, Colard A, Croll D, da Silva C, Gomez SK, Koul R, *et al.* 2012. The transcriptome of the arbuscular mycorrhizal fungus *Glomus intraradices* (DAOM 197198) reveals functional tradeoffs in an obligate symbiont. *New Phytologist* **193**: 755–769.

Tisserant E, Malbreil M, Kuo A, Kohler A, Symeonidi A, Balestrini R, Charron P, Duensing N, Frei Dit Frey N, Gianinazzi-Pearson V, *et al.* 2013. Genome of an arbuscular mycorrhizal fungus provides insight into the oldest plant symbiosis. *Proceedings of the National Academy of Sciences of the United States of America* **110**: 20117–20122.

Trouvelot, A., Kough, J., Gianinazzi-Pearson V. **1986**. Evaluation of VA infection levels in root systems. Researchfor estimation methods having a functional significance. *Physiological and Genetical Aspects of Mycorrhizae. INRA Press, Paris, France*: 217–221.

Uetake AY, Kojima T, Ezawa T, Saito M. **2002**. Extensive tubular vacuole system in an arbuscular mycorrhizal fungus, *Gigaspora margarita*. *New Phytologist* **154**: 761–768.

Ulrich PN, Lander N, Kurup SP, Reiss L, Brewer J, Soares LC, Miranda K, Docampo R. **2014**. The acidocalcisome vacuolar transporter chaperone 4 catalyzes the synthesis of polyphosphate in insect-

stages of *Trypanosoma brucei and T. cruzi*. *Journal of Eukaryotic Microbiology* **61**: 155–165.

Urbański DF, Małolepszy A, Stougaard J, Andersen SU. **2012**. Genome-wide LORE1 retrotransposon mutagenesis and high-throughput insertion detection in *Lotus japonicus*. *Plant Journal* **69**: 731–741.

Uttenweiler A, Schwarz H, Neumann H, Mayer A. **2007**. The vacuolar transporter chaperone (VTC) complex Is required for microautophagy. *Molecular Biology of the Cell* **18**: 166–175.

Van Aarle IM, Cavagnaro TR, Smith SE, Smith FA, Dickson S. **2005**. Metabolic activity of *Glomus intraradices* in *Arum*- and *Paris*-type arbuscular mycorrhizal colonization. *New Phytologist* **166**: 611–618.

Viereck N, Hansen PE, Jakobsen I. **2004**. Phosphate pool dynamics in the arbuscular mycorrhizal fungus *Glomus intraradices* studied by in vivo ^{31}P NMR spectroscopy. *New Phytologist* **162**: 783–794.

Walther T, Novo M, Rossger K, Le´tisse F, Loret M-O, Potasis J-C, Fancois J-M. **2010**. Control of ATP homeostasis during the respiro-fermentative transition in yeast. *Molecular Systems Biology* **6**:344.

Wang E, Schornack S, Marsh JF, Gobbato E, Schwessinger B, Eastmond P, Schultze M, Kamoun S, Oldroyd GED. **2012**. A common signaling process that promotes mycorrhizal and oomycete colonization of plants. *Current Biology* **22**: 2242–2246.

Wang E, Yu N, Bano SA, Liu C, Miller AJ, Cousins D, Zhang X, Ratet P, Tadege M, Mysore KS, *et al.* 2014. A H^+-ATPase That energizes nutrient uptake during mycorrhizal symbioses in rice and *Medicago truncatula*. *The Plant Cell* **26**: 1818–1830.

Wang L, Jia X, Zhang Y, Xu L, Menand B, Zhao H, Zeng H, Dolan L, Zhu Y, *et al.* 2021. Loss of two families of SPX domain-containing proteins required for vacuolar polyphosphate accumulation coincides with the transition to phosphate storage in green plants. *Molecular Plant* **14**: 838–846.

Watanabe FS, Olsen SR. **1965**. Test of an ascorbic acid method for determining phosphorus in water and $NaHCO_3$ extracts from soil. *Soil Science Society Proceedings **29***: 677–678.

Watts-Williams SJ, Jakobsen I, Cavagnaro TR, Grønlund M. **2015**. Local and distal effects of arbuscular mycorrhizal colonization on direct pathway Pi uptake and root growth in *Medicago truncatula*. *Journal of Experimental Botany* **66**: 4061–4073.

Werner TP, Amrhein N, Freimoser FM. **2007**. Specific localization of inorganic polyphosphate (poly P) in fungal cell walls by selective extraction and immunohistochemistry. *Fungal Genetics and Biology* **44**: 845–852.

Wild R, Gerasimaite R, Jung JY, Truffault V, Pavlovic I, Schmidt A, Saiardi A, Jacob Jessen H, Poirier Y, Hothorn M, *et al.* 2016. Control of eukaryotic phosphate homeostasis by inositol polyphosphate sensor domains. *Science* **352**: 986–990.

Wurst H, Kornberg A. **1994**. A soluble exopolyphosphatase of *Saccharomyces cerevisiae*. Purification and characterization. *Journal of Biological Chemistry* **269**: 10996–11001.

Wurst H, Shiba T, Kornberg A. 1995. The gene for a major exopolyphosphatase of *Saccharomyces-cerevisiae*. *Journal of Bacteriology* **177**: 898–906.

Xie X, Huang W, Liu F, Tang N, Liu Y, Lin H, Zhao B. **2013**. Functional analysis of the novel mycorrhiza-specific phosphate transporter AsPT1 and PHT1 family from *Astragalus sinicus* during the

arbuscular mycorrhizal symbiosis. *New Phytologist* **198**: 836–852.

Xie X, Lin H, Peng X, Xu C, Sun Z, Jiang K, Huang A, Wu X, Tang N, Salvioli A, *et al.* 2016a. Arbuscular mycorrhizal symbiosis requires a phosphate transceptor in the *Gigaspora margarita* fungal symbiont. *Molecular Plant* **9**: 1583–1608.

Xue L, Klinnawee L, Zhou Y, Saridis G, Vijayakumar V, Brands M, Dörmann P, Gigolashvili T, Turck F, Bucher M. **2018**. AP2 transcription factor CBX1 with a specific function in symbiotic exchange of nutrients in mycorrhizal *Lotus japonicus*. *Proceedings of the National Academy of Sciences* **115**: E9239–E9246.

Yang S-Y, Grønlund M, Jakobsen I, Grotemeyer MS, Rentsch D, Miyao A, Hirochika H, Kumar CS, Sundaresan V, Salamin N, *et al.* 2012a. Nonredundant regulation of rice arbuscular mycorrhizal symbiosis by two members of the *PHOSPHATE TRANSPORTER1* gene family. *The Plant Cell* **24**: 4236–4251.

Zhang H, Ishige K, Kornberg A. **2002**. A polyphosphate kinase (PPK2) widely conserved in bacteria. *Proceedings of the National Academy of Science* **99**: 16678–16683.